THE TURBULENT TRANSFER MECHANISMS IN THE ATMOSPHERIC SURFACE LAYER

by

GORDON ALMON McBEAN

B.Sc., University of British Columbia, 1964

M.Sc., McGill University, 1966

A THESIS SUBMITTED IN PARTIAL FULFILMENT OF THE REQUIREMENTS FOR THE DEGREE OF

DOCTOR OF PHILOSOPHY

in the Department of Physics

and

Institute of Oceanography

We accept this thesis as conforming to the required standard

THE UNIVERSITY OF BRITISH COLUMBIA

September, 1970

In presenting this thesis in partial fulfilment of the requirements for an advanced degree at the University of British Columbia, I agree that the Library shall make it freely available for reference and study. I further agree that permission for extensive copying of this thesis for scholarly purposes may be granted by the Head of my Department or by his representatives. It is understood that copying or publication of this thesis for financial gain shall not be allowed without my written permission.

Department of Physics

The University of British Columbia
Vancouver 8, Canada

Date September 30/70

ABSTRACT

The objective of this study was to investigate the turbulent transfer mechanisms near the surface. Direct measurements of the turbulent fluxes of momentum, heat, and moisture were made in the atmospheric surface layer: principally, 2 m above a grass surface at Ladner, Canada, and for comparison 8 m above the Atlantic Ocean near Barbados.

The spectral correlation coefficients were considered to be a measure of the transfer efficiency as a function of scale size. For momentum transfer the efficiency decreased at all scales as instability increased. It was postulated that this was due to greater amounts of momentum being transferred in bursts of short duration, thus making the spectral correlation coefficient, averaged over sufficient time, smaller.

The Ladner results for heat transfer showed that its transfer efficiency increased at all scales when instability increased. The ratios of the transfer efficiency of heat to that of momentum were greater than 1 for most scales, even for near neutral stratifications, and increased to between 2 and 3 for more unstable conditions.

The efficiency of moisture transfer, when moisture is a passive scalar, was usually smaller than that for heat transfer and was found to depend on the correlation between moisture fluctuations and those of temperature, which is the active scalar.

The results from Barbados pointed out two main differences between the subtropics and mid-latitudes: that the temperature spectrum is much narrower in bandwidth and that the humidity fluctuations make an equally important contribution to buoyancy. These features are reflected in the transfer mechanisms.

TABLE OF CONTENTS

LIST OF TABLES

LIST OF FIGURES

LIST OF APPENDICES

ACKNOWLEDGEMENTS

I am deeply grateful for the assistance of many people in the realization of this study. I would like to thank Dr. M. Miyake, my thesis advisor, Dr. R.W. Stewart, and Dr. R.W. Burling for their helpful advice at all stages of this study.

The main experiment was conducted at Canadian Forces Station Ladner and I am grateful to Capt. D.W. Bastock, the base commander, and his personnel for their complete cooperation.

During the Barbados experiment the temperature and humidity measurements were made with equipment of Dr. S. Pond of Oregon State University. I am especially grateful to Dr. Pond for his careful operation of the equipment and for making the data available to me.

All the students and staff at the Institute of Oceanography, University of British Columbia (IOUBC) helped at various stages of this study and I am grateful for their assistance. M.A. Donelan and J.A. Elliott deserve special thanks.

I would like to thank the Canadian Meteorological Service for supporting me while on educational leave.

Last I would like to thank most of all my wife Patricia for her encouragement and help throughout my study.

CHAPTER I

INTRODUCTION

The turbulent transfer processes play an important role in determining the motions of the atmosphere and the ocean. The atmosphere functions as a heat engine by receiving heat input from the surface in the forms of latent and sensible heat due to turbulent transfer and in the form of long wave radiation. The winds drive most of the ocean surface currents by transferring by turbulence momentum both into the waves and directly into the current. Further knowledge of the turbulent transfers of momentum, heat and moisture are thus essential to a further understanding of the whole circulations of the atmosphere and ocean. The aim of this thesis is to investigate the transfer mechanisms of the vertical transport of momentum, sensible heat, and moisture near the surface and to discover their similarities and dissimilarities.

To study the transfer mechanisms it is essential that direct measurements of the fluxes be made. Further, the results of direct measurements should be examined both in the time domain and in the frequency domain. It is by analysis in the frequency domain that, through Taylor's hypothesis, the effects of different scales of atmospheric motions can be investigated. Because the three transfers of momentum, heat and moisture are all very important it is necessary to study them simultaneously in order that possible interaction can be examined and so that their transfer mechanisms can be compared.

In the past considerable effort has gone into studying these transfers. However, usually one or more of the above measurements was missing. Studies have been made of the profiles alone in attempts to understand the transfers by measuring an effect of the transfer rather than by direct measurements.

Recently more direct measurements have been made (e.g. Dyer, 1965, 1968; Mordukhovich and Tsvang, 1966) but the frequency domain was not investigated. Businger et al (1967) studied heat transfers and Smith (1967), Elderkin (1968), Weiler and Burling (1967) and Miyake et al (1970) studied momentum transfers in the frequency domain while Zubkovsky and Koprov (1969) studied both. This thesis represents the first simultaneous direct measurements of all three transfers for which the results have been analysed extensively in the frequency domain.

CHAPTER 2

THEORETICAL BACKGROUND

The equations of conservation of momentum and mass and the entropy balance are fundamental to all problems of geophysical fluid dynamics. For atmospheric flows near the earth's surface an additional equation, that of conservation of water vapour, is frequently required. For turbulent fluids it is normal to use a Reynolds-type separation of mean and turbulent parts. This plus assumptions based on air behaving like an ideal gas, lead to (see Lumley and Panofsky, 1964, p.59; Phillips, 1966, p.7):

$$\frac{\partial \rho \bar{u}_i}{\partial t} + \frac{\partial}{\partial x_j}\left(\rho \bar{u}_i \bar{u}_j + \rho \overline{u_i' u_j'}\right) + \epsilon_{ijk}\,\rho\,\Omega_j\,\bar{u}_k + \frac{\partial \bar{P}}{\partial x_i} - \frac{g_i}{\bar{T}_v} T_v' = \mu \frac{\partial^2 \bar{u}_i}{\partial x_j \partial x_j}$$

$$\frac{\partial \bar{u}_i}{\partial x_i} = 0 \qquad (2.1)$$

$$\frac{\partial}{\partial t}\rho c_p \bar{T} + \frac{\partial}{\partial x_i}\left(\rho c_p \bar{u}_i \bar{T} + \rho c_p \overline{u_i' T'}\right) = D_T \frac{\partial^2 \bar{T}}{\partial x_j \partial x_j}$$

$$\frac{\partial}{\partial t}\rho \bar{q} + \frac{\partial}{\partial x_i}\left(\rho \bar{u}_i \bar{q} + \rho \overline{u_i' q'}\right) = D_q \frac{\partial^2 \bar{q}}{\partial x_j \partial x_j}$$

The terms in these equations due to the turbulence are the Reynold stresses, $\rho\overline{u_i'u_j'}$, the turbulent transport of sensible heat (or enthalpy), $\rho c_p \overline{u_i'T'}$, and the turbulent advection of moisture, $\rho \overline{u_i'q'}$, where q is the specific humidity. All other terms are standard notation; a list of symbols is given at the end of the thesis. Near the surface and over terrain homogeneous for scales large relative to the height it is usually possible to neglect the molecular terms and to assume horizontal homogeneity. This leads to three

predictor equations for the local horizontal momentum, $\rho\bar{u}_1$, the heat content per unit volume, $\rho\, c_p\, \bar{T}$ and the moisture content per unit volume, $\rho\bar{q}$:

$$\frac{\partial}{\partial t}\rho\bar{u}_1 = -\frac{\partial \bar{P}}{\partial x_i} - \rho\Omega_3\bar{u}_2 - \frac{\partial}{\partial x_3}\rho\overline{u_1'u_3'}$$

$$\frac{\partial}{\partial t}\rho c_p\bar{T} = -\frac{\partial}{\partial x_3}\rho c_p\overline{u_3'T'} \qquad (2.2)$$

$$\frac{\partial}{\partial t}\rho\bar{q} = -\frac{\partial}{\partial x_3}\rho\overline{u_3'q'}\,.$$

Note that the effects of the radiation flux divergence have been assumed negligible in obtaining (2.2b). A typical value of $\bar{q}$ is about 10 g/Kg for the Ladner experiment and about 18 g/Kg during BOMEX. To use these equations it is necessary to specify the turbulent fluxes $\rho\overline{u_1'u_3'}$, $\rho c_p\overline{u_3'T'}$ and $\rho\overline{u_3'q'}$. These fluxes are hence essential to further the understanding of the dynamics of the lower atmosphere.

For steady-state conditions within the constant flux layer $\overline{u_1'u_3'} = \overline{u'w'}$ $\overline{u_3'T'} = \overline{w'T'}$ and $\overline{u_3'q'} = \overline{w'q'}$ are constant with height.

In order to examine these fluxes more completely they can be represented in a spectral form as:

$$\overline{u'w'} = -\int_{n_L}^{n_H}\phi_{uw}(n)\,dn$$

$$\overline{w'T'} = \int_{n_L'}^{n_H'}\phi_{wT}(n)\,dn \qquad (2.3)$$

$$\overline{w'q'} = \int_{n_L''}^{n_H''} \phi_{wq}(n)\, dn$$

where, for example, $\phi_{uw}(n)\, dn$ is the contribution to the u-w covariance due to those eddies with frequencies in the range n to n + dn. It would be desirable that the limits of integration, which may be different for each integral, include all frequencies that contribute to the flux, yet, at the same time, exclude those frequencies associated with large time scale trends. It is only by first computing and then examining the cospectrum that the limits of integration can be determined.

The cospectra can be normalized so that, for example:

$$\int_{n_L}^{n_H} \frac{n\phi_{uw}(n)}{u_*^2}\, d\ln n = 1. \qquad (2.4)$$

Thus $n\phi_{uw}(n)/u_*^2$ or $n\phi_{wT}(n)/\overline{w'T'}$ are measures of the relative importance of scales associated with frequency n to the total transfer. Taylor's hypothesis is that $\lambda = \bar{u}/n$, where λ is the wave length. In this thesis the "non-dimensional frequency", f, defined as $f = z/\lambda = nz/\bar{u}$, where z is the level of observation, will normally be used.

Of special importance to examining the transfer mechanisms are the spectral correlation coefficients:

$$R_{uw}(f) = \frac{\phi_{uw}(f)}{\left[\phi_{uu}(f)\,\phi_{ww}(f)\right]^{1/2}}$$

$$R_{wT}(f) = \frac{\phi_{wT}(f)}{\left[\phi_{ww}(f)\,\phi_{TT}(f)\right]^{1/2}} \qquad (2.5)$$

$$R_{wq}(f) = \frac{\phi_{wq}(f)}{\left[\phi_{ww}(f)\,\phi_{qq}(f)\right]^{1/2}}$$

These are measures of the transfer efficiency associated with any particular

scale. Note that the spectral correlation coefficient provides different information than the cospectrum. For example $\phi_{uw}(f)/u_*^2$ and $\phi_{wT}(f)/\overline{w'T'}$ may have different shapes yet, $R_{uw}(f)$ and $R_{wT}(f)$ can be similar. Thus the cospectrum specifies which scales are important to the total transfer but the spectral correlation coefficient is an actual measure of the transfer efficiency as a function of scale size and hence is more directly related to the transfer mechanism. The importance of the spectral correlation coefficient appears to have been neglected in the literature. Zubkovsky and Koprov (1969) presented data on $R_{uw}(f)$ and $R_{wT}(f)$ but placed more emphasis on the cospectra. Weiler and Burling (1967) and Smith (1967) also analysed $R_{uw}(f)$.

The behaviour of $R_{wq}(f)$ and the dependence of $R_{uw}(f)$ and $R_{wT}(f)$ on stability has not previously been investigated. In this thesis the three transfers will be examined for stability dependence based on the non-dimensional stability parameter, z/L (Monin and Obukhov, 1954). This is defined here as:

$$z/L = -\frac{\kappa z}{u_*^3}\left[\frac{g}{T_v}\left(\overline{w'T'} + 0.61\,\bar{T}\,\overline{w'q'}\right)\right]$$

$$= -\frac{\kappa z}{u_*^3}\frac{g}{T_v}\overline{w'T'} - \frac{\kappa z}{u_*^3}\frac{g\bar{T}}{T_v}0.61\,\overline{w'q'} \qquad (2.6)$$

$$= z/L_T + z/L_q.$$

L_T is what is usually defined as the Monin-Obukhov length. The correction due to moisture content, L_q, can be important over water but is usually negligible over land surfaces.

The criteria for the similarity of the transfer mechanisms is, for a given z/L, that the spectral correlation coefficients agree scale by scale for all scales associated with the transfer. In other words, the transfer mechanisms for momentum transfer and for heat transfer can be considered similar

only if $R_{uw}(f) = R_{wT}(f)$ for all f.

It is useful to be able to compare the overall transfer mechanisms regardless of scale. The correlation coefficients can be defined, as usual:

$$\Gamma_{uw} = \frac{\overline{u'w'}}{\left[\overline{u'^2}\ \overline{w'^2}\right]^{1/2}} = -\frac{u_*^2}{\sigma_u \sigma_w}$$

$$\Gamma_{wT} = \frac{\overline{w'T'}}{\left[\overline{w'^2}\ \overline{T'^2}\right]^{1/2}} = \frac{k u_* T_*}{\sigma_w \sigma_T} \qquad (2.7)$$

$$\Gamma_{wq} = \frac{\overline{w'q'}}{\left[\overline{w'^2}\ \overline{q'^2}\right]^{1/2}} \qquad \frac{k u_* q_*}{\sigma_w \sigma_q}$$

The ratios Γ_{wT}/Γ_{uw} or Γ_{wq}/Γ_{uw} are measures of the relative efficiencies of the transfer mechanism for heat or moisture transfer compared to that for momentum transfer.

In the literature it is more common to investigate the similarity by comparing the exchange coefficients or turbulent diffusivities:

$$K_M = u_*^2 \Big/ \frac{\partial \bar{u}}{\partial z}$$

$$K_H = k u_* T_* \Big/ \frac{\partial \bar{T}}{\partial z} \qquad (2.8)$$

$$K_E = k u_* q_* \Big/ \frac{\partial \bar{q}}{\partial z}.$$

The ratios K_H/K_M and K_E/K_M, which are usually considered, are more measures of the transfer effects than measures of the transfer mechanisms. For example, K_M is a measure of the type of profile $\frac{\partial \bar{u}}{\partial z}$, that will result for a given value of the momentum transfer. The ratios K_H/K_M and K_E/K_M are, however, closely related to Γ_{wT}/Γ_{uw} and Γ_{wq}/Γ_{uw} since:

$$\frac{\Gamma_{wT}}{\Gamma_{uw}} = \frac{k u_* T_*}{u_*^2} \frac{\sigma_u}{\sigma_T} = \frac{K_H}{K_M} \left[\frac{\sigma_u \Big/ \frac{\partial \bar{u}}{\partial z}}{\sigma_T \Big/ \frac{\partial \bar{T}}{\partial z}} \right] \qquad (2.9a)$$

$$\frac{\Gamma_{w\xi}}{\Gamma_{uw}} = \frac{k u_* \xi_*}{u_*^2} \frac{\sigma_u}{\sigma_\xi} = \frac{K_E}{K_M} \left[\frac{\sigma_u / \frac{\partial \bar{u}}{\partial z}}{\sigma_\xi / \frac{\partial \bar{\xi}}{\partial z}} \right] . \qquad (2.9b)$$

Experimental evidence (Tsvang, 1960; Garratt, 1969) indicates that the term in the square bracket in (2.9a) is near unity for unstable stratifications. This implies that $\sigma_u / \sigma_T \simeq \partial \bar{u} / \partial \bar{T}$ or that the relative variances of u to T are uniquely related to the local gradients.

In the past the ratios K_H/K_M and K_E/K_M have been investigated either by directly measuring both the fluxes and the gradients, as was done by Dyer (1965, 1967) and Mordukhovich and Tsvang (1966) or by investigating the profiles alone, since:

$$\frac{K_H}{K_M} = \frac{k u_* T_*}{u_*^2} \frac{\partial \bar{u}/\partial z}{\partial \bar{T}/\partial z} \propto \frac{\partial \bar{u}}{\partial \bar{T}}$$

$$\frac{K_E}{K_M} = \frac{k u_* \xi_*}{u_*^2} \frac{\partial \bar{u}/\partial z}{\partial \bar{\xi}/\partial z} \propto \frac{\partial \bar{u}}{\partial \xi} \qquad (2.10)$$

(e.g., Swinbank and Dyer, 1967).

In summary it should be pointed out again that the spectral correlation coefficient is the most fundamental measure of the transfer mechanisms. Further, similarity of the transfer mechanism of two transfers can only be shown by showing that the spectral correlation coefficients of each transfer are similar for all scales.

CHAPTER 3

THE EXPERIMENTS

The data used in this thesis are from two separate experiments. The main source of data was from an over ground experiment at Ladner, British Columbia. The other source of data was an experiment conducted by an Institute of Oceanography group on Flip, the floating instrument platform of Scripps Institution of Oceanography, University of California, San Diego, as described by Rudnick, 1964, during the Barbados Oceanographic and Meteorological Experiment (BOMEX) near Barbados. These two experiments will be described in the next two sections of this chapter. The equipment, much of which was common to both experiments, will be described in Section 3.3.

3.1 The Ladner Experiment.

The Ladner experiment was conducted over an unused airport at Canadian Forces Station Ladner in mid-August, 1969. This station is at 123.03° west and 49.05° north and located in the flat delta region of the Fraser River. The terrain around the station (Fig. 1) is fairly iniform in elevation and vegetation. All data were collected in winds ranging in direction between 160° and 330° "true' (see Fig. 2 for the mean wind direction for each run). For winds from 142° through to 192° the fetch was over about 30 km of water (Strait of Georgia and Boundary Bay), then over a dyke rising 2 m above land level followed by 1 to $1\frac{1}{2}$ km of mown grass surface (interrupted by one runway) to the observation point. The runways were asphalt and 40 to 60 m wide. For winds from 192° to about 230° the over-water fetch was interrupted by a hilly peninsula 5 to 10 km from the observation point. For winds between 230° and 330° the fetch was over several kilometers of mixed farmland and then over about 800 m of grass (again except for one or two runways) before

Figure 1. Air photograph of Ladner experimental site.

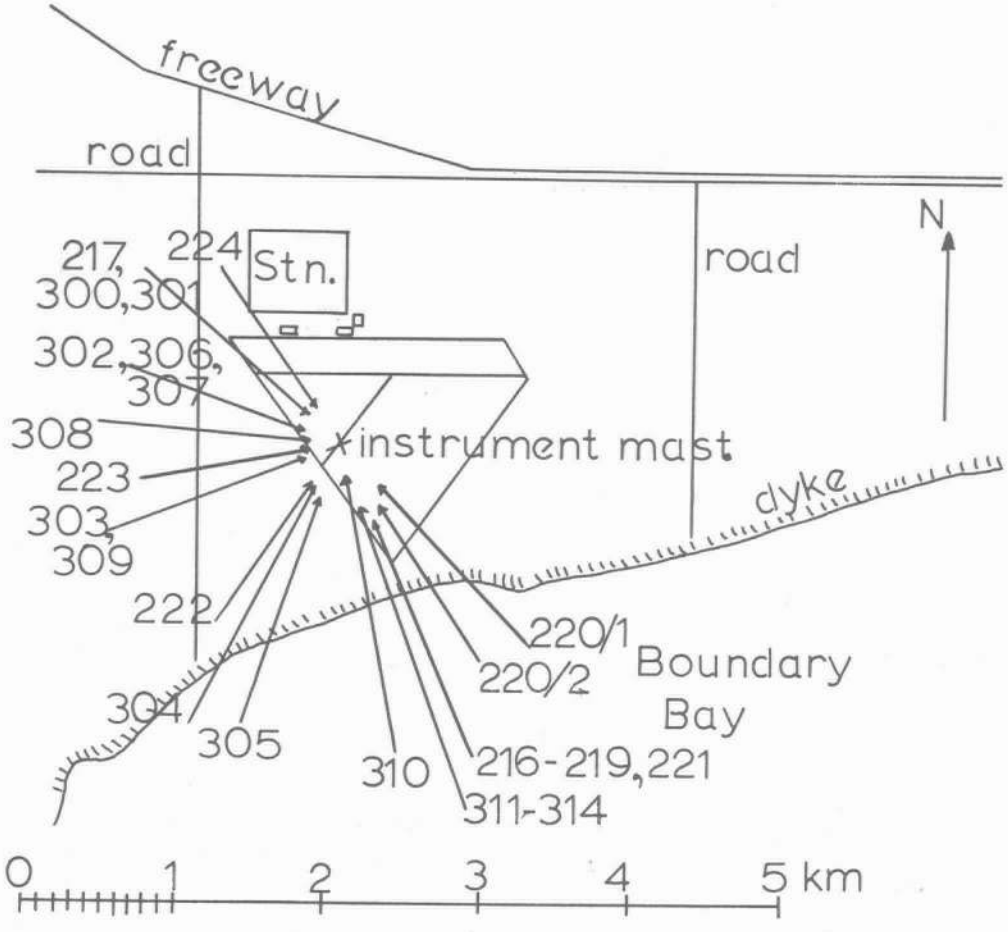

Figure 2. Map of Ladner site showing wind directions for each run.

the observation point. The portable instrument mast was always located near the upwind edge of a runway during each run.

The 10 cm diameter aluminium instrument mast was 4.3 m high, and supported by a tripod clamped at the 0.75 m level. The mast itself could be rotated about its vertical axis to orientate all the instruments into the mean wind direction. Cup anemometers were mounted 30 cm to one side of the mast at the 1 m, 2 m, and 4 m levels. All turbulence sensors were mounted on a 3 cm diameter pipe extending 85 cm horizontally from the mast (see Fig. 3). This was mounted so that the centre of a sonic anemometer array was at the end of the pipe and 2 m above the surface. A dew point hygrometer probe and air intake for the humidiometer were all mounted within the sonic array. A hot wire anemometer, fast response platinum resistance thermometer and thermistor bead temperature sensor were mounted on a vertical support arm 40 cm to the side of the sonic anemometer. A Lyman-α humidiometer and sonic anemometer preamplifier box were also mounted on this horizontal pipe. Most electronics and the recording equipment were housed in a 4'x6'x6' instrument trailer located 50 m to the east of the mast.

The Ladner experiment began on August 15, 1969. Three data runs were made during the evening of August 15th and another seven runs were made on August 16th (see Appendix III for a summary of the data runs). During these runs the humidity sensors and fast response anemometer and thermometer were not used. When the experiment continued on August 21 the humidity and fast response sensors were used. Twelve data runs were collected on August 21st; thirty-three on August 22nd; twenty-five on August 23rd and twelve on August 24th. The program was concluded in the early afternoon on August 24th due to rain. A summary of the prevailing weather conditions for each day is as follows. The weather on August 15 was mainly cloudy while on August 16th it was mainly sunny. On both days the winds were southerly. August 21st;

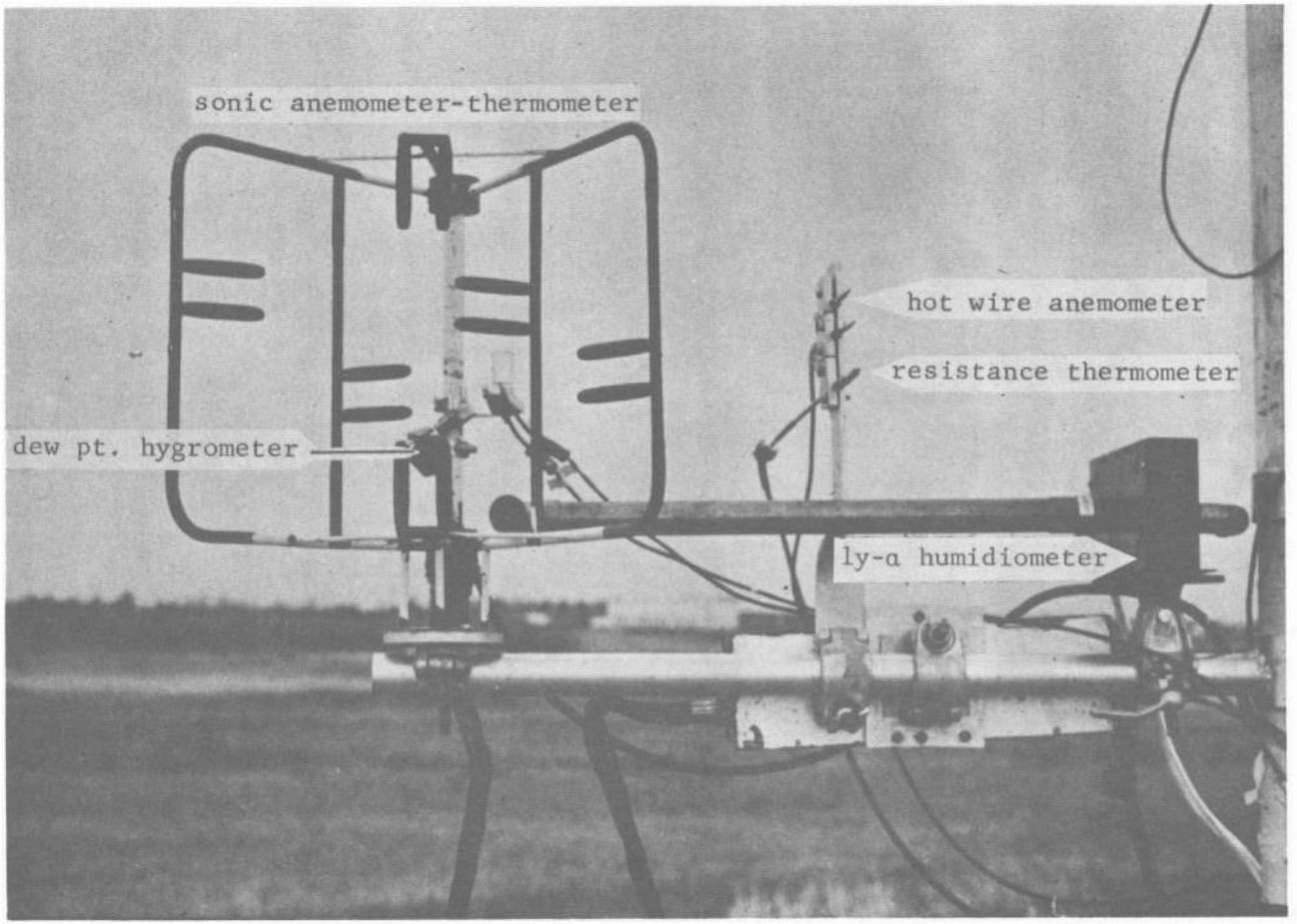

Figure 3. Photograph of measuring instruments for Ladner experiment.

scattered cumulus and heavy cumulus with southerly winds changing to westerly by the end of the day. August 22nd: clear with winds from the northwest but shifting to southwest by midnight. August 23rd: sunny with scattered altocumulus castellanus in the afternoon. Winds were generally westerly becoming light southerly in the evening. August 24th: scattered to broken altocumulus becoming thicker as the day progressed. A few showers in the afternoon and evening. Winds southerly.

3.2 The Flip Experiment

Flip (see Fig. 4) is a manned spar buoy designed to provide a stable platform at sea. It can be towed with its long axis horizontal to the experimental site. Once on position ballast tanks are flooded such that Flip adopts a stable position with its long axis vertical. Of the total length of 116 m only 26 m are above water and its effective center of mass is 60 m below mean water line (Rudnick 1967). Because of Flip's shape, her vertical motions correspond to wave motions about 60 m below the surface which are much less than those of surface waves. During periods of this experiment the main Flip motions were tilting about horizontal axes due to waves and a rotation about its vertical axis due to differential wind forces. These and their effects on the data will be discussed further in Chapter 5.

BOMEX was a large multi-institutional experiment involving a dozen oceanographic ships and more than two dozen aircraft. The objectives and operational setup of BOMEX have been described by Kuettner and Holland (1969). The Flip experiment was only a small part of BOMEX but it still involved two teams of ten scientists each for two week periods. IOUBC cooperated with Oregon State University (OSU), University of Washington,

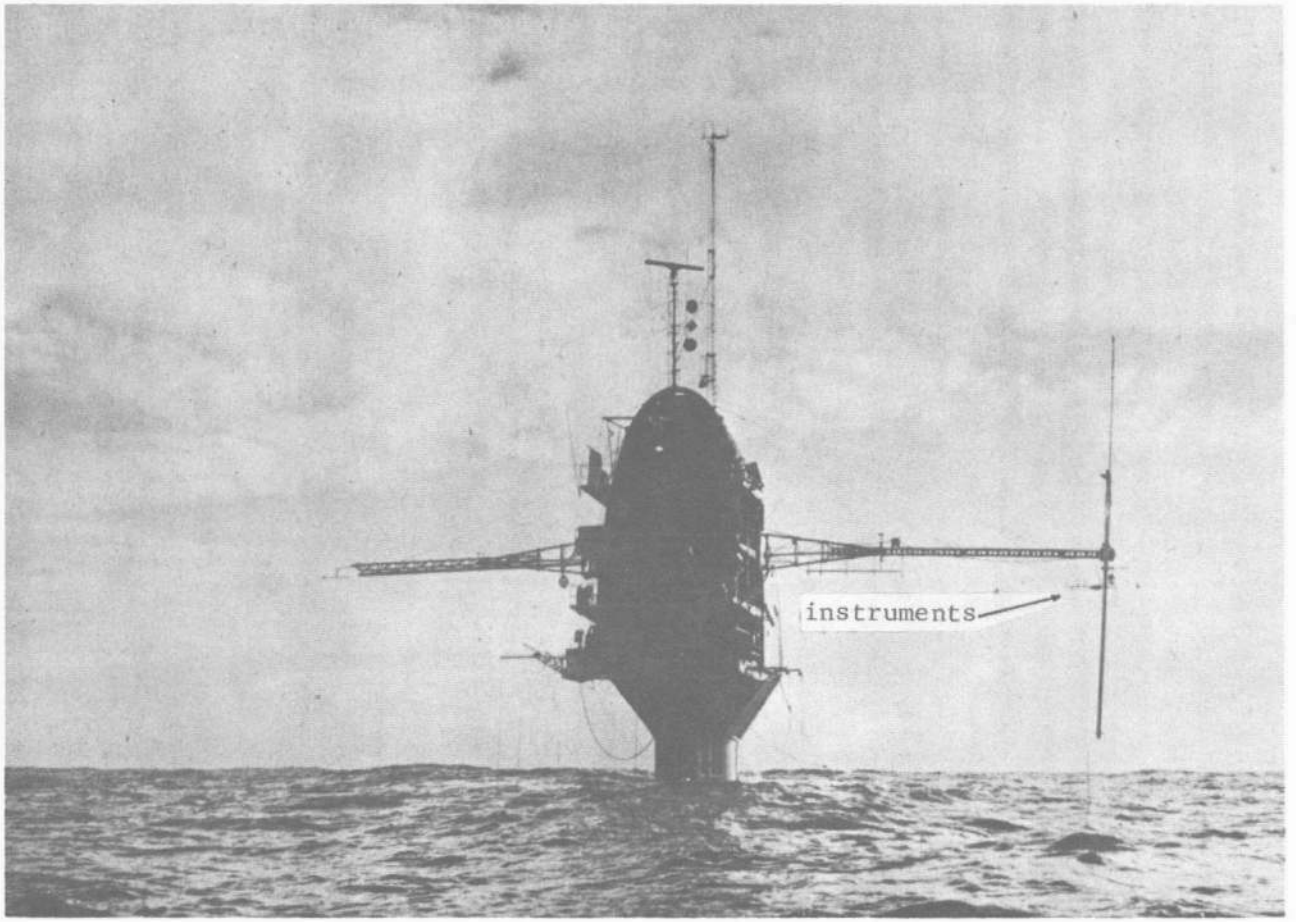

Figure 4. Photograph of Flip, indicating instruments' location.

and University of California, San Diego. A three dimensional sonic anemometer-thermometer and the Oregon State University Lyman-α humidiometer (Phelps et al, 1970) were mounted approximately 8 m above the mean water surface and 16 m to the starboard side of Flip's hull (see Fig. 4). The sonic anemometer was mounted upside-down below a 5 cm diameter horizontal pipe. The Lyman-α humidiometer was mounted 15 cm further outboard and at a slightly higher level. These instruments were about one metre directly below and upwind of the horizontal open lattice support beam which was one half metre wide. A platinum resistance wire thermometer (see Phelps et al, 1970) was mounted so that the platinum element was approximately 5 cm in front of and slightly below the intake port of the Lyman- α . A resistance wire wave gauge was supported from Flip's lower deck. The data reported here were collected on May 6, 1969, and coincided with aircraft measurements by the Institute of Oceanography.The remaining data will be analysed later.

3.3 The Equipment

The principle of operation, advantages and limitations of the equipment used will now be described. Since most of the equipment is commercially available the descriptions will be brief and references given to the appropriate instruction manuals or published reviews.

A schematic diagram of the instrument setup for the Ladner experiment is given in Fig. 5. All electrical signals were recorded on a 14 channel instrumentation tape recorder (Ampex Corp., Model FR1300). The tape recorder was operated in the FM mode so that at $7\frac{1}{2}$ ips (the tape speed used at Ladner) frequencies from DC to 2.5 Khz could be recorded. During the Flip experiments a tape speed of 1 7/8 ips was used so that the response was limited to 625 Hz. All input signals were kept within the range of $\pm$ 1.5 volts while the tape

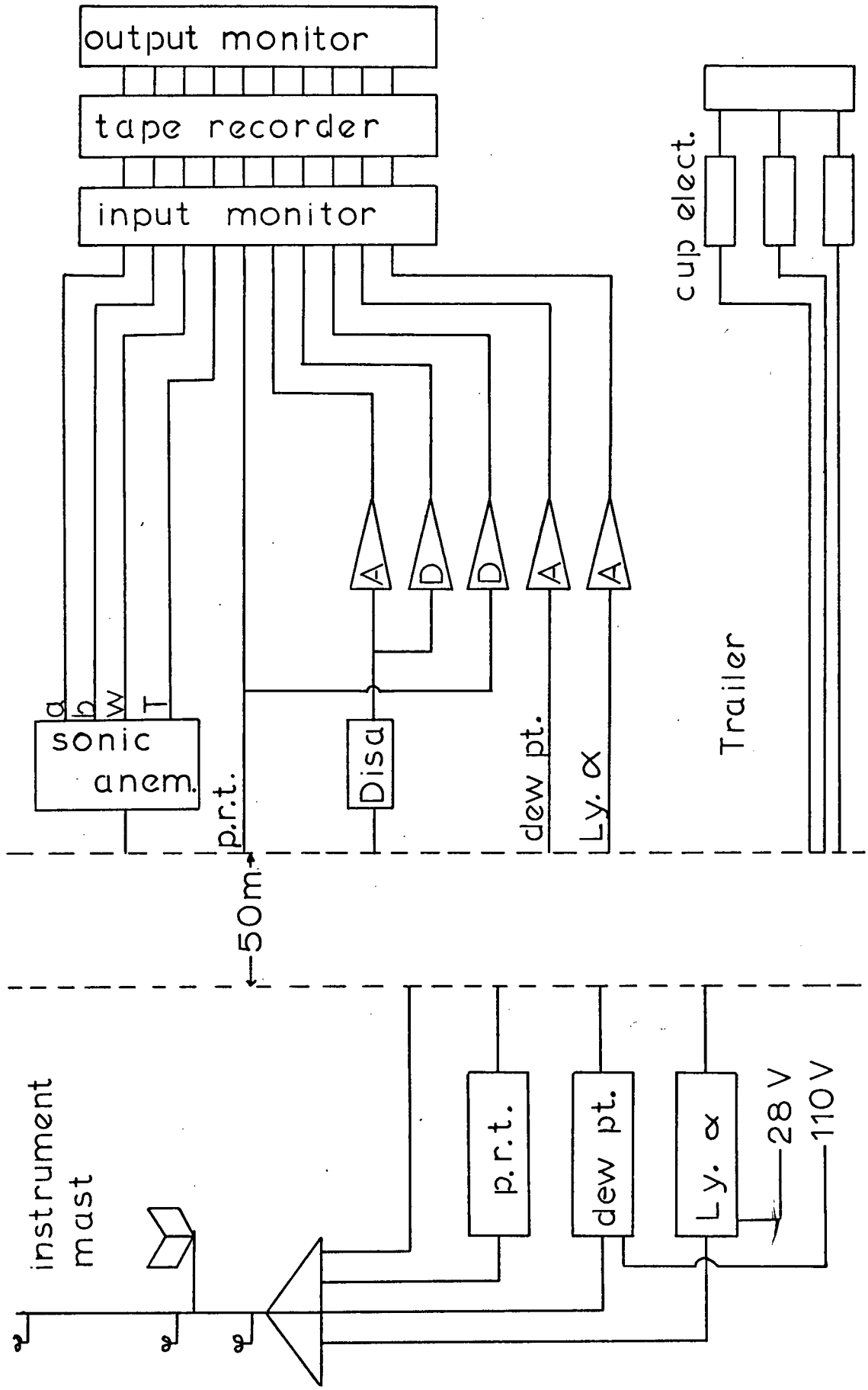

Figure 5. Schematic of the instrument-recording system for Ladner experiment.

recorder noise level was about 20 mv peak to peak. A meter panel was constructed so that the input or output signals of each channel could be monitored. During data runs the outputs from the reproduce heads of the tape recorder were always monitored so that the quality of recorded signals at DC and low frequency (less than 1 Hz) could be visually checked. A six channel chart recorder (Clevite Brush Model 260) was used to follow more rapid fluctuations (to 100 Hz).

The principal measuring device used in the measurement program was a three dimensional ultrasonic anemometer-thermometer (Kaijo Denki, Model PAT-311-1). This anemometer has been described by Mitsuta (1966) and incorporates the advantages of both the pulse and continuous wave type sonic anemometers. Three 20 cm long sound paths are used to determine the three wind components. One path is mounted vertically and the other two are in a horizontal plane and separated by 120°, to avoid structural interference. The effect of the path length is to limit the wavenumber resolution of the sonic anemometer to scale sizes of about 1 m. The noise level of the tape recorder was equivalent to $\pm$ 4 cm sec^{-1} on the sensitivity usually used (full scale $\pm$ 3 m sec^{-1}). The maximum error in calibration was $\pm$ 2%.

Sound virtual temperature fluctuations are measured by sensing the fluctuations in the mean speed of sound along the vertical path length. The sound virtual temperature fluctuations, T'_{sv}, are related to the temperature by (Kaimal and Businger, 1963):

$$T'_{sv} = T' + \left(\frac{0.32\,\bar{T}}{\bar{P}}\right) e' - \left(\frac{2\,\bar{T}\,\bar{u}}{c^2}\right) u'$$

where c is the speed of sound and e is the vapour pressure. The maximum error in equating T' and T_{sv}' will, for the Ladner experiment, always be less than 20%; about 12% due to velocity contamination and 8% due to

humidity contamination. During BOMEX the humidity contamination errors were much larger so that the sonic temperature was not used.

Atmospheric humidity is one of the most difficult parameters to measure. The physical principles and a variety of methods are described in a four volume series under the general editorship of A. Wexler (1965). The two sensors used in this study are commercially made versions of sensors reported on in the series. The Lyman-α humidiometer (Electromagnetic Research Corporation, Model B) is described by Randall et al (1965). It senses the water vapour content of the air by measuring the absorption of Lyman-α radiation (1215.6A) across about a 1 cm path length. In this study the response and sensitivity of the sensor were limited by a 65 cm long tube (3.5 cm diameter) used to transport the air from an intake within the sonic array to the humidiometer. The tube was considered necessary as the humidiometer electronics were too large to put near the sonic anemometer. The effects of this tube and the corrections made for it will be discussed in Appendix II.

To add to the confidence in the humidity measurements, a second humidity sensor, a dew point hygrometer (Cambridge Systems, Model 137-C3), was used in conjunction with the humidiometer. This instrument measures the dew point temperature by sensing photoelectrically the formation of dew on a mirrored surface and then measuring the temperature of the surface (Francisco and Beaubian, 1965). The platinum resistance thermometer used in this system is relatively easy to calibrate and its calibration is quite stable. The dew point hygrometer was thus used to provide an "in situ" calibration for the faster responding Lyman-α humidiometer. The following relation, derived in Appendix II, was used to relate humidity and dew point temperature fluctuations.

$$q' = \left(\frac{19.9\,\overline{q}}{273 + \overline{T_d}} \right) T_d'$$

The humidiometer and dew point hygrometer had very similar spectra for frequencies below 0.05 Hz (see fig. 41).

In addition to the sonic thermometer, a fast response platinum wire resistance thermometer was also used. This system is constructed by National Electrolab, Vancouver, who modified an IOUBC design (Pond, 1965) and employs an 80 KHz A.C. bridge with less than 0.01°C overheat. The probes are 0.25 micron diameter platinum wire with a resistance of about 800 ohms. The response at high frequency is flat throughout the range of temperature fluctuations. The OSU resistance wire thermometer used during BOMEX is of similar design but employs 2.5 micron diameter probes of resistance near 60 ohms.

The mean wind speeds at three levels (1m, 2m, 4m) were measured with cup anemometers (Makino Photoelectric Anemometers, Model AF 701). The cups were calibrated in the low wind speed wind tunnel of the Department of Mechanical Engineering of U.B.C. A hot wire anemometer (Disa Type 55D05) was used to extend the frequency analysis range for the longitudinal wind fluctuations.

During the Ladner experiment both the resistance wire thermometer and hot wire anemometer were calibrated 'in situ' against the sonic anemometer-thermometer by comparing the low frequency spectral densities.

3.4 Summary of Data Presented

For the Ladner experiment the data were divided into 91 data runs of 12 to 17 minutes duration. Two longer runs L300L and L307L which were 54 min. and 47 min. respectively included several shorter runs. A complete list of the data runs, their dates, durations, wind speeds and stabilities are in Appendix III. All the Ladner experiment times are in Pacific Day-

light Saving Time while those for BOMEX (in Appendix IV) are in GMT. For those runs where z/L_q is zero no humidity flux measurements were available. A plot of wind speed against stability is given in Fig. 6. The different symbols represent different days observations. The results show, as expected, that for higher wind speeds the stability tends to be near zero. Note further that during most of the stable cases, $\bar{u} < 2$ m/sec with the lowest speed being 1 m/sec. For these low wind speeds the humidiometer did not ventilate properly and any results from these runs must be treated with extreme caution in considerations involving measurements of moisture.

In order to analyse the Ladner data systematically the data were divided into stability groups. These groups and their limits are indicated in Table I. Groups VI and VIII can each be further subdivided because of differences in results. Gp. VI includes three runs for $|z/L| < 0.01$ which will not be included in plots involving temperature because T_* is approximately zero. Gp. VIII appears to change character around $z/L = 4.0$ but all runs are low wind speed cases. Group VIIIB will refer to those runs for which $z/L > 4.0$.

To consider the effects of stability on spectral shape the following procedure was used. For each group a composite plot of seven spectra was plotted and a mean value for each of 10 frequency bands ($\Delta \mathrm{Log}_{10} F = 0.5$) determined. For groups with more than seven runs, the plotted runs were chosen by choosing every second run when listed chronologically. Low wind speed cases and incomplete data runs were excluded when possible. On the averaged cospectra that are presented, the means for Group I will be represented by (.), for Group VI by a (+), and for Group VIIIB by a (∇). In addition the standard error of the means will be indicated by the use of horizontal lines; ⊢⊣ for Group I, — for Group VI, and ≈ for Group VIIIB. The original composite cospectrum for Group I will also be presented.

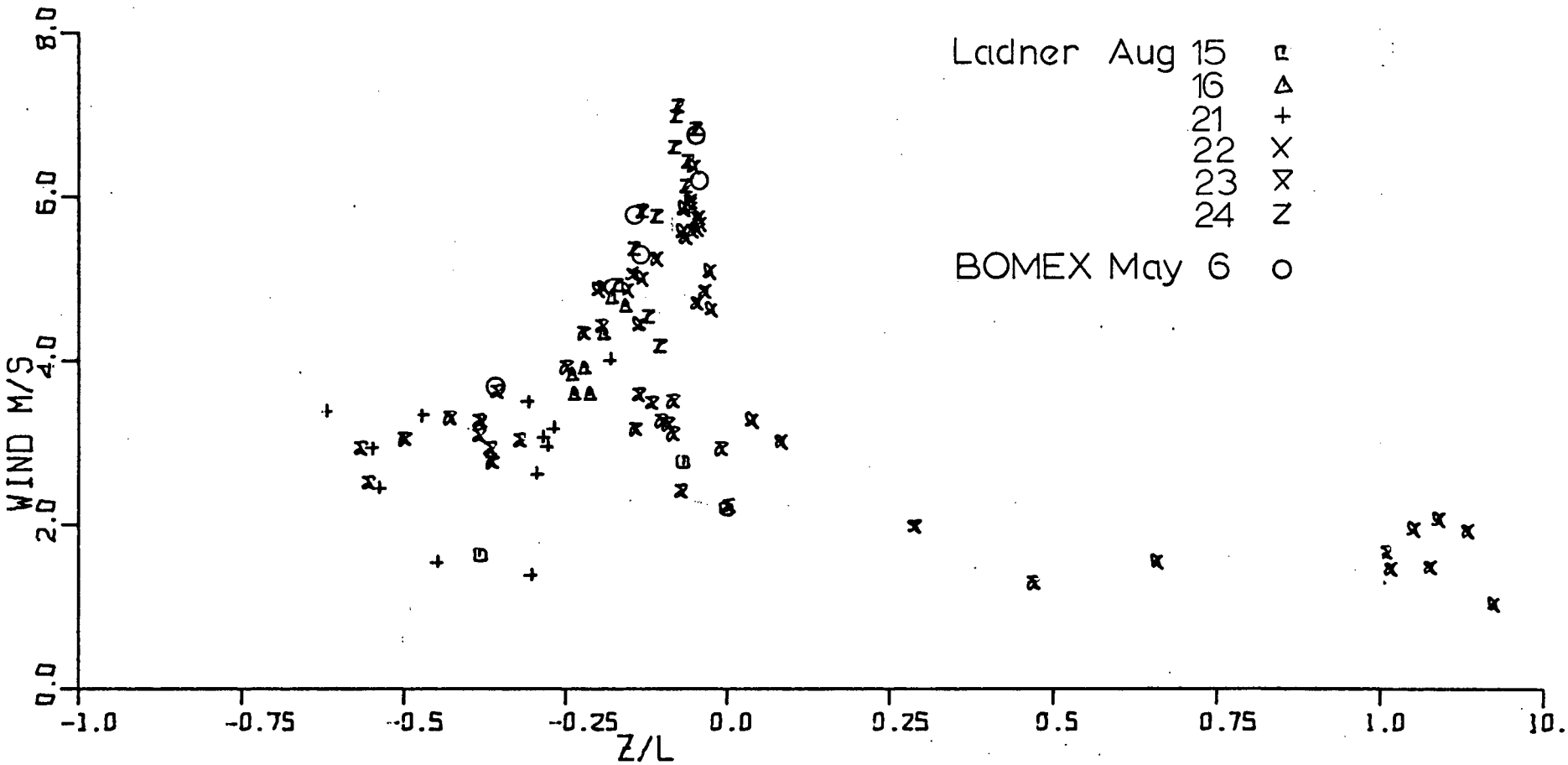

Figure 6. Summary of data: wind speed against stability.

Table I. Stability Groups for Ladner Data

Group	Limits of z/L	No. of Cases
I	-0.63 : -0.46	7
II	-0.46 : -0.34	9
III	-0.34 : -0.18	19
IV	-0.18 : -0.10	17
V	-0.10 : -0.04	23
VI	-0.04 : 0.10	8
VII	+0.1 : 1.0	4
VIII	1.0 : 10.0	6

The original composite cospectra or spectral correlation coefficients for Groups III, V, VI, and VIIIB are given in Appendix V. A complete tabulation of all the integrated statistics is given in Appendices III (Ladner) and IV (BOMEX).

The Flip data analysed were all for . May 6, 1969. Five data runs of 45 minutes each were analysed and the results are presented in Chapter 5. All Flip experimental data were for unstable conditions.

CHAPTER 4

TURBULENT FLUXES OF MOMENTUM, HEAT AND MOISTURE

4.1 Time Series Representation

Time series traces of $w'q'$, $w'T'$, and $u'w'$ representing unstable, near neutral, and stable stratifications are presented in Fig. 7. Note for case L220/1/1 (an unstable case, $z/L = -0.47$) that the transfers are dominated by periods of active transfer; longer series show that these are typically about a minute duration. Separating these periods are quieter periods of approximately the same duration. During the active periods there is a preferred direction of transport while during the quiet periods the direction is more random. Even within the active periods there are shorter time scale variations between active and quiet periods. Visual inspection of the traces seems to indicate that the momentum transfer has a lower correlation coefficient than either heat or moisture transfer.

For the neutral case (Fig. 7b) $w'T'$ is usually non-zero but there is no preferred direction of transport so when averaged over time, $w'T'$ is near zero. However, there is still appreciable moisture transfer. The active periods that dominated the unstable case are now not evident.

For the stable record (Fig. 7c, $z/L = 0.29$) the transfers are all significantly reduced in magnitude. The scales are only one-quarter of the magnitude of those of Figs. 7a and 7b. The scale and trace (Fig. 7c) for $w'T'$ are inverted. In this case there is some heat transfer (downwards) but very little moisture transfer. Although there are periods of relatively high heat transfer the transfers are generally more continuous in time than they were for the unstable case.

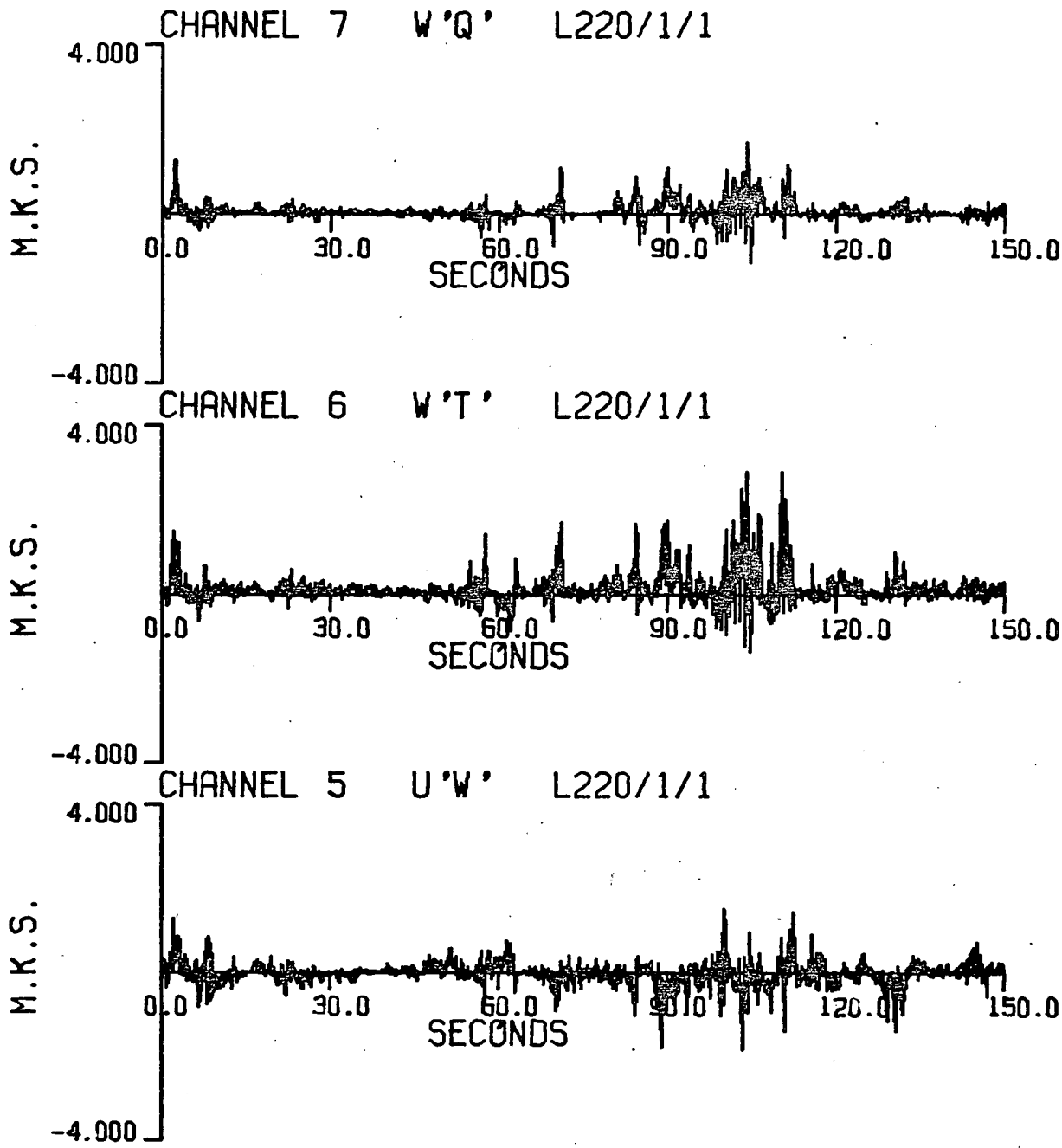

Figure 7a. Time series traces of w'q', w'T', and u'w'.

Run 220/1/1, z/L = -0.47.

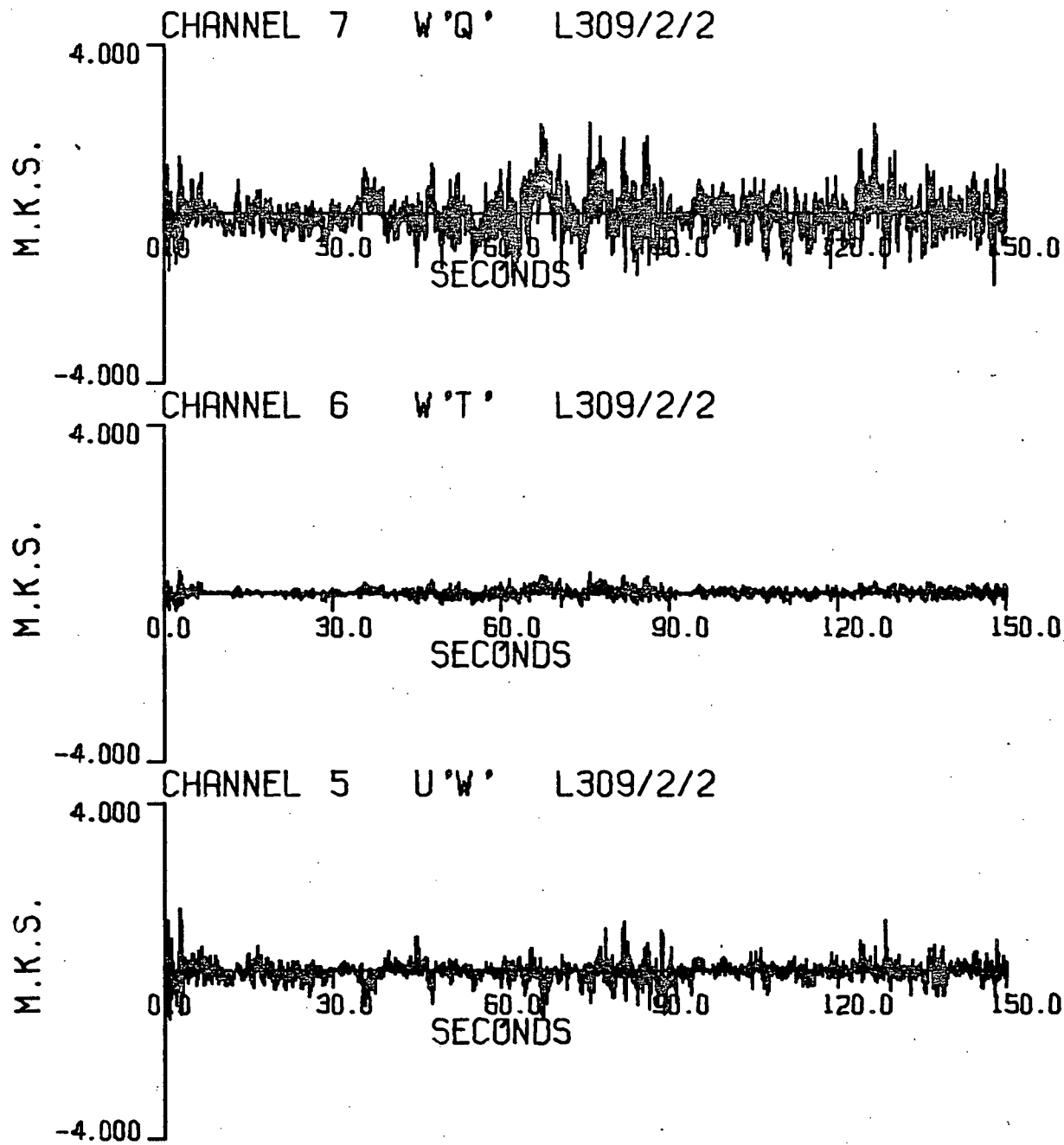

Figure 7b. Time series traces of w'q', w'T', and u'w'.

Run 309/2/2, $z/L \approx 0.0$.

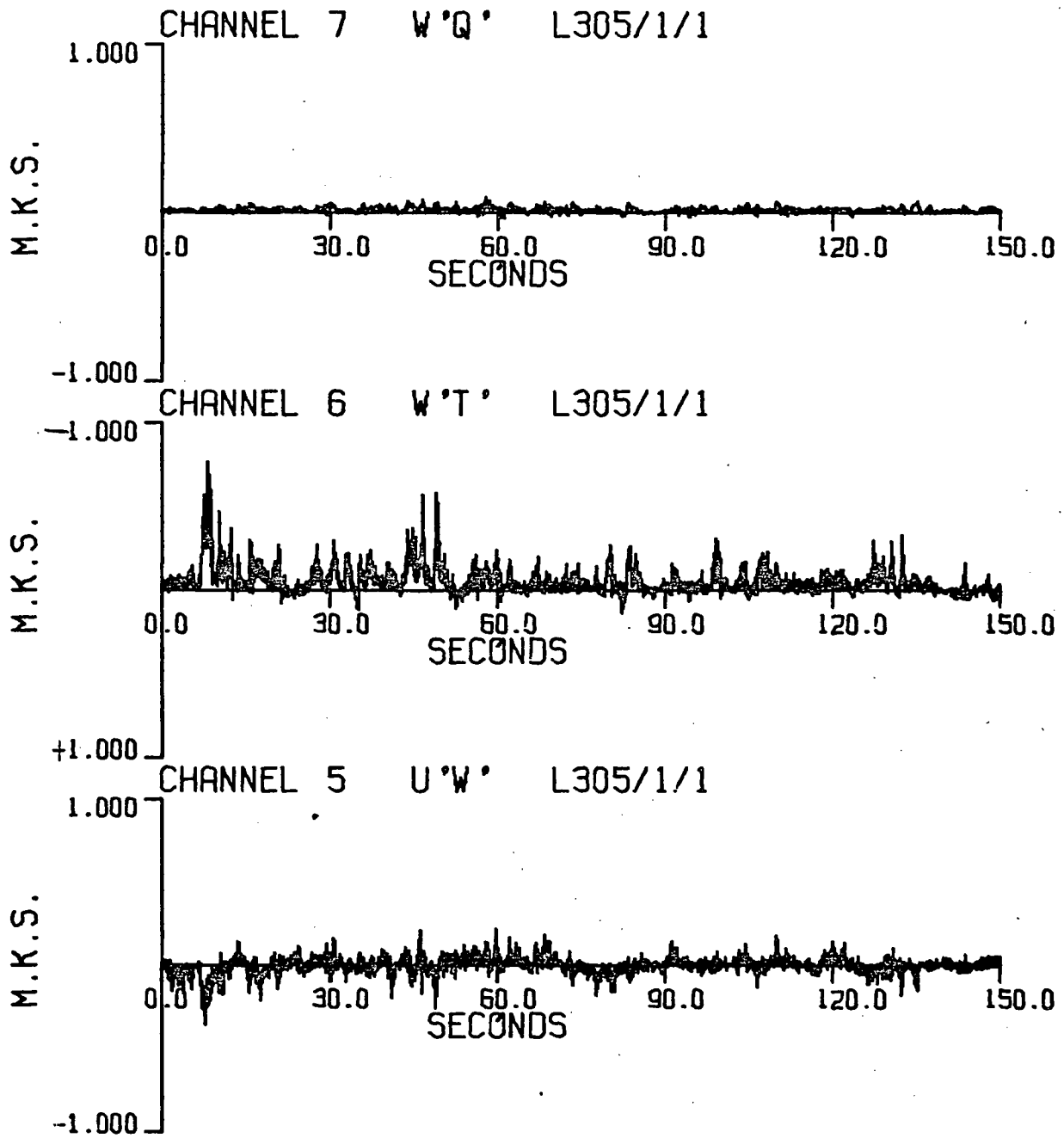

Figure 7c. Time series traces for w'q', w'T', and u'w'. Run 305/1/1, z/L=0.29. The trace and scale for w'T' is inverted.

4.2 Cospectra of the Transfers of Momentum, Heat, and Moisture

The cospectra of the turbulent transfers were computed as described in Appendix I. For each transfer the composite cospectrum for stability Group I will be presented. To demonstrate the variation with stability the mean cospectra plus error bars for Gp. I (most unstable), Gp. VI (near neutral) and Gp. VIIIB (most stable) will be compared.

4.2.1 Momentum Transfer Cospectra

In Fig. 8 the composite momentum cospectrum for the most unstable group is given. The scatter within a data run and from run to run was higher for this group than any other (except for the low frequency part of the cospectra for very stable conditions). The standard error of the mean, as determined for the data blocks (see Appendix I) is indicated for a few cospectral estimates on Fig. 8 and is a measure of the variation in the transfer due to that scale over the length of the data run. These results indicate that, for this stability group, the momentum transfer can be quite variable in time.

The shape of the momentum transfer cospectrum does not change significantly as the stability changes from unstable ($z/L \approx -0.5$) to near neutral (see Fig. 9). However the peak frequency of the logarithmic cospectrum, $n\phi(n) = f\phi(f)$, shifts from near $f = 0.06$ for z/L -0.5 to near $f = 0.2$ for $z/l \approx 0.0$. The curves for the other stability groups were intermediate to those shown. At low f or large scales the cospectral dependency of f is approximately $f^{0.5}$, being slightly steeper in the near neutral case compared to the most unstable case. The fall-off at high f is greater than $f^{-2/3}$ but appears to be less than the $f^{-5/3}$ suggested by Panofsky and Mares (1968). Because of instrumental response effects it is not possible to define this

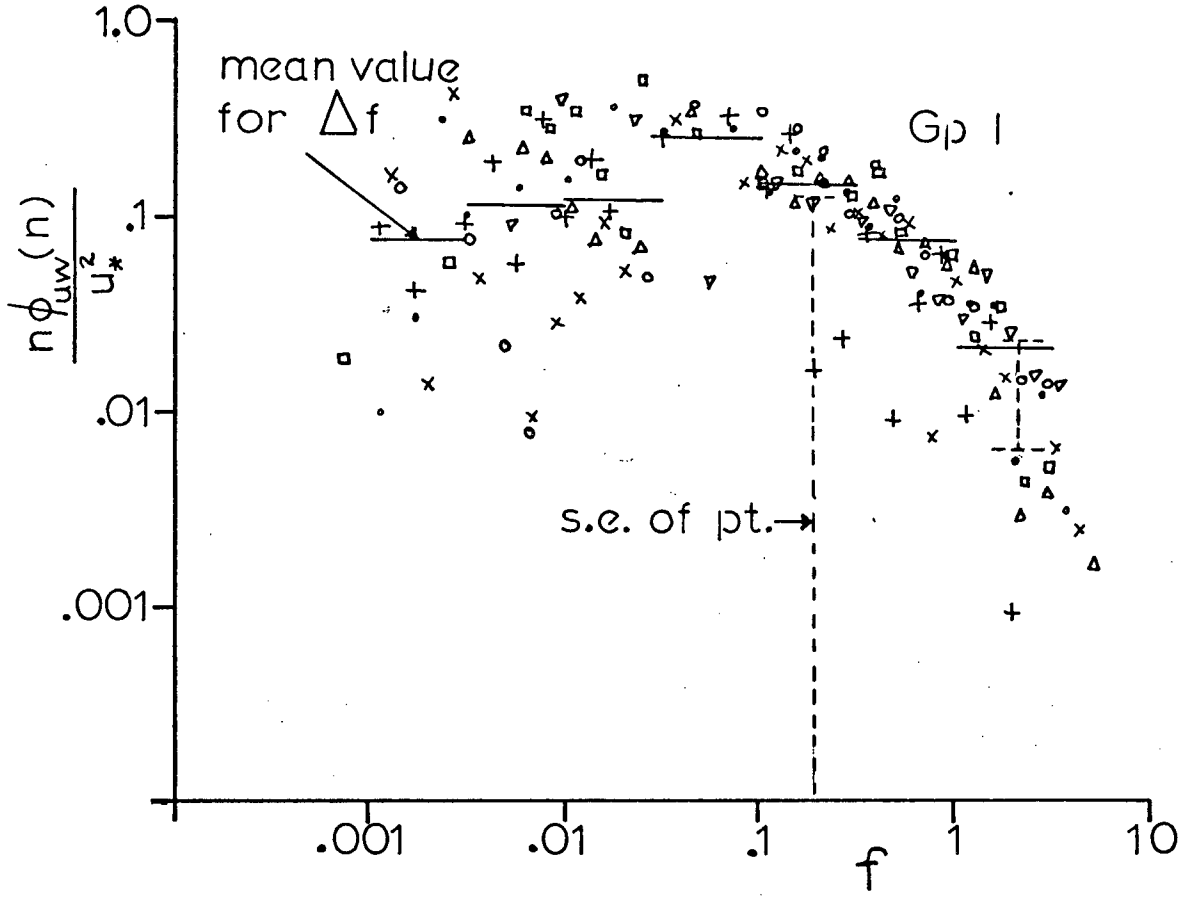

Figure 8. Composite momentum transfer cospectrum for Gp. I.

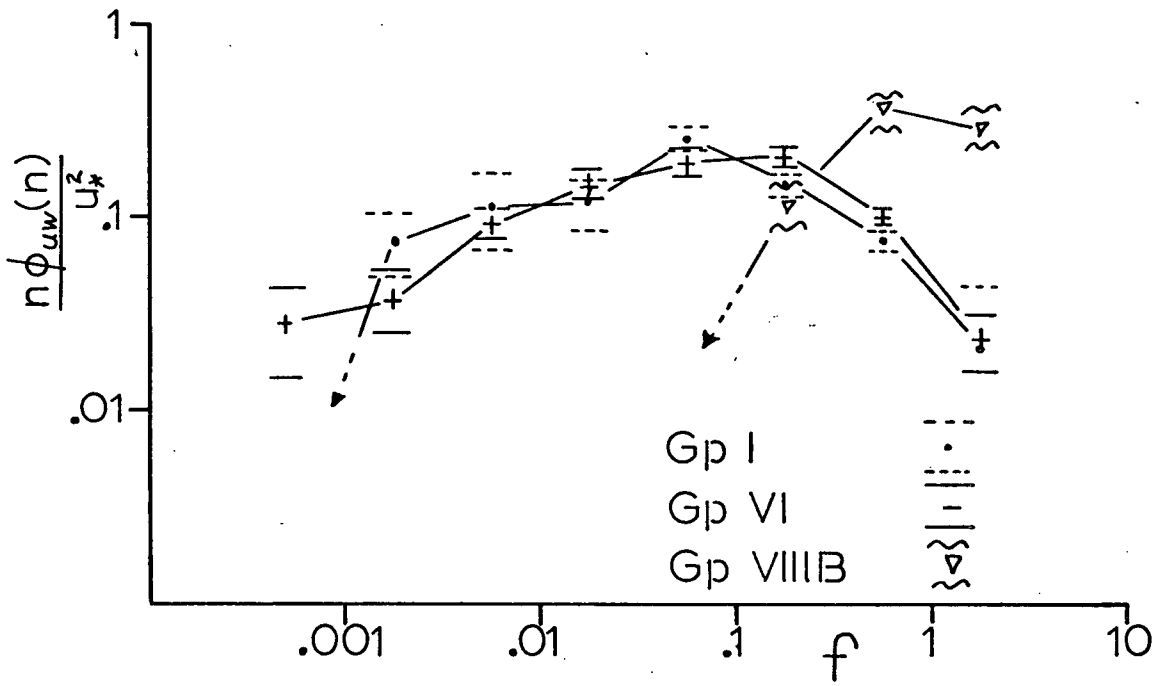

Figure 9. Variation of momentum transfer cospectrum with stability.

fall-off slope very accurately.

The cospectra for stable stratifications are considerably different from those for neutral to unstable stratifications (Fig. 9). The cospectral shape is much narrower and is shifted in peak frequency to near f = 0.8 for z/L about 4. At low f (below f = 0.1) the cospectra were generally positive indicating upward momentum transfer. This feature of the cospectrum changing sign was also evident in the heat flux cospectrum and will be discussed after considering that cospectrum.

4.2.2 Heat Transfer Cospectra

The heat flux cospectra (Fig. 10) generally showed much less variation within runs and less scatter in their composite graphs for stability groups than did either momentum or moisture transfer. The mean curves for Gps. I, VI and VIIIB are represented in Fig. 11. The characteristics of the normalized heat flux cospectrum appear to be similar to those for the normalized momentum flux cospectrum for f less than 0.3. For higher f, the heat flux cospectra fall off less rapidly than the stress cospectra. However this difference may be due to the instrument response not responding correctly to u fluctuations. The fall-off is only slightly faster than $f^{-2/3}$.

For stable stratifications the heat flux cospectrum behaves similarily to that of momentum transfer. There is a marked shift to higher f with the peak near f = 1.0 for z/L near 4. For these stable stratifications the normalization of frequency by z is probably not correct; L is a more meaningful length. It was found that the stable groups, VII, VIIIA, and VIIIB, all had regions at small f (large scales) for which the transfers of heat and momentum were upward; since $\partial \bar{u}/\partial z$ was always positive and $\partial \bar{T}/\partial z$ likely positive this indicated momentum and heat transfer against their gradients

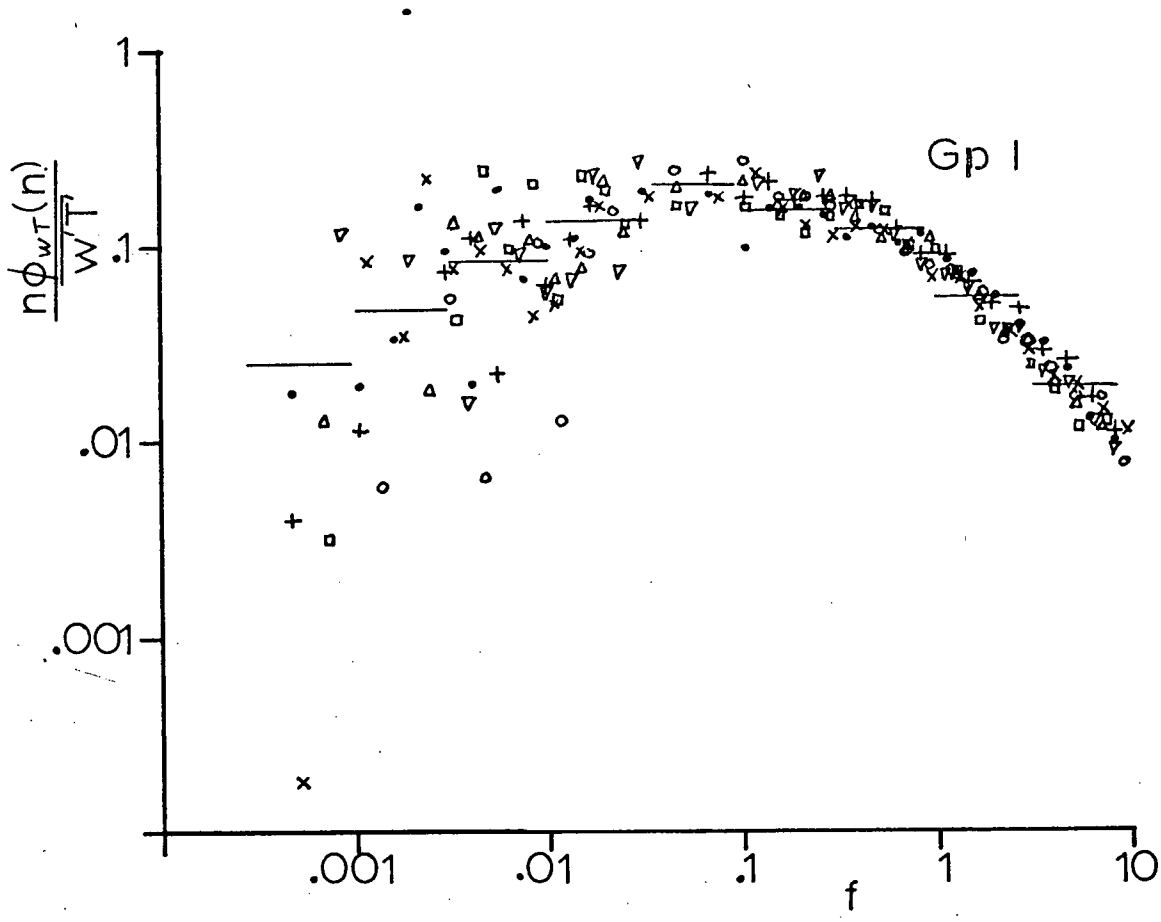

Figure 10. Composite heat flux cospectrum for Gp. I.

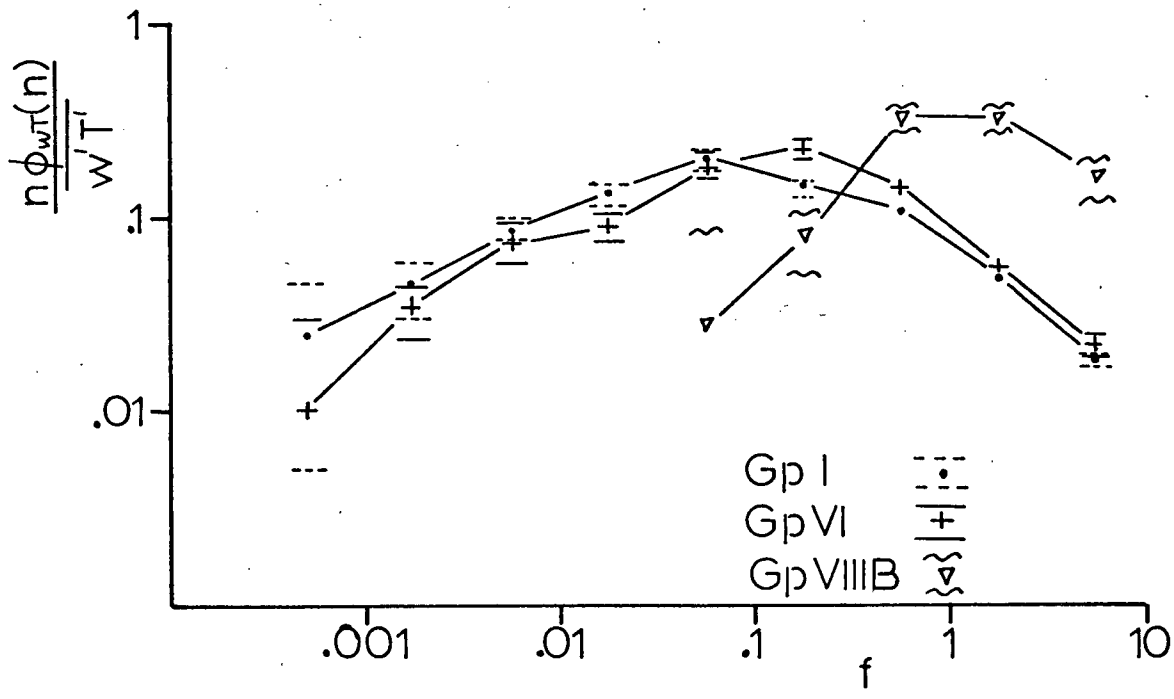

Figure 11. Variation of heat transfer cospectrum with stability.

at these scales. In most cases a changeover frequency, f_c, could be determined such that for $f < f_c$ the transfer was mainly upward or variable with f and for $f > f_c$ the transfer was consistently downward and the cospectra had a consistent shape with less scatter. The value of f_c was found to decrease with z/L. As was suggested by Stewart (1969), in stable stratifications atmospheric inertial wave motions will frequently be mixed with turbulence. One way of identifying the presence of wave motions is by examining the w-T coherence-phase relationships. When the w-T coherence is high the phase angle will be either near zero or near 180° for turbulence at these scales but will be near $\pm$ 90° for wave motions. Fig. 12 shows the coherence and phase angles as a function of f for three stable runs. Note that the coherence is mainly high but quite variable for $f < f_c$, small for $f \approx f_c$ and mainly between 0.2 and 0.4 for $f > f_c$. The phase angles scattered for $f < f_c$ but are usually between 50° and -90° whereas for $f > f_c$ the phase angles are consistently between $\pm$ 150°. This indicates that for $f > f_c$ the fluctuations of w and T are due to turbulence. For $f < f_c$ it seems that there is a mixture of turbulence and wave motions. For the purposes of this study it was decided to restrict attention to that region dominated by turbulence. The fluxes were defined as the integrals between $f_L = f_c$ and $f_H \approx 20$. However, the sonic anemometer response is valid only to about f = 2 or 3.

A small tilt of the sonic anemometer could introduce an apparent positive u-w correlation. The maximum likely tilt was about one degree. It was found, however, by rotating the coordinates both ways by one degree that tilt could not account for the positive u-w correlation and the results were thus considered valid.

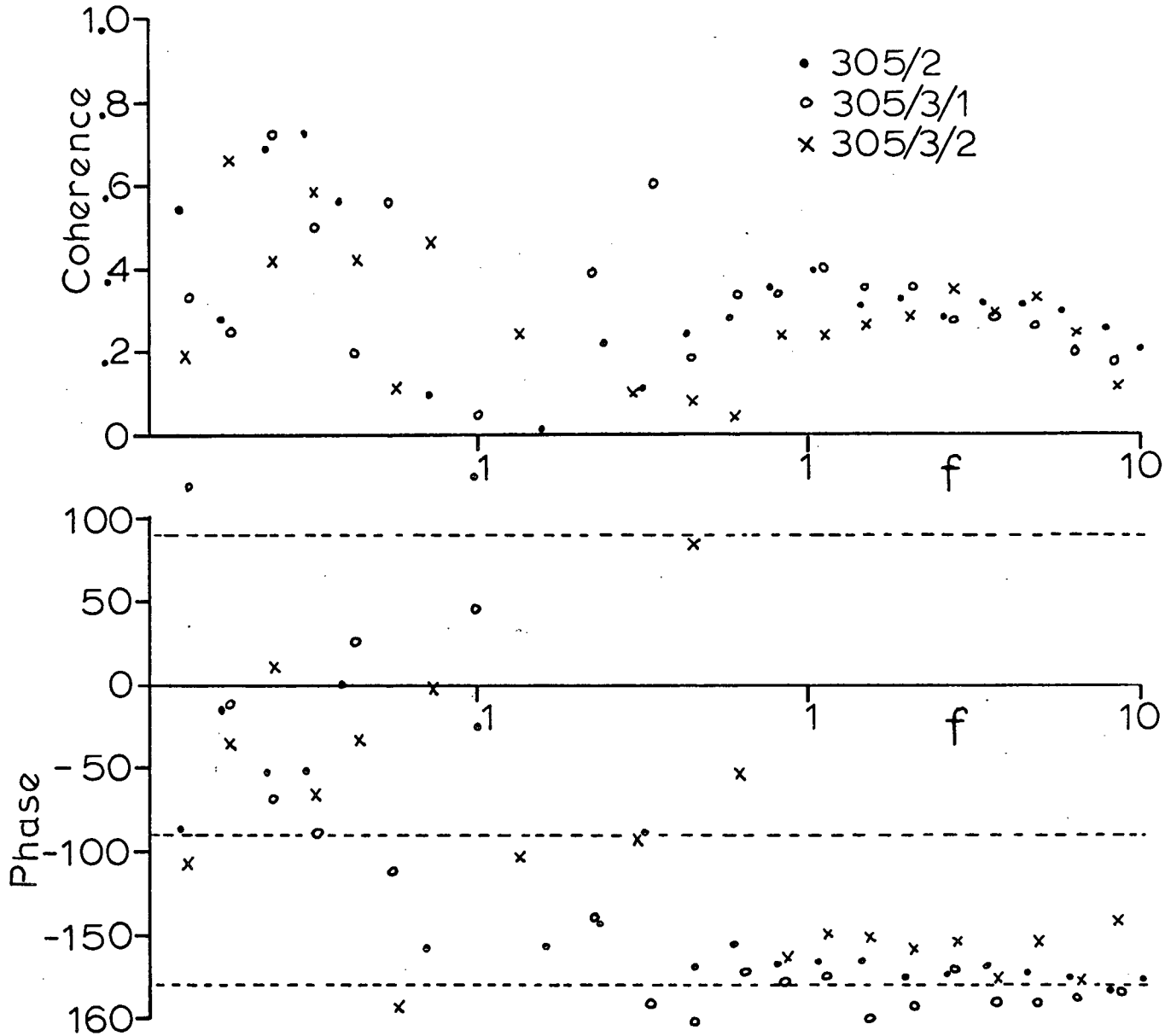

Figure 12. Coherence and phase angles for three stable runs.

4.2.3 Moisture Transfer Cospectra

The moisture transfer cospectra were computed only for the unstable through to neutral cases and for wind speeds greater than 2 m sec^{-1}. The moisture transfer composite cospectrum for Gp.I is shown in Fig. 13 and the mean curves for Gps. I and VI compared in Fig. 14. Note that the scatter of the moisture composite cospectrum is less than that for momentum transfer but appreciably more than that for heat transfer. The moisture transfer cospectra have shapes very similar to those for momentum transfer throughout the range of f measured. The method of correcting these cospectra for the phase lag due to the humidiometer intake pipe is described in Appendix II. Despite uncertainties in this technique the difference in cospectral shape at high frequencies between the moisture transfer cospectra and the heat transfer cospectra appears to be real.

4.3 Spectral Correlation Coefficients.

The normalized cospectra indicate which scales are important in contributing to the transfers but the correlation coefficient as a function of frequency is more useful in investigating how these transfers are taking place.

4.3.1 Momentum Transfer Spectral Correlation Coefficients.

In Fig. 15 are the spectral correlation coefficients for momentum transfer for Group I. Note that although at large scales the correlation coefficient is sometimes very large and negative and at other times large and positive these scales do not contribute much to the total transfer because the spectral densities of w, and hence of uw, at those frequency bands are very small. In addition these points at low frequencies are statistically very unreliable in that they each have only a few degrees of freedom. Only

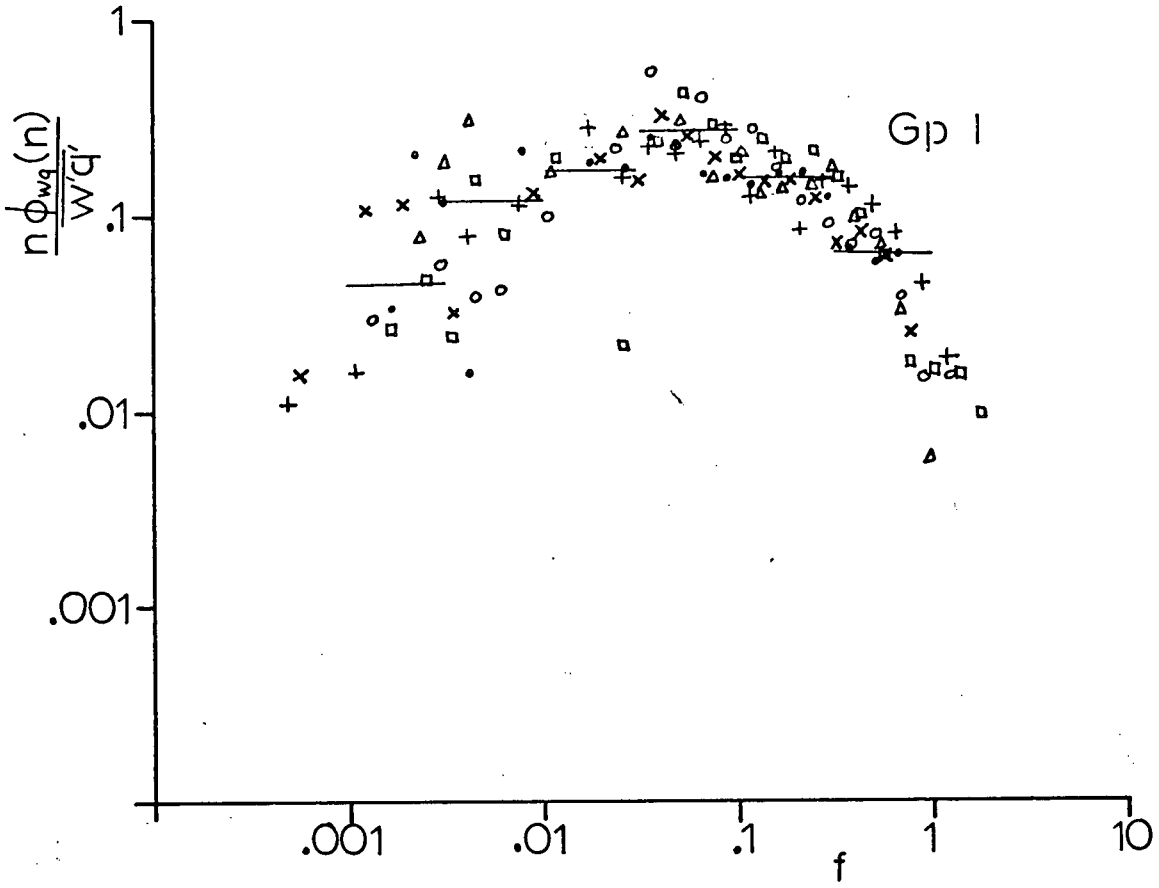

Figure 13. Composite moisture transfer cospectrum for Gp. I.

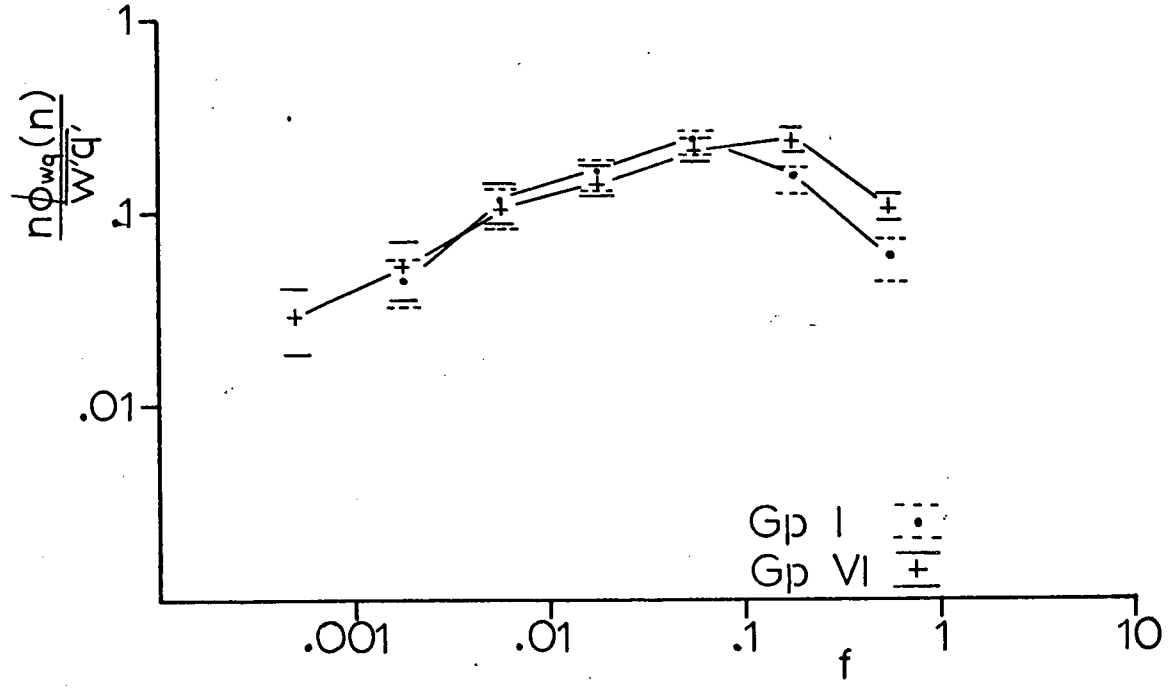

Figure 14. Variation of moisture transfer cospectrum with stability.

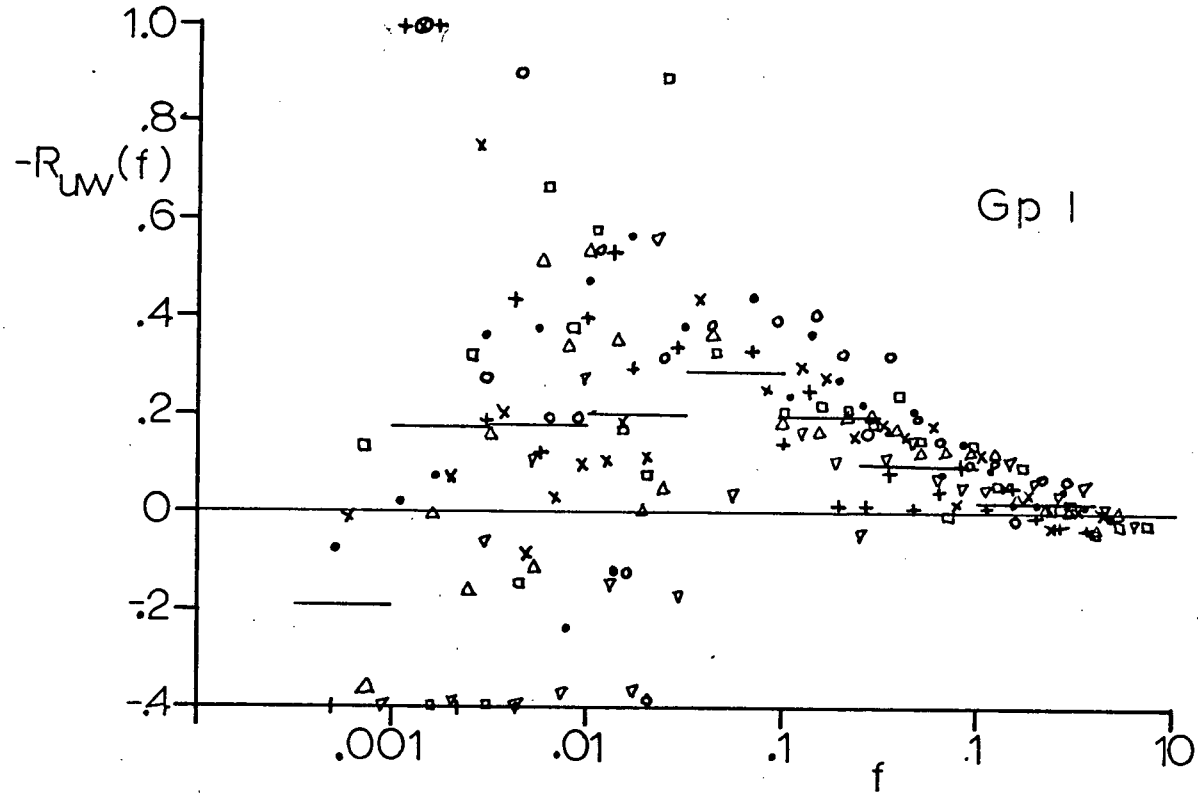

Figure 15. Spectral correlation coefficients for momentum transfer for Gp. I.

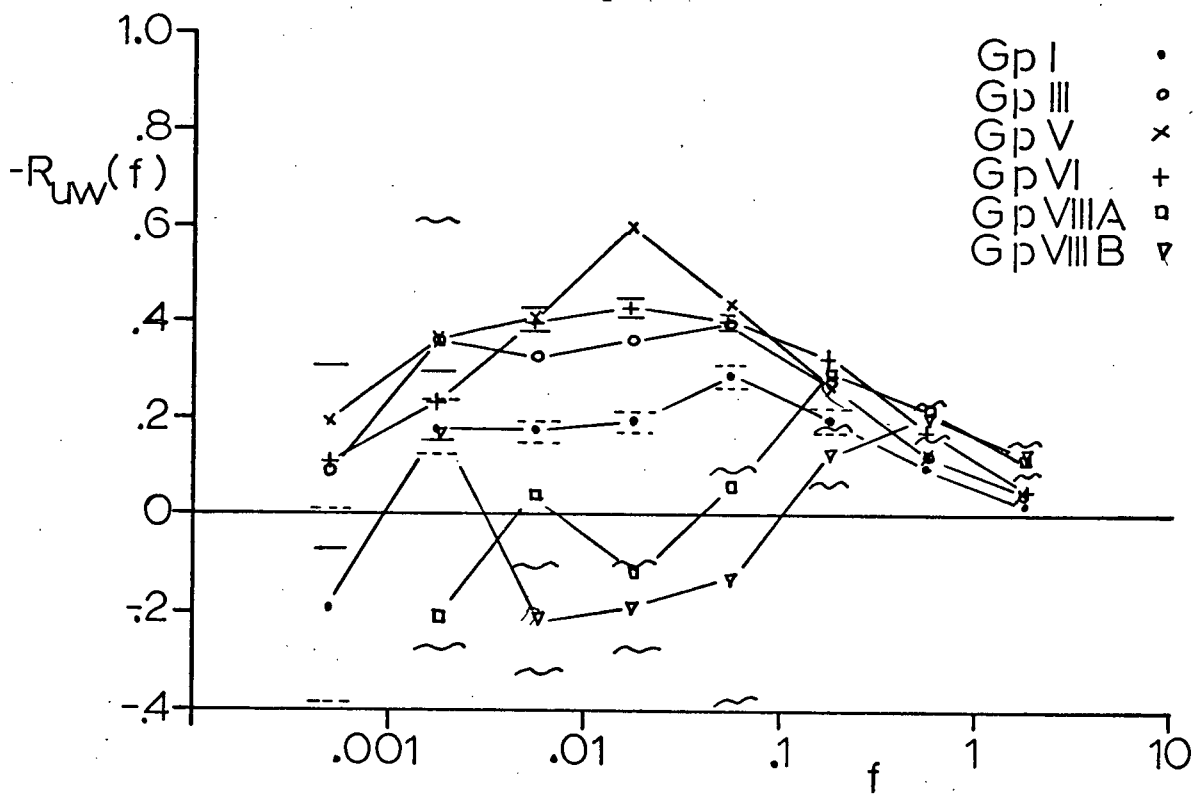

Figure 16. Variation of momentum transfer spectral correlation coefficients with stability.

when averaged over several data runs do these points have any significant meaning.

For this most unstable group (Fig. 15) there was frequently evidence of upward momentum transfer by eddies of size 200 metres or larger. These estimates are statistically unreliable but may be associated with organized meso-scale circulations and will require further investigations involving the whole planetary boundary layer.

The mean spectral correlation coefficients for Gps. I, III, V, VI, VIIIA and VIIIB are given in Fig. 16. The error limits, indicated for Gps. I, VI, and VIIIB are indicative of those for the other stability groups. $R_{uw}(f)$ for near neutral stratification, Gp. VI, is a smooth curve increasing with f to a peak near f = 0.02 and then decreasing with f. The rate at which $R_{uw}(f)$ decreases with increasing f beyond f about 1.0 may be due to the instrument's u velocity measurement being contaminated by v component. Since the v-w correlation is near zero any v contamination will reduce the apparent u-w correlation. As the stratification becomes more unstable $R_{uw}(f)$ generally decreases, although not consistently for Gps. III and V, until for Gp. I $R_{uw}(f)$ is for all scales significantly less than $R_{uw}(f)$ for Gp. VI. Note that the largest relative reduction in $R_{uw}(f)$ between Gp. VI and Gp. I is for f less than about 0.02 or for scales of about 100 metres or larger. The peak of $R_{uw}(f)$ for Gp. I is near f = 0.06 which is higher than for Gp. VI. This shift (based actually only on one point) of the peak to higher f for increasing instability is in the opposite direction to the shift in the peak of the cospectrum.

For stable stratifications $R_{uw}(f)$ follows the behaviour of the cospectrum and shifts to higher frequencies. For f less than 0.1, $R_{uw}(f)$ for Gp. VIIIB was usually positive and the scatter was much larger.

4.3.2 Heat Transfer Spectral Correlation Coefficients.

The spectral correlation coefficients for heat transfer have less scatter than those for momentum transfer, especially in the unstable case (Fig. 17). The change of $R_{wT}(f)$ with stability (as shown in Fig. 18) is more consistent than for momentum transfer, especially for f greater than 0.06. Note that the standard errors of the means for f greater than 0.1 were too small to plot (except in stable cases). For the near neutral group, Gp. VI, excluding the runs with $|z/L| < 0.01$, $R_{wT}(f)$ increases with increasing f to a peak near $f = 0.02$, the same place as $R_{uw}(f)$ for Gp. VI, and then decreases with increasing f. As the stratification becomes more unstable $R_{wT}(f)$ increases at all f. The largest relative increases are a low f or large scales so that for Gps. I and III $R_{wT}(f)$ is approximately constant with f for f less than about 0.06. At higher f the fall-off has a similar slope to that for Gp. I. For the stable cases $R_{wT}(f)$ shifts to higher f in the same manner as did $R_{uw}(f)$. Note that for all stability groups $R_{wT}(f)$ has a significant value to values of f near 10.

4.3.3 Moisture Transfer Spectral Correlation Coefficients.

For Gp. I (Fig. 19) spectral correlation coefficient for moisture transfer, $R_{wq}(f)$, is similar to that for heat transfer but it decreases more rapidly at smaller scales with decreasing f. Fig. 20 compares the values of $R_{wq}(f)$ for the four unstable to near neutral stability groups. Generally there is a decrease in $R_{wq}(f)$ with decreasing instability but there is a lot of scatter to the diagram. The composite plot for Gp. V, in particular, had a considerable amount of scatter.

The variation of $R_{wq}(f)$ needs further amplification. Four specific cases (see Table II) grouped into two pairs will be described in more detail.

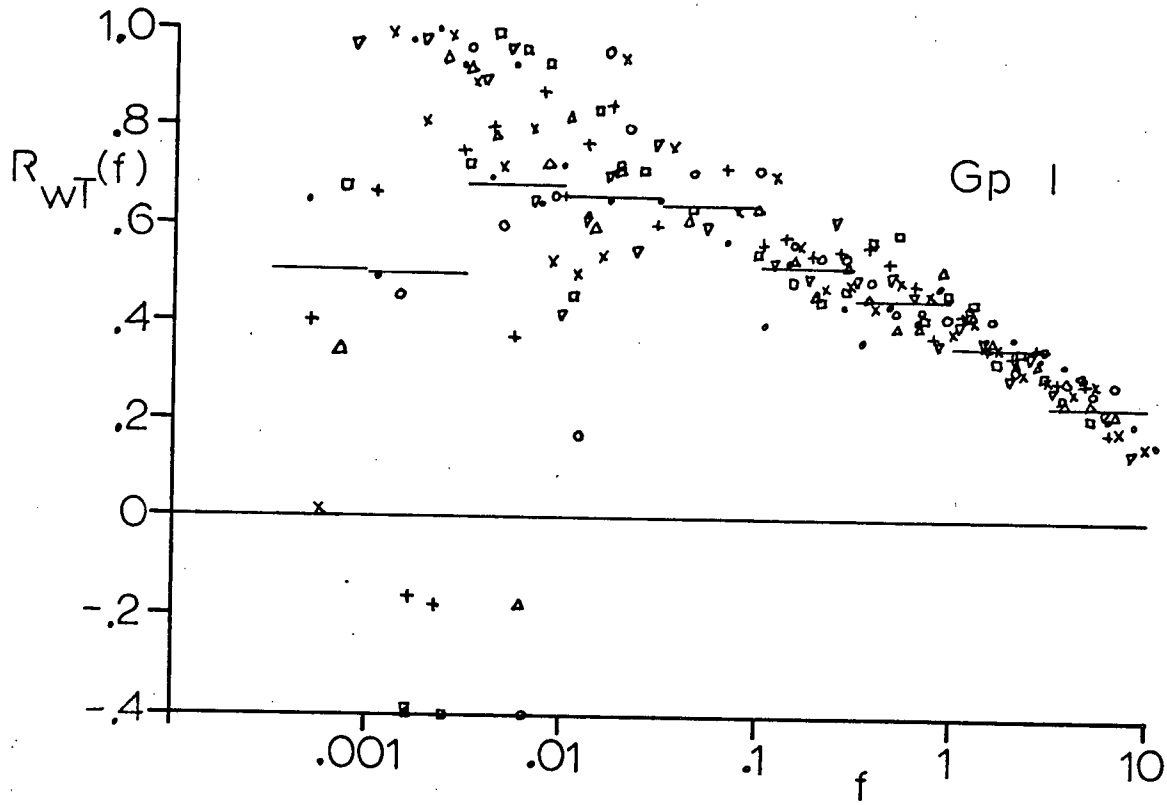

Figure 17. Spectral correlation coefficients for heat transfer for Gp. I.

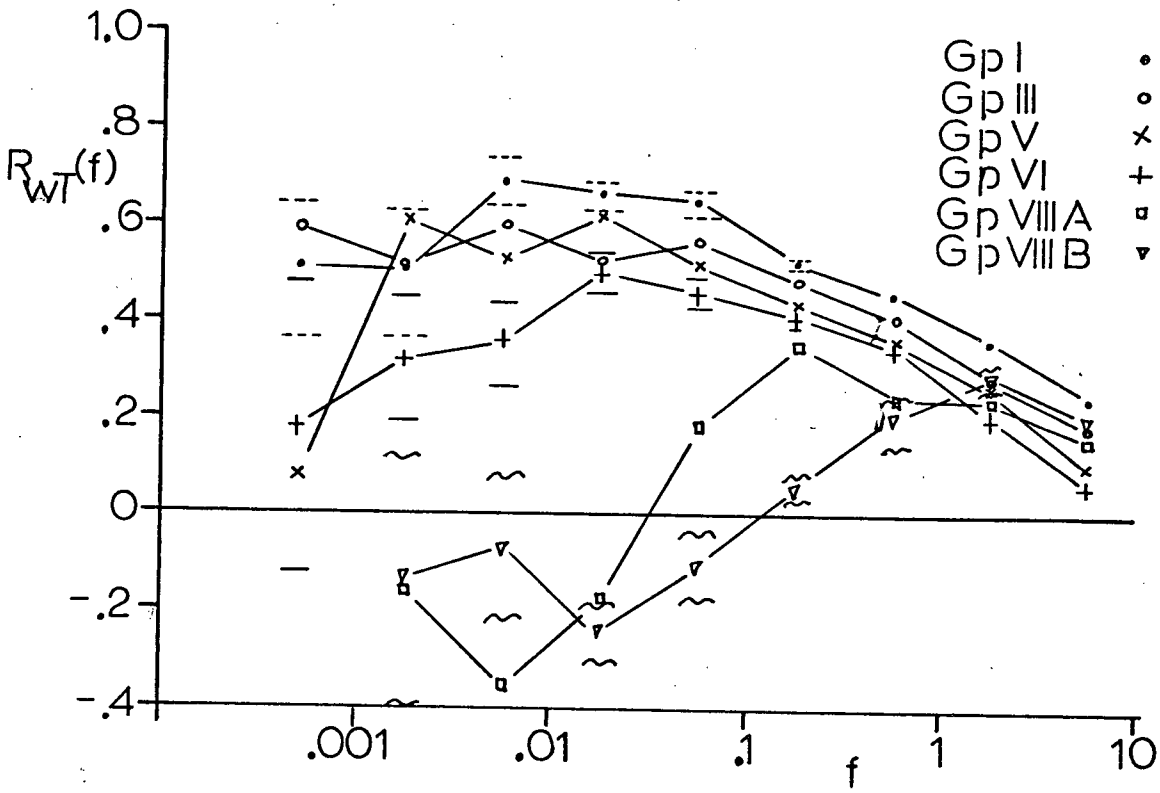

Figure 18. Variation of heat transfer spectral correlation coefficients with stability.

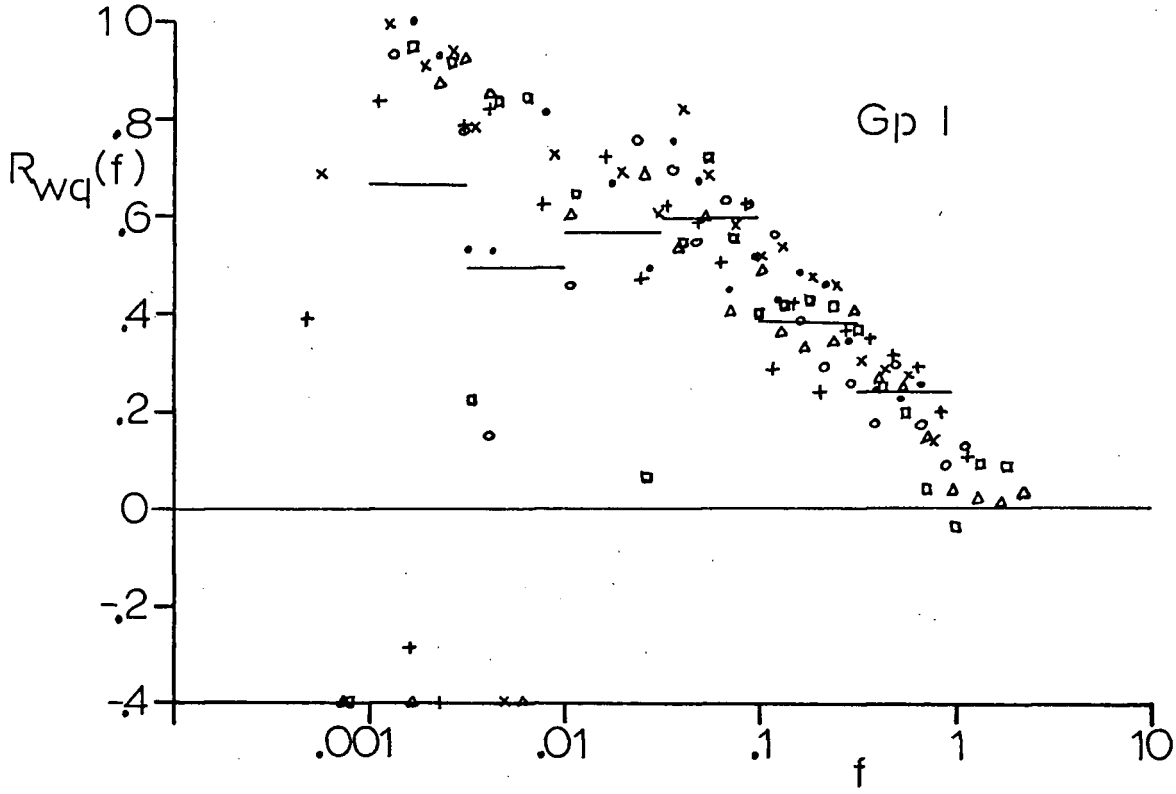

Figure 19. Spectral correlation coefficients for moisture transfer for Gp. I.

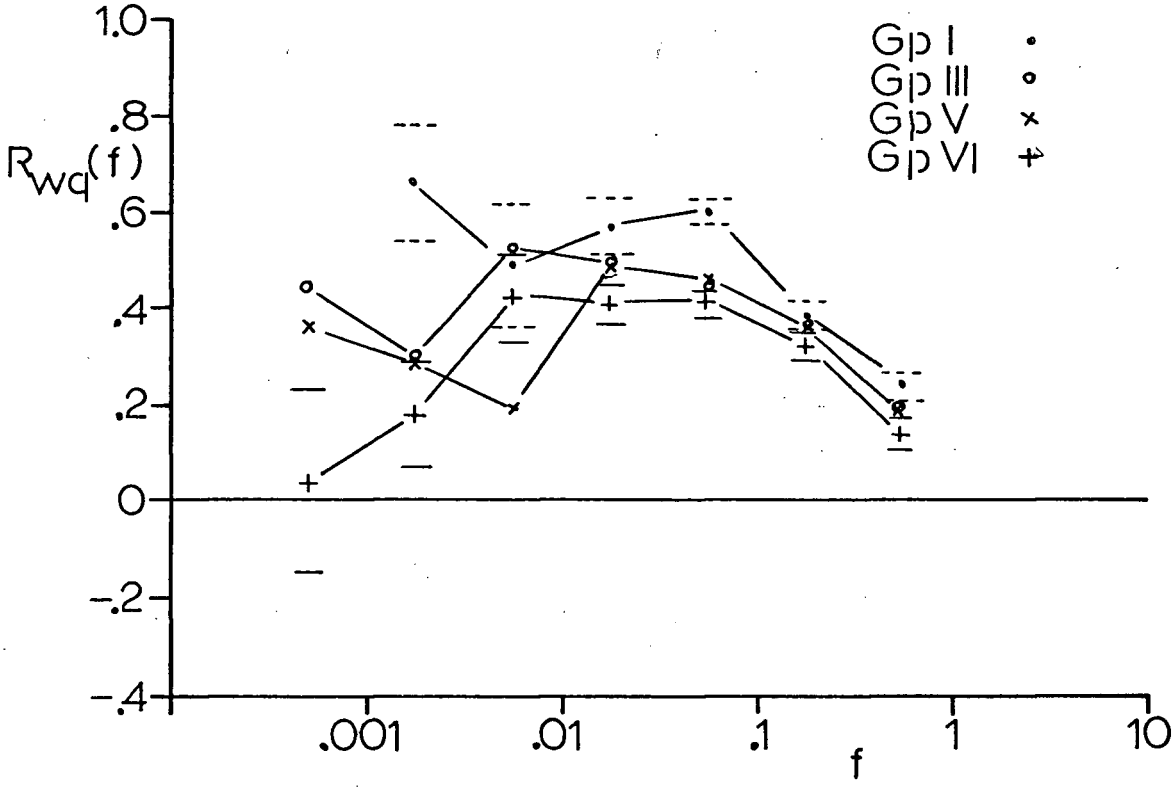

Figure 20. Variation of moisture transfer spectral correlation coefficients with stability.

Table II. Comparison of Correlation Coefficients for Two Pairs of Data.

	Pair A		Pair B	
	L221/2	L222/2	L224/4	L311/2/1
z/L	-0.29	-0.28	-0.15	-0.14
$\bar{u}$(cm s^{-1})	307	297	487	538
r_{uw}	-0.34	-0.30	-0.30	-0.23
r_{wT}	0.52	0.50	0.47	0.43
r_{wq}	0.49	0.25	0.49	0.16

Note that in each pair of runs the only statistic in the table which differs significantly is that of r_{wq}, the integrated correlation coefficient, which is high and approximately equal to r_{wT} in one run of each pair and small and much less than r_{uw} for the other run in the pair. The spectral correlation coefficients $R_{Tq}(f)$ and $R_{wq}(f)$ are plotted for each pair of runs in Figs. 21 and 22. The T-q correlation for L221/2 is more than twice as high as that for L222/2 for f greater than 0.05. The w-q correlation for L221/2 is higher than that for L222/2 for all scales, except in a short range near f = 0.1. For pair B, similar differences are noted although the differences between T-q correlations are not as large. These results demonstrate the dependence of the transfer efficiency for moisture transport on the correlation between q, which is an essentially passive scalar being transported, and T, the active scalar that causes the convective motions and is highly correlated with the vertical velocity fluctuations.

These differences in the T-q correlation must be explained in terms of inhomogeneities on all scales. The large scale inhomogeneities of the site (the land-sea contrasts) can not explain the differences. For example L221/2 with a high T-q correlation and L311/2/1 with a low T-q correlation had the same wind direction (southerly off Boundary Bay) while L222/2 and L224/4 had mainly over-land trajectories. The small scale inhomogeneities must be associated with differences in the surface boundary conditions. August 21st, the day on which L221/2 and L222/2 were made, was a warm, sunny day that followed a few days of light showers. If the evaporation rate varied across the grass surface either due to differences in vegetation or differences in moisture supply then small scale inhomogeneities in both surface temperature and surface moisture would develop during the day. These differences would tend to be anticorrelated due to cooling caused by evaporation. August 22nd, on

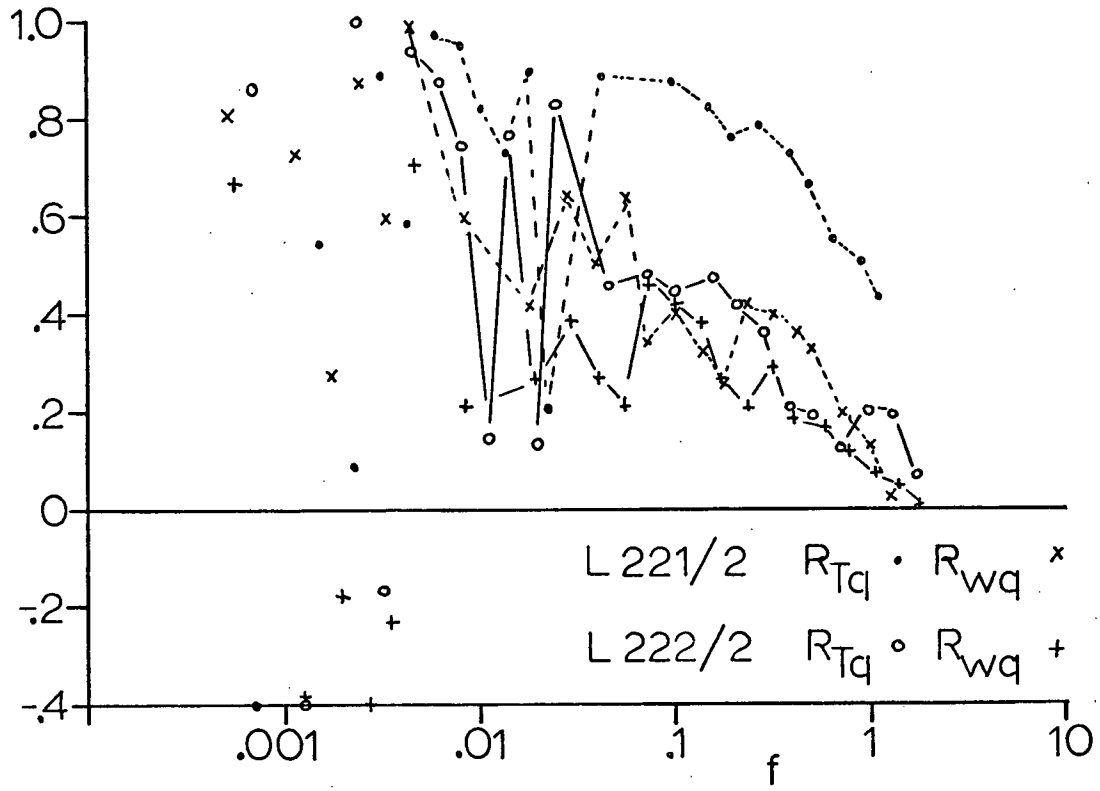

Figure 21. Spectral correlation coefficients for runs L221/2 and L222/2.

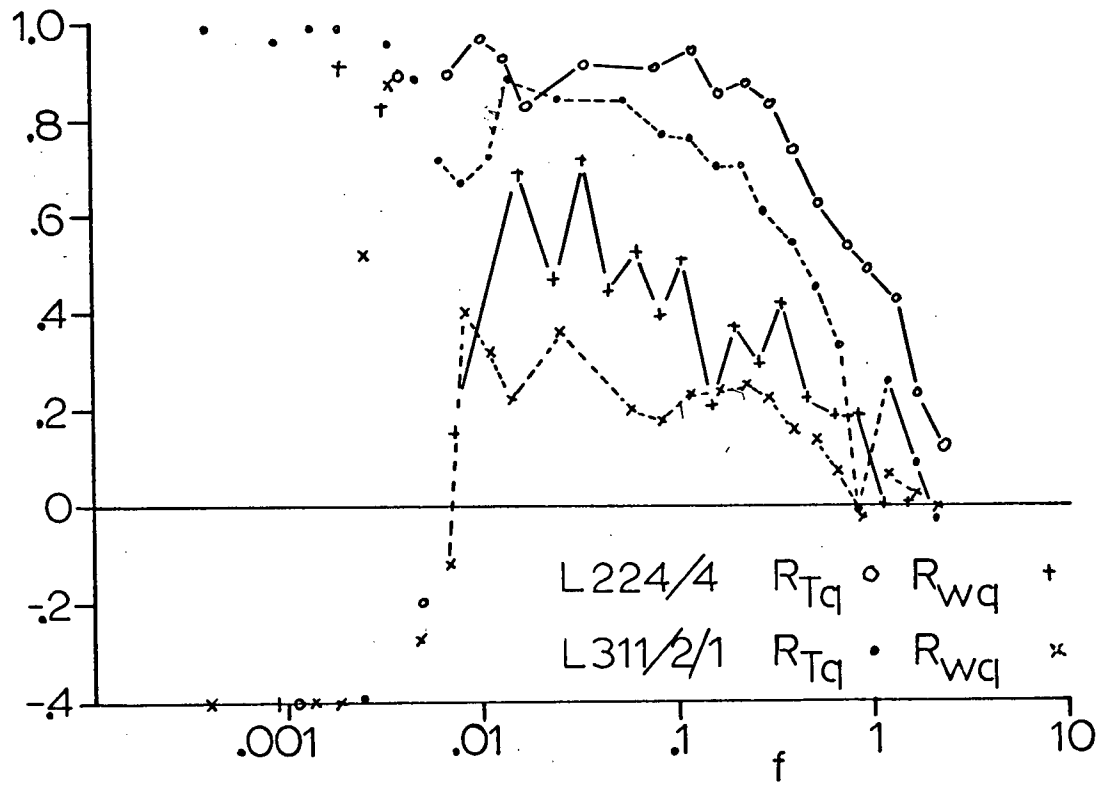

Figure 22. Spectral correlation coefficients for runs L224/4 and L311/2/1.

which L22/4 was run, was sunny and windy while August 24th on which L311/2/1 was run was cloudy, cooler and windy. Here one might expect the T-q correlation associated with the meso-scale circulations to also effect the transfers. The mean $R_{wq}(f)$ over all groups for unstable stratifications is indicated in Fig. 23.

4.3.4 Comparison of the Spectral Correlation Coefficients.

The ratios of the spectral correlation coefficients at different scales is a measure of the relative transfer efficiencies at each scale for the different fluxes. The ratios $R_{wT}(f)/R_{uw}(f)$ are shown in Fig. 24. The ratio of near neutral stratification is indicated with a double line. Recall that $R_{uw}(f)$ and $R_{wT}(f)$ for near neutral correlations both had a peak near $f = 0.02$ and the same fall-off with f. However, at the peak $R_{wT}(f)$ was about 0.50 while $R_{uw}(f)$ was about 0.43. Hence the ratio $R_{wT}/R_{uw}(f) \approx 1.2$ for f greater than 0.02. By f higher than 0.6, $R_{uw}(f)$ is decreasing slightly more rapidly and is near zero while $R_{wT}(f)$ is still relatively large. Hence the ratio $R_{wT}(f)/R_{uw}(f)$ increases rapidly and is not well defined. It is important to note that $R_{wT}(f)/R_{uw}(f)$ is significantly greater than 1.0 for scales smaller than 100z and that its average is about 1.4. For this near neutral case (the z/L values of the component runs are -0.03, -0.03, -0.02, 0.04 and 0.08) the effects of buoyancy are still important. In order to investigate the effects of buoyancy in more nearly neutral stratifications will require very accurate measuring equipment. Consideration of the ratio $R_{wT}(f)/R_{uw}(f)$ for exactly neutral cases is not worthwhile because no heat transfer takes place and occurrances of those conditions will be very rare.

As the stratification becomes more unstable the ratio $R_{wT}(f)/R_{uw}(f)$ generally increases. For the most unstable group, Gp.I, the ratio averages near three and is significantly higher than the value of the ratio for any

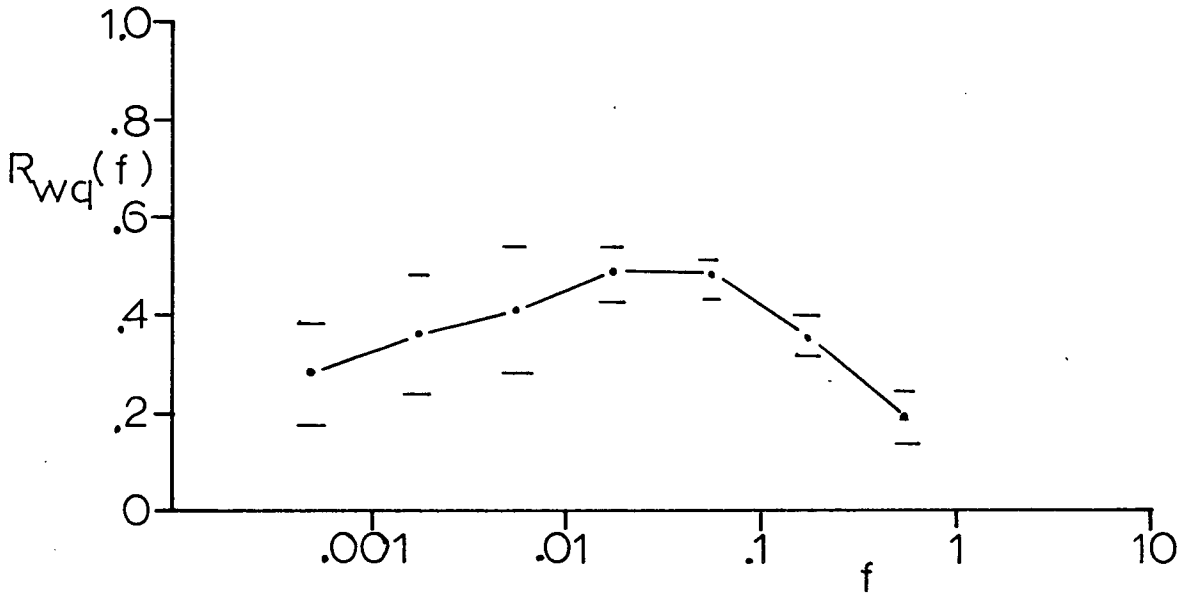

Figure 23. Spectral correlation coefficients for moisture transfer averaged over stability Groups I to VI.

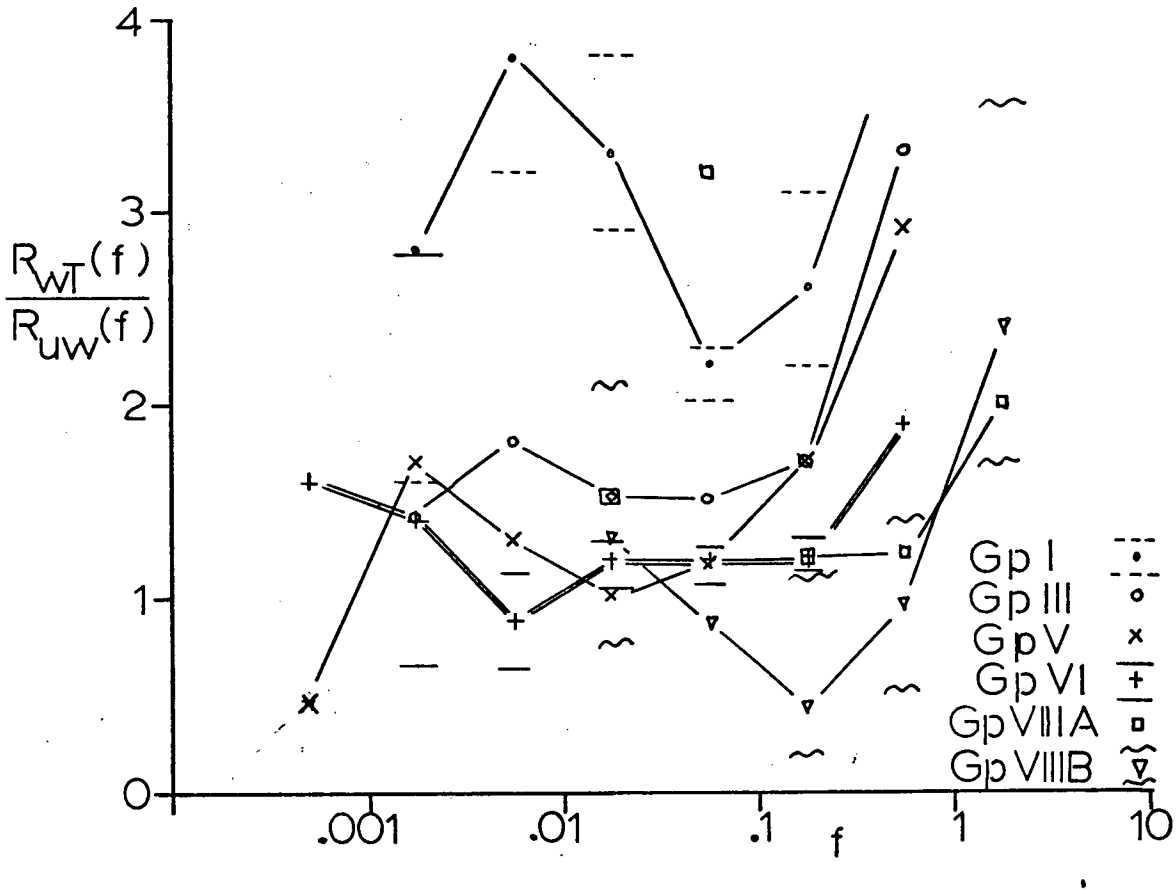

Figure 24. The ratios of the spectral correlation coefficients for heat transfer to those of momentum transfer.

other stability groups. These marked increases in the ratio $R_{wT}(f)/R_{uw}(f)$ for decreasing stability are due to the fact that $R_{wT}(f)$ increases and $R_{uw}(f)$ decreases so that both act to increase the ratio. The increase is larger at both large scales (f less than 0.01) and at small scales (f greater than 0.2) than at the intermediate scales. The increases at small scales are somewhat less reliable because $R_{uw}(f)$ is small and effected by instrument response and the ratio is poorly defined. The increases at larger scales may be attributed to the effects of buoyancy acting most efficiently at these larger scales. For a strongly convecting regime a high w-T correlation would be expected for the scales appropriate to those of the buoyant plumes. However the reasons for the reduced $R_{uw}(f)$ for convecting regimes are not so obvious. Recall that although the peak of the momentum transfer cospectrum shifted to lower f (larger scales) for increasing instability, the peak of $R_{uw}(f)$ shifted to higher f (smaller scales) and that the largest relative reduction in $R_{uw}(f)$ was for large scales. In a buoyant situation the large updrafts would originate near the surface and hence carry air with a small horizontal velocity or relative to the mean wind at the observing level these large positive w fluctuations would carry large negative u fluctuations and hence a large amount of momentum would be transported during the updraft. For a constant flux layer the amount of momentum transfer will be determined near the surface where buoyant forces are not important. Since only a certain amount of mcmentum transfer is required the u-w correlation between updrafts would be relatively low. This implies that the momentum transfer should take place in bursts and would be quite variable during the duration of a data run. These points are in agreement with observations on the data made earlier in this chapter. Thus during a sufficiently long time in a freely convecting regime the same amount of momentum can be transported vertically at specific scales

while the correlation coefficient will be lower than in neutral conditions.

For the stable case $R_{wT}(f)/R_{uw}(f)$ is not significantly different than unity for $f<1.0$ but appears to be higher for $f>1.0$. Thus in the small scale region in which mechanical turbulence is believed to dominate the transfer mechanism, the efficiency of heat transfer is greater than that of momentum transfer. It has generally been believed that the opposite should be true (Lumley and Panofsky, 1964,p.106). Further investigations under a variety of conditions are needed to confirm this.

4.4 Correlation Coefficients

The correlation coefficients, as defined in Eq. 2.7, have been averaged over stability intervals as indicated in Table I. For each point on the graph the vertical line represents the standard error of the mean of the data averaged to obtain the point. The line is plotted for the average z/L value of the group. The horizontal line shows the stability range averaged over. Note that the z/L scale is linear from -0.7 to 0.1 and is logarithmic for higher values of z/L.

4.4.1 Momentum Transfer Correlation Coeffiecients

The correlation coefficient, r_{uw}, (Fig. 25a) is negative for all z/L and has a value near -0.3 for neutral conditions. For increasing z/L r_{uw} decreases approximately linearly. For unstable stratifications r_{uw} can be represented as $r_{uw} = -0.31(1 - 0.66|z/L|)$. This empirical relation and all others presented in this section are least squares best fits to the data. For stable stratifications r_{uw}, when forced to go to -0.31 at z/L = 0, was $r_{uw} = -0.31(1 - 0.16|z/L|)$. Thus the efficiency of momentum transfer decreases more rapidly for increasing instability than it does for increasing stability.

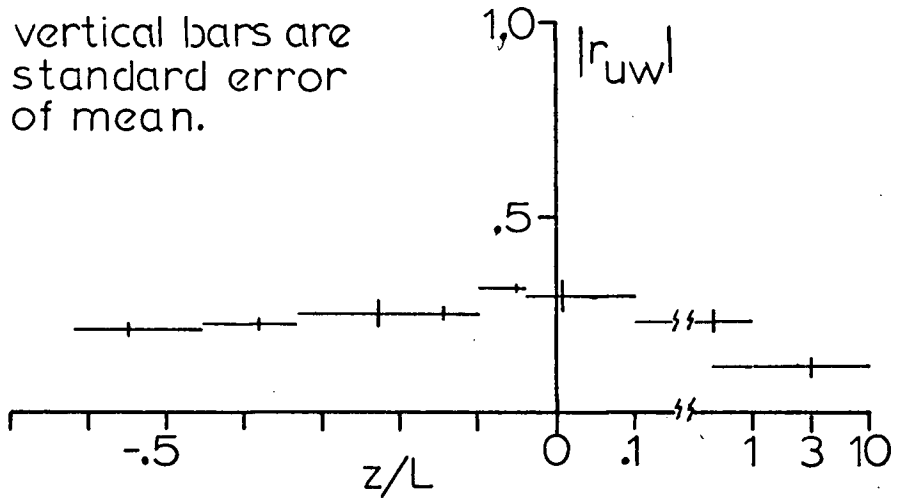

Figure 25a. Variation of the correlation coefficients for momentum transfer with stability.

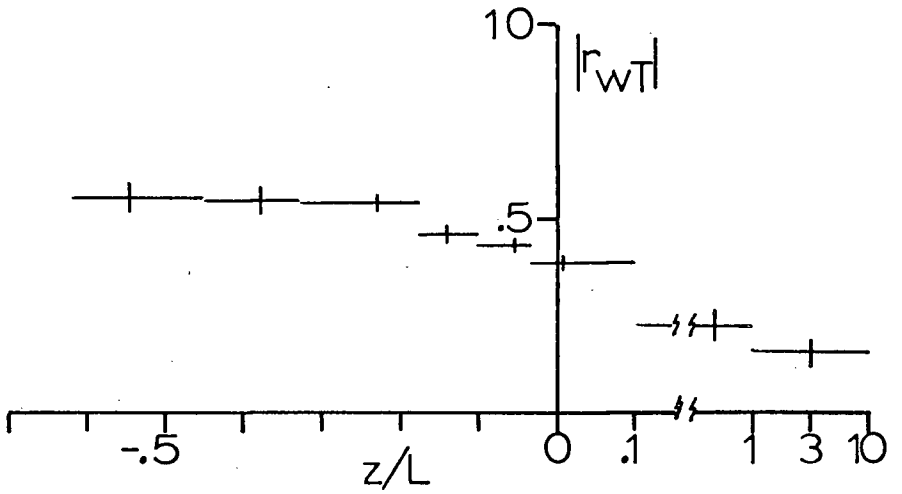

Figure 25b. Variation of the correlation coefficients for heat transfer with stability.

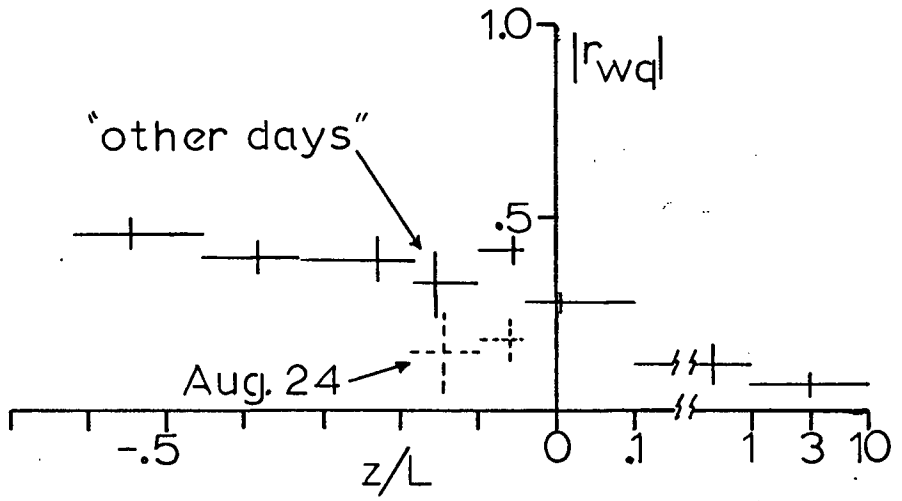

Figure 25c. Variation of the correlation coefficients for moisture transfer with stability.

Neither equation can be expected to apply for very large values of $|z/L|$; the limits being about 0.7 on the unstable side and about 5 on the stable side.

The results quoted here for unstable stratifications agree with those of Haugen et al (1970) but disagee with those of Mordukhovich and Tsvang (1966) who found r_{uw} increased in magnitude as z/L decreased from zero. This result may have been due to nstrumental limitations. If an instrument does not properly measure the high frequency part of the uw-cospectrum (see Fig. 9) then the error or reduction in $\overline{uw}$ would be greatest for near neutral conditions and would decrease as z/L decreased.

4.4.2 Heat Transfer Correlation Coefficients

The magnitude of the correlation coefficient for heat transfer, r_{wT}, as a function of z/L is shown in Fig. 25b. Since z/L is determined almost entirely by the heat flux, r_{wT} is naturally positive when z/L is negative and vice versa. The magnitude of r_{wT} appears to be a montonically decreasing function of z/L. The least squares best fit over all z/L gave $|r_{wT}| = 0.46 (1 - 0.19z/L)$. The three points of very nearly neutral stability ($|z/L|<0.01$) were excluded from the data used to fit the curve. Although r_{wT} is usually considered as being zero for z/L = 0, it must from the point of view of similarity theory be considered as undefined. This is because for neutral conditions meeting the criteria of horizontal homogeneity both $\overline{w'T'}$ and σ_T would be zero. Hence the empirical relation is valid for z/L near but not exactly zero at which point r_{wT} is undefined. The range of applicability of this empirical relation is about the same as that for r_{uw}.

These results are in fairly good agreement with those of Haugen et al (1970), Wesley et al (1970), and Mordukhovich and Tsvang (1966).

4.4.3 Moisture Transfer Correlation Coefficients

In section 4.3.3 the spectral correlation coefficient for moisture transfer was shown to depend on the T-q correlation. When averaged over stability qroups the correlation coefficient, r_{wq}, does show a variation with z/L similar to that for r_{wT} . These averaged values of r_{wq} are always less than those of r_{wT}. The scatter is also much larger. For stability groups IV and V the data could be divided into two groups; those on August 24th and those on the other days. These groups are plotted separately on Fig. 25c. The "other days" group did have some low values of r_{wq} (for example, 1222/2 discussed in section 4.3.3) but were generally higher than those of August 24th. The best fit to all the data was $|r_{wq}| = 0.33(1-0.23z/L)$. Note that the slope of this line is not significantly different from that for r_{wT}. The mean ratio of $|r_{wT}/r_{wq}|$ is thus about 1.4 without much dependence on stability. The data does indicate, though, that for less unstable stratifications the likelihood of r_{wq} values being different from the mean is higher than for more unstable cases.

4.4.4 Comparison of the Correlation Coefficients

The relative values of these correlation coefficients are of as much interest as their actual values. The ratios $|r_{wT}/r_{uw}|$ are plotted in Fig. 26. The variation of the ratio is quite consistent. The best linear fit is $|r_{wT}/r_{uw}| = 1.4(1+1.8|z/L|)$ for unstable conditions. For stable stratifications the ratio averages about 1.1 and the variation with z/L is small and insignificant. The fact that the ratio is significantly greater than unity for near neutral and averages greater than unity for stable conditions is in contradiction to the generally believed ideas that the mechanisms are similar for near neutral and stable stratifications (Lumley and Panosky, 1964).

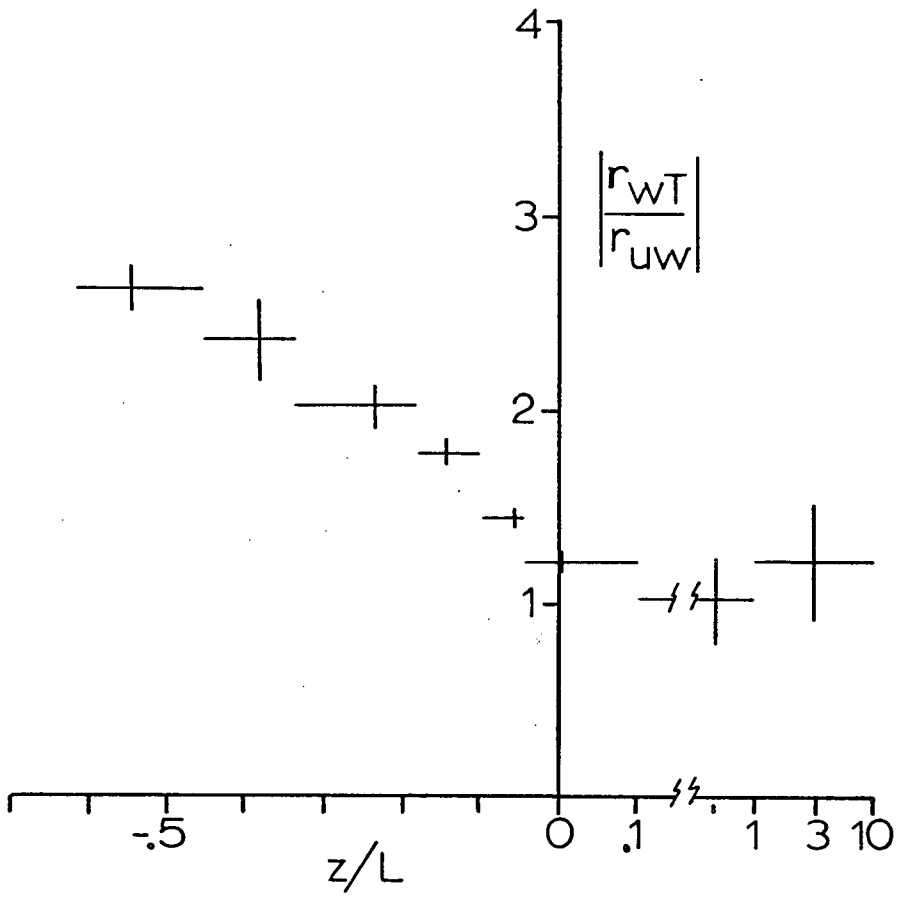

Figure 26. Variation of the ratio of the correaltion coefficients of heat transfer to those of momentum transfer with stability.

For unstable conditions the ratios increase at first rapidly and then less rapidly as z/L decreases from zero. This implies a power law type dependence on z/L. The best fit of the data on a log-log plot gave $|r_{wT}/r_{uw}| = 3\,|z/L|^{\frac{1}{4}}$. This fits the data better than a linear fit. For the most unstable stratifications the effects of buoyancy make the transfer efficiency for heat transfer about 2.7 times that for momentum transfer. As more buoyant energy is added it does not seem to increase the comparative efficiency by the same amount. This implies that there is probably an upper limit on the ratio $|r_{wT}/r_{uw}|$.

The variation of $|r_{wq}/r_{uw}|$ with stability is given in Fig. 27. The variation is effected by the T-q correlations variation and the scatter for Gps. IV and V is very large. As before, the data from August 24 in Gps. IV and V are separated from those recorded on other days. The data can be fit by $|r_{wq}/r_{uw}| = 0.86(1+2.2|z/L|)$ for z/L less than zero and $|r_{wq}/r_{uw}|$ approximately constant, 0.7, for z/L greater than zero. The behaviour is similar to that of $|r_{wT}/r_{uw}|$ but the values are much lower. Since it has been shown that r_{wq} depends on the T-q correlation and not directly on z/L it is not worthwhile pursuing the variation of r_{wq}/r_{uw} any further.

4.5 Consideration of K_H/K_M

The ratio of the turbulent diffusivity of heat transfer or of moisture transfer to that of momentum transfer has been widely debated in the literature (see, for example, Lumley and Panofsky, 1964). Since neither temperature nor humidity profiles were measured in this study no direct estimates of K_H or K_E are possible. However, as was pointed out in Chapter 2,

$$\frac{\Gamma_{wT}}{\Gamma_{uw}} = \frac{K_H}{K_M}\left[\frac{\sigma_u/\frac{\partial \bar{u}}{\partial z}}{\sigma_T/\frac{\partial T}{\partial z}}\right]$$

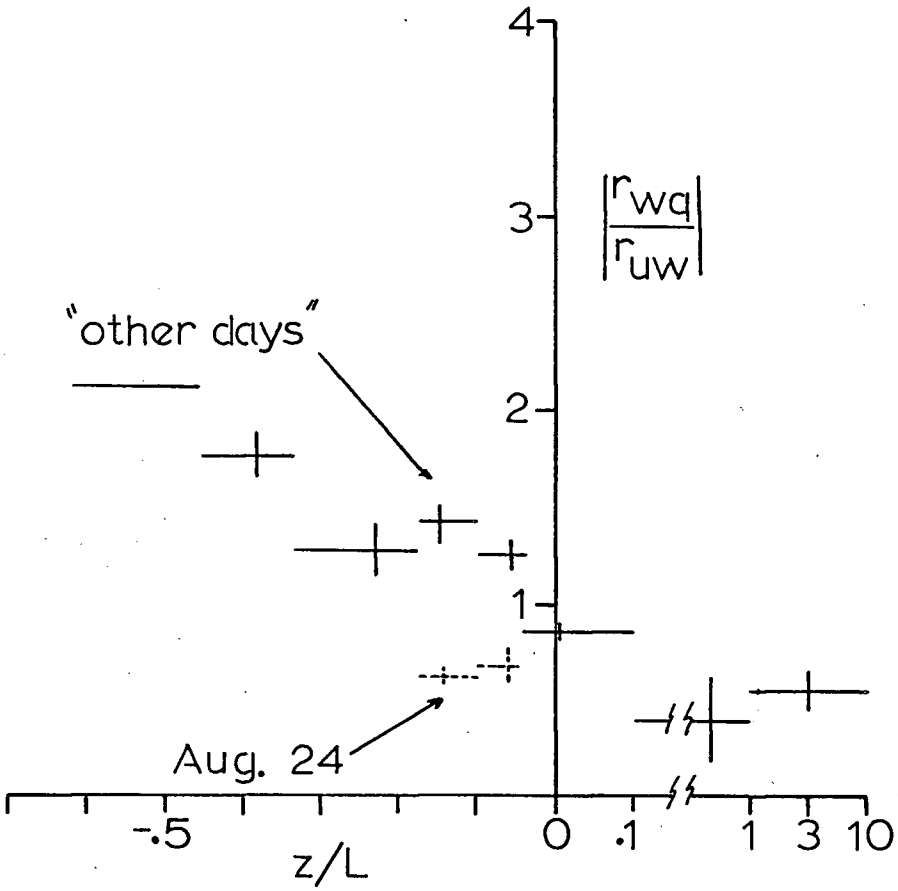

Figure 27. Variation of the ratio of the correlation coefficients of moisture transfer to those of momentum transfer with stability. On Aug. 24th the T-q correlation was generally lower than on the "other days".

Tsvang (1960) has shown that $\sigma_T/z\frac{\partial\bar{T}}{\partial z}$ is approximately unity for unstable stratifications. This could be expected if all the temperature fluctuations were created locally by the vertical velocity fluctuations acting on the temperature gradient. Similar arguments would apply to $\sigma_u/z\frac{\partial\bar{u}}{\partial z}$. In Fig. 28, $\sigma_u/z\frac{\partial\bar{u}}{\partial z}$ is plotted against z/L. The gradient $\frac{\partial\bar{u}}{\partial z}$ was computed from the best log-linear profile fit to the data. The results indicate that $\sigma_u/z\frac{\partial\bar{u}}{\partial z}$ is also approximately constant for unstable conditions and its value is not too far from unity (about 1.2). Hence it can be assumed that the ratio $\left(\sigma_u/z\frac{\partial\bar{u}}{\partial z}\right)\left(\sigma_T/z\frac{\partial\bar{T}}{\partial z}\right)^{-1}$ is approximately unity over the z/L rang 0 to -0.5 and that $r_{wT}/r_{uw} \simeq K_H/K_M$.

Two recent estimates of the ratio K_H/K_M have been made. One, due to Swinbank (1968), led to the empirical formula $K_H/K_M = 2.7|z/L|^{\frac{1}{4}}$. Unfortunately no direct measurements of stress were made and u_* was inferred from the wind profiles. Businger et al (1970) measured directly both the transfers and the profiles. Their measurements were analysed within the framework of the Businger-Dyer theory (see Paulson, 1967) and led to:

$$\frac{K_H}{K_M} = 1.35\ \frac{[1 - 9(z/L)]^{1/2}}{[1 - 15(z/L)]^{1/4}}$$

for unstable stratifications and K_H/K_M approximately constant (about 1.35) for the stable range of z/L. In Fig. 29 the results of Swinbank and of Businger are compared with the results shown here, assuming $r_{wT}/r_{uw} = K_H/K_M$. For stable stratifications there is good agreement that K_H/K_M is approximately constant and greater than unity (between 1.1 and 1.4). For unstable stratifications my results are higher than either Swinbank's or Businger's but all results show that K_H/K_M increases as instability increases and indicate that the rate of increase decreases as z/L becomes more negative.

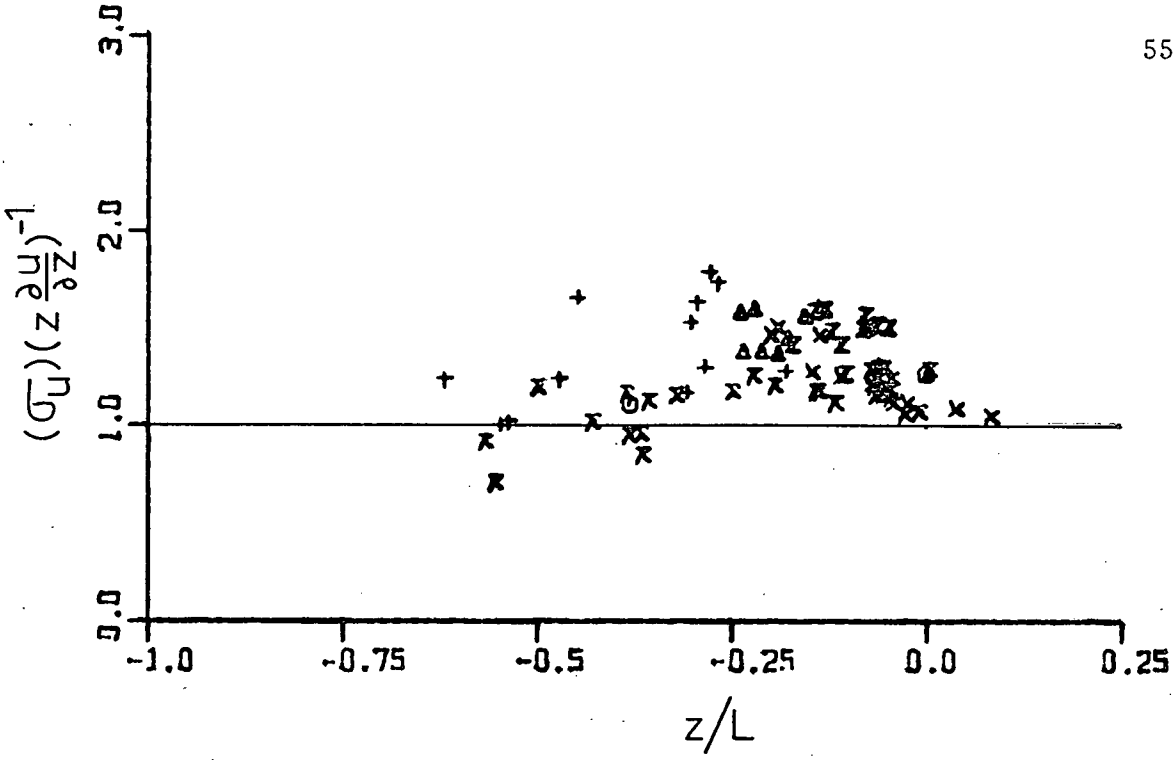

Figure 28. $\sigma_u/z\,\frac{\partial u}{\partial z}$ aqainst stability.

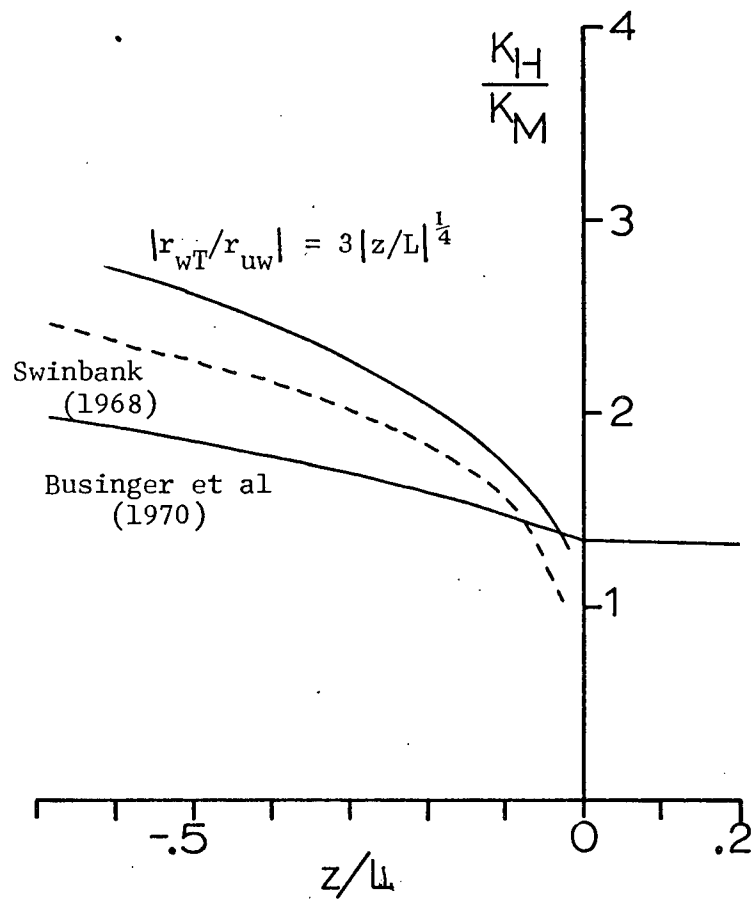

Figure 29. Variation of K_H/K_M with stability.

CHAPTER 5

TURBULENT TRANSFERS DURING BOMEX

In this chapter the results of direct measurements of momentum, heat and moisture transfer in a sub-tropical environment (near Barbados) will be presented. Because these data required special analysis procedures these procedures will be presented first, in Section 5.1. In Section 5.2 the turbulent transfers during BOMEX will be compared with one another and in Section 5.3 the results will be compared with those for the Ladner experiment.

5.1 Special analysis for Flip Data.

The analysis of the Flip experiment data was complicated by the motion of Flip and also by the disturbance of the mean flow pattern due to the presence of Flip. Flip's motion is principally in two modes. The first is the tilting about horizontal axes due to the ocean waves while the second is the rotation of Flip around its vertical axis due to differential wind pressures. The latter proved to be far more serious for these measurements. Flip's disturbance of the mean flow pattern appears to have resulted in a mean negative vertical wind at the 8 m location of the sonic anemometer (see Fig. 4).

The effect of Flip's rotations about its vertical axis, when large enough, was to cause the sonic anemometer's horizontal wind channels (channels A and B) to saturate. Since the Lyman-α humidiometer required the air to flow through a section of 1 cm diameter tubing to be sampled it too would not function when the rotation angle exceeded about 50°. Because of these problems with Flip's rotation it will be very difficult, if indeed possible, to analyse some of the data. The data analysed for this thesis only dealt with cases

where the relative wind direction did not exceed $\pm$ 20° during the run.

At the Institute of Oceanography at U.B.C. considerable effort has gone into studying the momentum transfer into waves, and a good deal is known about the cospectral shape (Smith, 1967; Weiler and Burling, 1967). The stress cospectrum is also the spectrum that will be most effected by Flip's motion and flow disturbances. Hence, if the stress can be made meaningful then the other turbulent transfers (i.e., heat and water vapour) will also be meaningful.

The effects of Flip's motion due to the ocean waves can be seen in Fig. 30. The effects on the u and v spectra are similar to the effects on the w spectrum. As can be seen the wave spectrum is very narrow and effects only a small band-width of the turbulence spectra. The fact that the wave peak appears in the v spectra indicates that the mean wind direction and the response of Flip to the waves were not always in the same vertical plane, at least for the long period waves that influence the spectra. This wave-effect peak in the spectra is considered to be due to Flip's response to the waves, and hence to varying the tilt of the anemometer, rather than due to a direct wind-wave coupling. The waves at the peak of the spectrum have a period of about 8 seconds and hence a wavelength of about 100 metres. The phase speed of the waves was about 12 m sec $^{-1}$ and the wind speeds about 6 m sec $^{-1}$. Elliott (1970) has shown that potential flow theory, in cases where $\bar{u} < c$, is a good approximation to the measured results. The wave induced velocities at a height of 8 metres, can thus be calculated from potential flow theory (see Lamb, 1945, Sec. 231). The amplitude of the wave induced velocities, A, will be:

$$A = \eta \left(\frac{\bar{u} - c}{c}\right) k e^{-kz} \qquad (5.1)$$

where η is the sea wave amplitude

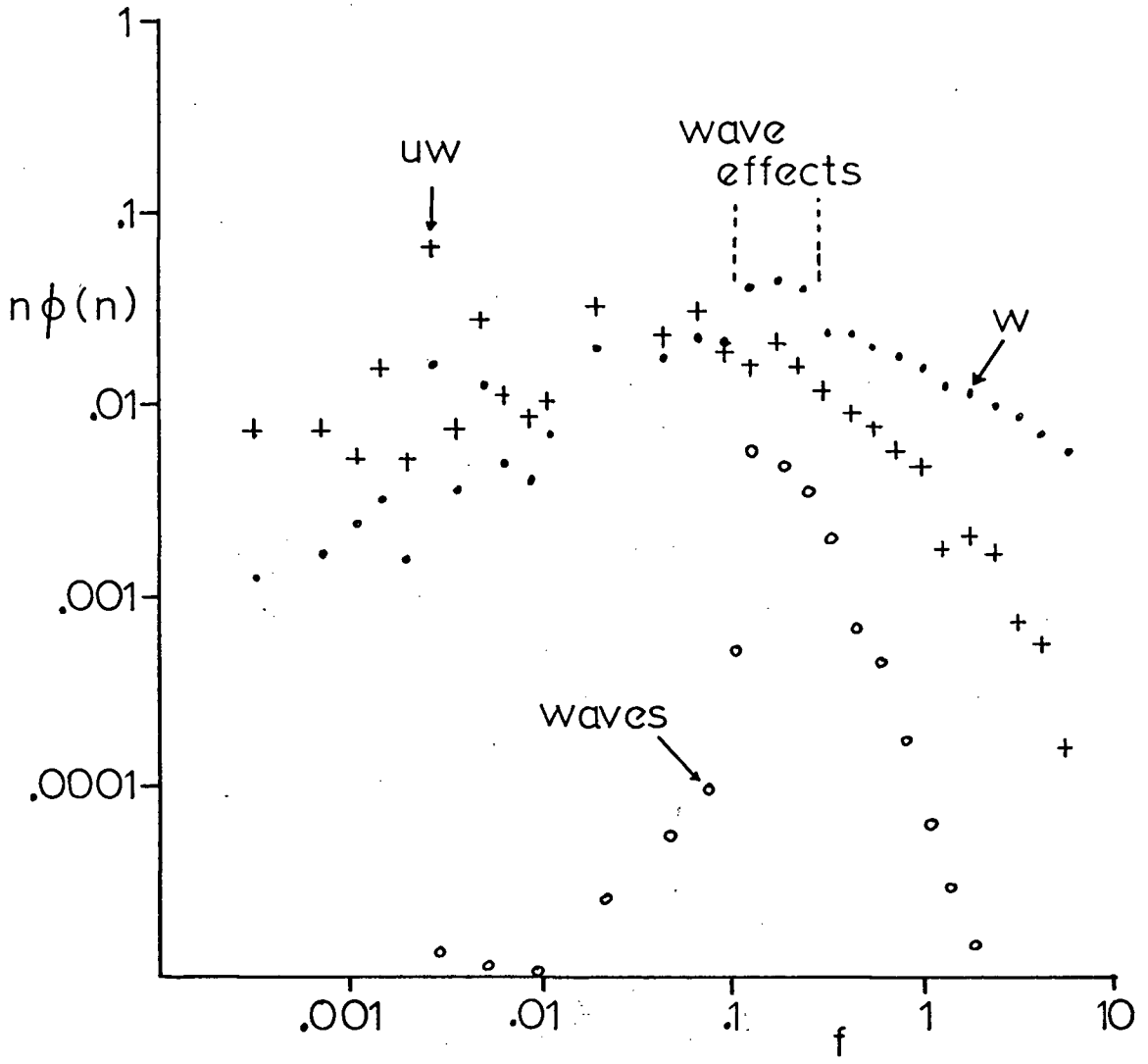

Figure 30. Effect of Flip's response to ocean waves on the w-spectrum and uw-cospectrum. The u and v-spectra had peaks similar to that observed on the w-spectrum.

c is the sea wave phase velocity,

k is the wave number of the sea waves,

$\bar{u}$ is the mean wind speed,

z is the height above the mean wave surface.

For η = 1 m and k = 0.063 m^{-1}, and (5.1) gives A $\approx$ 0.02 m sec^{-1}. Hence the wave induced energy will be of the order 4 x 10^{-4} m^2 sec; however the observed turbulent velocities at the wave peak had energy levels of the order of 2 x 10^{-2} m^2 sec^{-2}. Since the potential flow estimate of wave induced turbulent energy is more than an order of magnitude smaller than that observed it is believed that the wave peaks in the velocity spectra are due to Flip's motion and would not have been present if the measurements had been made from a fixed platform. Measurements of velocity made at IOUBC's fixed platform do not show wave peaks at comparable heights (relative to the wave height). To correct the statistics for the wave motion a smooth curve was drawn connecting the unaffected spectral estimates. The integrals under the curves were then recomputed for the new spectral shape.

Since the analysis has been restricted to cases where the relative wind direction was not rapidily changing, the only correction necessary was to correct the spectra for lack of alignment of the sonic anemometer array into the mean wind. Because all three velocities were measured it was possible to do these tensor transformations. The SCOR program (see Appendix I) computed the mean wind speed and direction (relative to Flip) for each block and the average over the data run. Hence an estimate of the wind direction variance was readily available. The ROTATE program was then used to compute the spectra and cospectra for the aligned coordinate system from the spectra and cospectra for the sonic array coordinates. The aligned coordinate system will have the mean wind vector $\vec{u}$ in its x - z plane but not necessarily along the x axis. The transformation equations (Kaimal et al, 1968) used assume the

$\bar{u}$ is in the x - y plane but the error is negligible since the tilt of the coordinates is less than 15°. The effect of Flip obviously altered the mean flow pattern around the instruments (see Mollo-Christensen, 1969). How it effected the structure of the turbulence is not known. As a first step to correcting for Flip's presence it seems reasonable to correct for the relative tilt of the sonic anemometer to the mean wind speed, i.e. to bring x along $\bar{u}$. The relative tilt was the total of the angle due to the array not being mounted exactly vertically and the angle due to the distortion of the near flow around Flip in tilting the $\bar{u}$ plane. The obvious technique to correct for this, to rotate until $\bar{w} = 0$, was not desirable in this case because of the uncertainty of the zero adjustment of the vertical channel of the sonic anemometer. Two other techniques were tried. One was to rotate the coordinates to obtain a given correlation coefficient between the low frequency u and w components while the other was to rotate to minimize the low frequency w spectrum. Let γ be the angle that the measuring instrument coordinate x^m, z^m are from the true coordinates x, z. The true velocities u' and w' are related to the measured velocities u^m and w^m by:

$$u' = u^m \cos\gamma - w^m \sin\gamma$$

$$w' = w^m \cos\gamma + u^m \sin\gamma$$

which lead to the spectral relations:

$$\phi_{uu}(n) = \phi^m_{uu}(n)\cos^2\gamma + \phi^m_{ww}(n)\sin^2\gamma - 2\phi^m_{uw}(n)\cos\gamma\sin\gamma$$

$$\phi_{ww}(n) = \phi^m_{ww}(n)\cos^2\gamma + \phi^m_{uu}(n)\sin^2\gamma + 2\phi^m_{uw}(n)\cos\gamma\sin\gamma$$

$$\phi_{uw}(n) = \phi^m_{uw}(n)\left[\cos^2\gamma - \sin^2\gamma\right] + \left[\phi^m_{uu}(n) - \phi^m_{ww}(n)\right]\cos\gamma\sin\gamma$$

At low frequencies and assuming small tilt angle these equations become:

$$\phi_{uu}(n) = \phi^{m}_{uu}(n)$$

$$\phi_{ww}(n) = \phi^{m}_{ww}(n) + \phi^{m}_{uu}(n)\,\gamma^2 + 2\phi^{m}_{uw}(n)\,\gamma$$

$$\phi_{uw}(n) = \phi^{m}_{uw}(n) + \phi^{m}_{uu}(n)\,\gamma$$

Hence for positive γ the measured $\phi^{m}_{uw}(n)$ will be too negative at low frequencies where $\phi^{m}_{uu}(n)$ is large and the stress integral will probably not be defined for periods of about an hour. For high frequencies and small γ the measured values of each of these spectra is a good approximation to the true value.

In order to calculate the tilt angle γ for these spectra the technique of forcing the low frequency u and w correlation coefficient to a given value, β was used. Smith (1967) used this technique with $\beta = -0.5$ to correct some data and obtained satisfactory results.

Using the approximations appropriate to low frequencies the correlation coefficient can be written as:

$$R_{uw}(n) = \frac{\phi_{uw}(n)}{\left[\phi_{uu}(n)\,\phi_{ww}(n)\right]^{1/2}}$$

$$= \frac{\phi^{m}_{uu}(n)\,\gamma + \phi^{m}_{uw}(n)}{\left[\phi^{m}_{uu}(n)\left(\phi^{m}_{ww}(n) + 2\phi^{m}_{uw}(n)\,\gamma + \gamma^2\phi^{m}_{uu}(n)\right)\right]^{1/2}}$$

this can be solved for γ to give

$$\gamma = \frac{\phi^{m}_{uw}(n)}{\phi^{m}_{uu}(n)} \pm \left[\left[\frac{\phi^{m}_{uw}(n)}{\phi^{m}_{uu}(n)}\right]^2 - \frac{1}{1-\beta^2}\left[\left(\frac{\phi^{m}_{uw}(n)}{\phi^{m}_{uu}(n)}\right)^2 - \beta^2\frac{\phi^{m}_{ww}(n)}{\phi^{m}_{uu}(n)}\right]\right]^{1/2}$$

The value of γ will, of course, be a function of frequency. The ROTATE program computed the average value of γ over a band of frequencies. A value

of -0.5 was chosen for the range from 0.01 Hz to 0.01 Hz. Because of the scatter of the data for $R_{uw}(f)$, it was decided to see the effects of other values of β. The results are given in Fig. 31 and the integrals summarized in Table III. Note that for correlation coefficients -0.3 the low frequency uw cospectrum is pushed positive which is unrealistic. For β = -0.6 the cospectra has a much wider bandwidth than previous results had indicated. This indicated that -0.5 was a good choice for β for that frequency interval.

The other technique tried was minimize the low frequency w spectrum. $\phi^{*}_{ww}(n)$ was calculated as:

$$\left[\phi_{ww}(n)\right]_{k\Delta\gamma} = \phi^{m}_{ww}(n)\ \cos^2(k\Delta\gamma) + 2\,\phi^{m}_{uw}(n)\ \cos k\Delta\gamma \sin k\Delta\gamma + \phi^{m}_{uu}(n)\ \sin^2(k\Delta\gamma)$$

for values of $k = 0, \pm 1, \pm 2, \pm 3, \ldots, \pm \frac{\gamma_{max}}{\Delta\gamma}$ where γ_{max} and $\Delta\gamma$ could be specified. The value of γ was found that made the average of $\phi_{ww}(n)$ over a frequency band a minimum. Fig 31 showed the effect of doing this over the frequency range f = 0.01 to 0.1 Hz, but the resulting cospectrum became positive at low f and was considered as unreasonable. If the length of the data run is sufficiently long then there will be a band of very low frequencies (e.g. f = 0.0001 to 0.001 Hz) for which this technique is useful. For run 14/2 minimizing the $\phi_{ww}(f)$ spectrum at very low frequencies led to a tilt angle of 11.5 degrees, in good agreement with the β = -0.5 technique for the same run which gave 12.5 degrees. However, for this technique the value of γ is based on spectral estimates that are statistically less reliable than any other region of the spectrum. For this reason it was decided to use the β=-0.5 technique to correct for anemometer tilt.

5.2 Comparison of the Turbulent Transfers During BOMEX

All the BOMEX data were for unstable stratifications. A complete

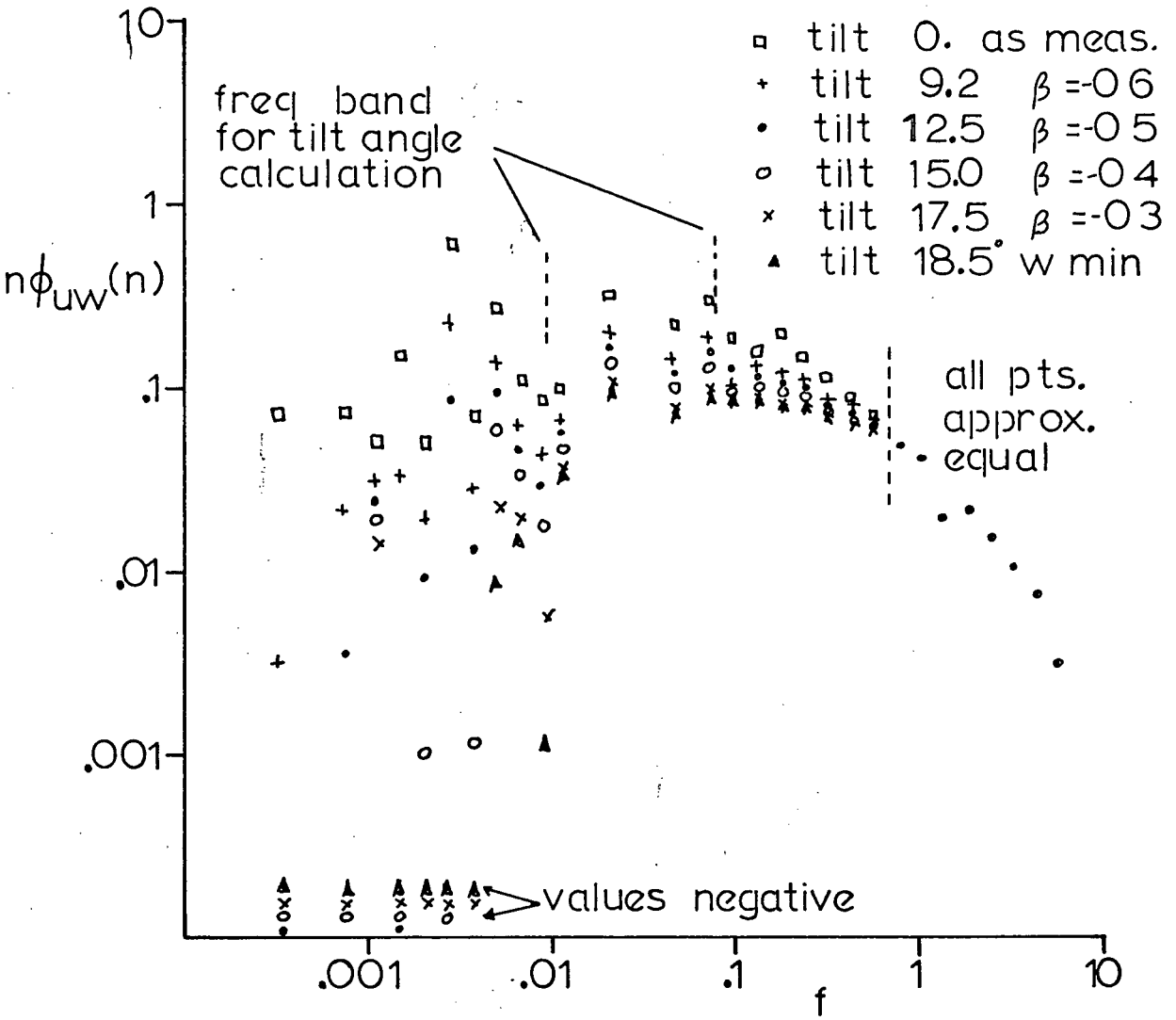

Figure 31. Effect of tilt on the uw-cospectrum for run B14/2. The angles 9.2 to 17.5 degrees were computed for the specified correlation coefficient over the indicated frequency range. The 18.5 degree tilt results from minimizing the w-variance in the same frequency range.

TABLE III Effects of Tilt Angle on Drag Coefficient and w variance

Correlation Coefficient β	Tilt Angle γ		Drag Coefficient		w Variance	
	14/1 Deg	14/2 Deg	14/1	14/2 $\times 10^3$	14/1 cm^2/sec^2	14/2
	0	0	2.8	3.5	1340	1310
-0.6	5.0	9.2	2.1	2.2	1240	960
-0.5	8.9	12.5	1.6	1.6	1120	870
-0.4	12.0	15.0	1.3	1.2	1000	810
-0.3	15.0	17.5	1.0	1.2	990	780
w minimized	17.5	18.5	.83	1.0	990	770

For a given spectral correlation coefficient the tilt angles were computed by the ROTATE program. Varying the tilt angle varied the computed stress and hence the drag coefficient (defined as $C_D = u_*^2/u_{10}^2$). The w-variance also depends on the tilt angle used.

tabulation is in Appendix IV. Because of the high evaporation rates over the sub-tropical ocean the contribution to buoyancy due to the moisture flux term is very significant. The contribution by z/L_q to z/L (see Equation 2.6) was equally as important as the contribution of z/L_T. The ratio $(z/Lq)(z/L_T)^{-1}$ was between 0.6 and 1.3 for the five data runs analysed. The variation of z/L was between -0.08 for B14/1 to -0.36 for B15/3.

The non-dimensional cospectral results for momentum, heat, and moisture transfers are compared in Fig. 32. Note that the shapes of $n\emptyset_{uw}(n)$ and $n\emptyset_{wq}(n)$ are very similar; the shape of $n\emptyset_{wT}(n)$ however, is significantly different. The heat flux cospectrum is much narrower in bandwidth and also extends to higher frequencies. The cospectral peaks for momentum and moisture transfer are between f = 0.03 and f = 0.2 whereas for heat transfer the cospectral peaks are near f = 0.3 and well-defined.

Before discussing the transfers further it is necessary to consider the temperature spectra and the T-q correlation functions. The spectra of temperature fluctuations are presented in Fig. 33. For comparison purposes an average temperature spectrum from Ladner and the humidity spectra from BOMEX are included. Notice the marked dissimilarity of the BOMEX temperature spectra and either the BOMEX humidity spectra or the Ladner temperature spectrum. The BOMEX temperature spectrum has an appearance more similar to that of a vertical velocity spectrum whereas the humidity spectrum has a shape nearer to that of a longitudinal velocity spectrum. The BOMEX temperature variance was contributed almost entirely by scales between 30_z and 0.3_z (z is the height of observation, 8m) whereas for humidity there were contributions from scales as large as those measured, approximately 3000z. The reason for the dominance of these scale temperature fluctuations may be attributed to the high degree of organization of convective scales in the subtropics.

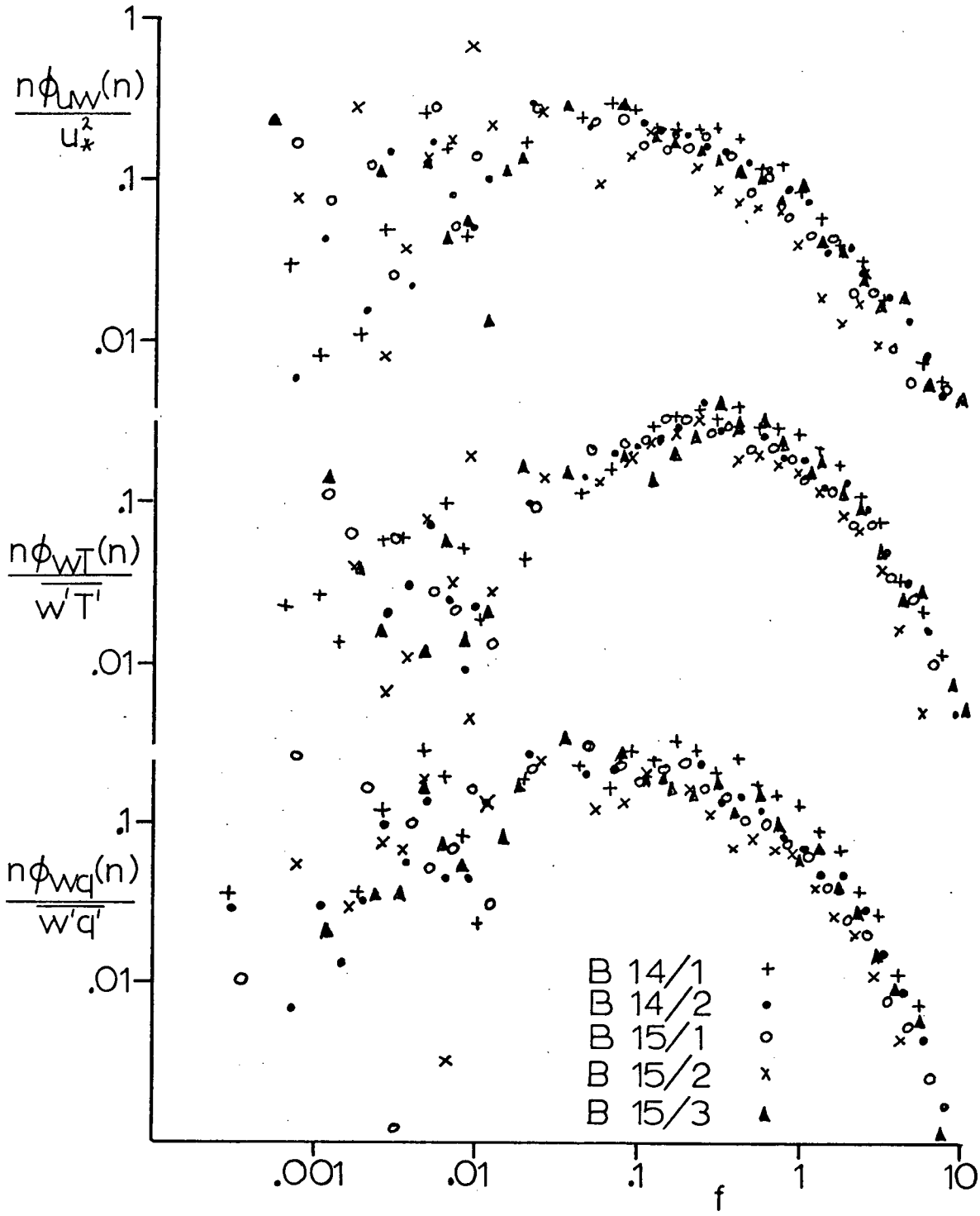

Figure 32. Cospectra of momentum, heat, and moisture transfer for the Flip experiment.

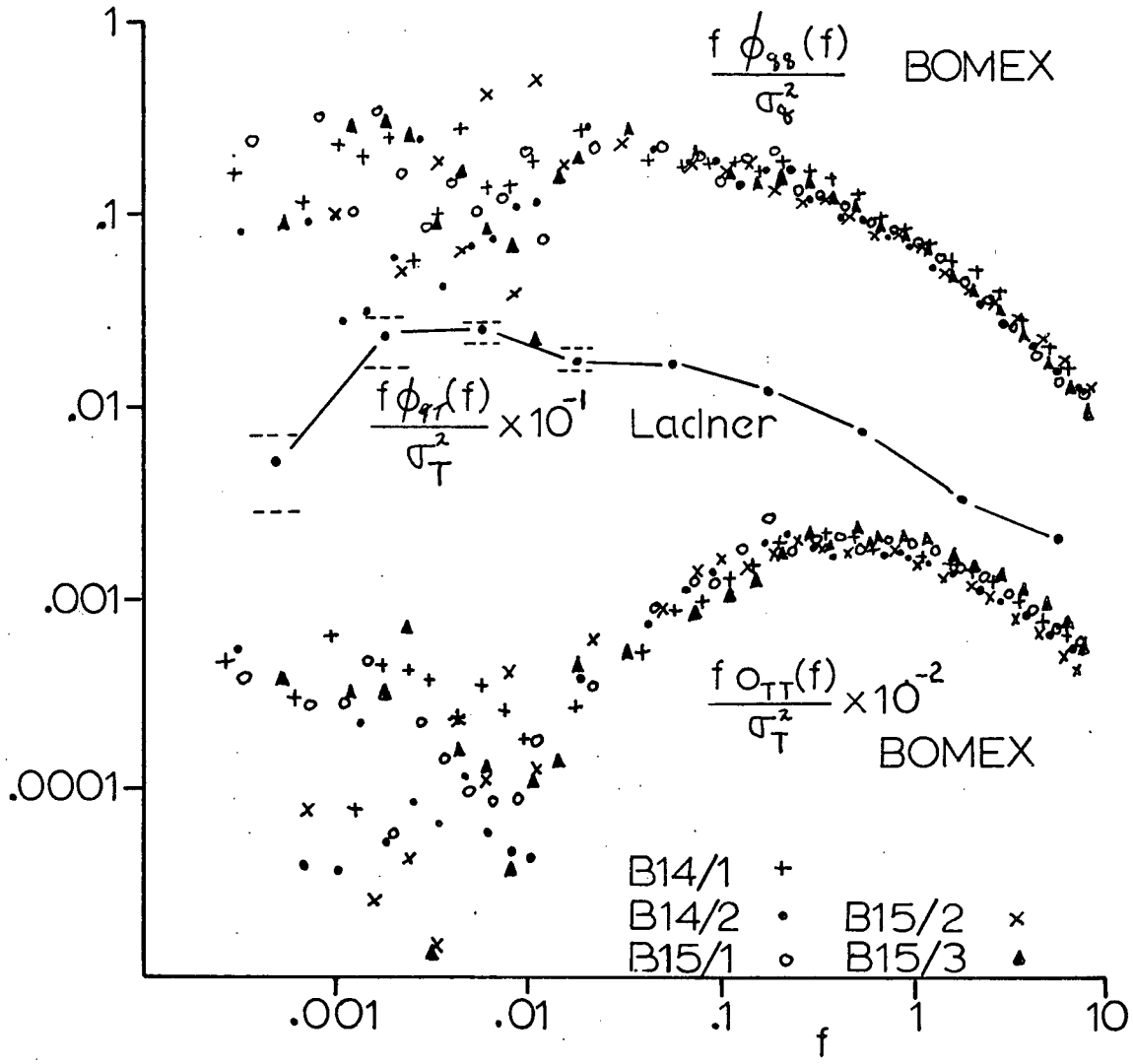

Figure 33. Spectra of temperature and humidity fluctuations for Flip experiment. A mean temperature spectrum from the Ladner experiment is included for comparison.

The convective elements of scales of a few hundred metres are in patches separated by larger areas of descending stable air. This descending air is warm, dry and less turbulent and more homogeneous than that in the convective regions. Hence the temperature fluctuations will be mainly of scales of the size of or smaller than the convective regions. There is some evidence of a second peak in the temperature spectrum of scales of several kilometers which might be associated with the combined system of convective and descending air regions.

Supporting evidence for this explanation is in the T-q spectral correlation coefficients (see Fig. 34). For scales smaller than about 10z temperature and humidity had a correlation coefficient of higher than 0.8. The high frequency fall-off may be instrumental. For scales about 1000z and larger the correlation coefficients are between -0.8 and -1.0. For scales in between $R_{Tq}(f)$ varies gradually (but somewhat erratically) between these limits for some runs and abruptly changes for other runs. These results indicate that at large scales (several Kilometers) warm air is dry and vice versa. At small scales the correlation is warm and wet; cold and dry. These data support the explanation given for the temperature spectrum. Further investigations in both space and time will be needed before the phenomenon is understood.

The narrow bandwidth of the temperature spectrum, of course, reflects itself in the transfers. The heat flux cospectrum has a shape similar to that of the temperature spectrum. This is because no matter how large $R_{wT}(f)$ happens to be $f\emptyset_{wT}(f)$ will still be small if $f\emptyset_{TT}(f)$ is small. The spectral correlation coefficients for B14/1, the least unstable run, and for B15/3, the most unstable run, are shown in Figs. 35 and 36. At low frequencies the correlation coefficients have a large scatter but above f = 0.01 the data are

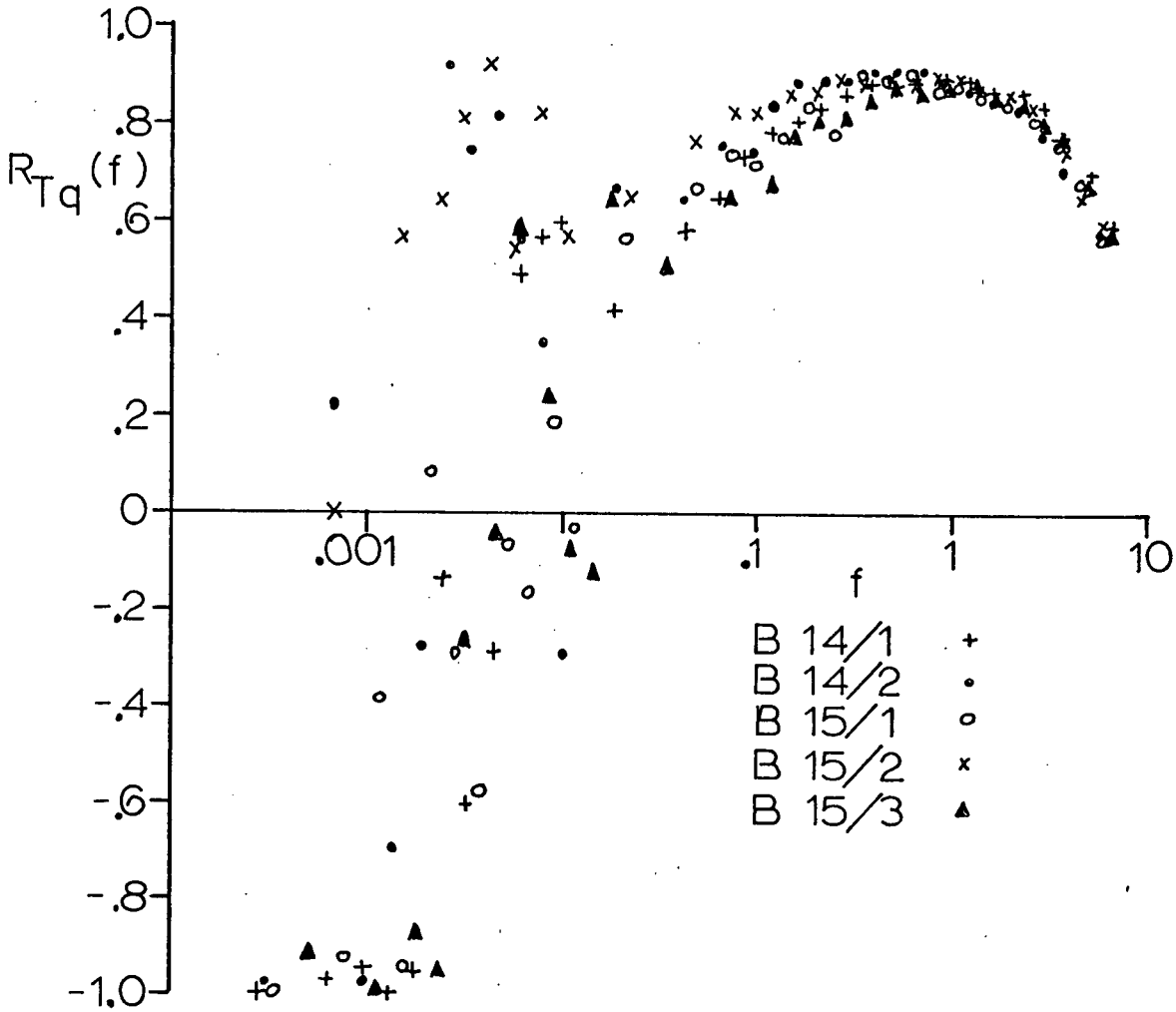

Figure 34. Temperature-humidity spectral correlation coefficients for the Flip experiment.

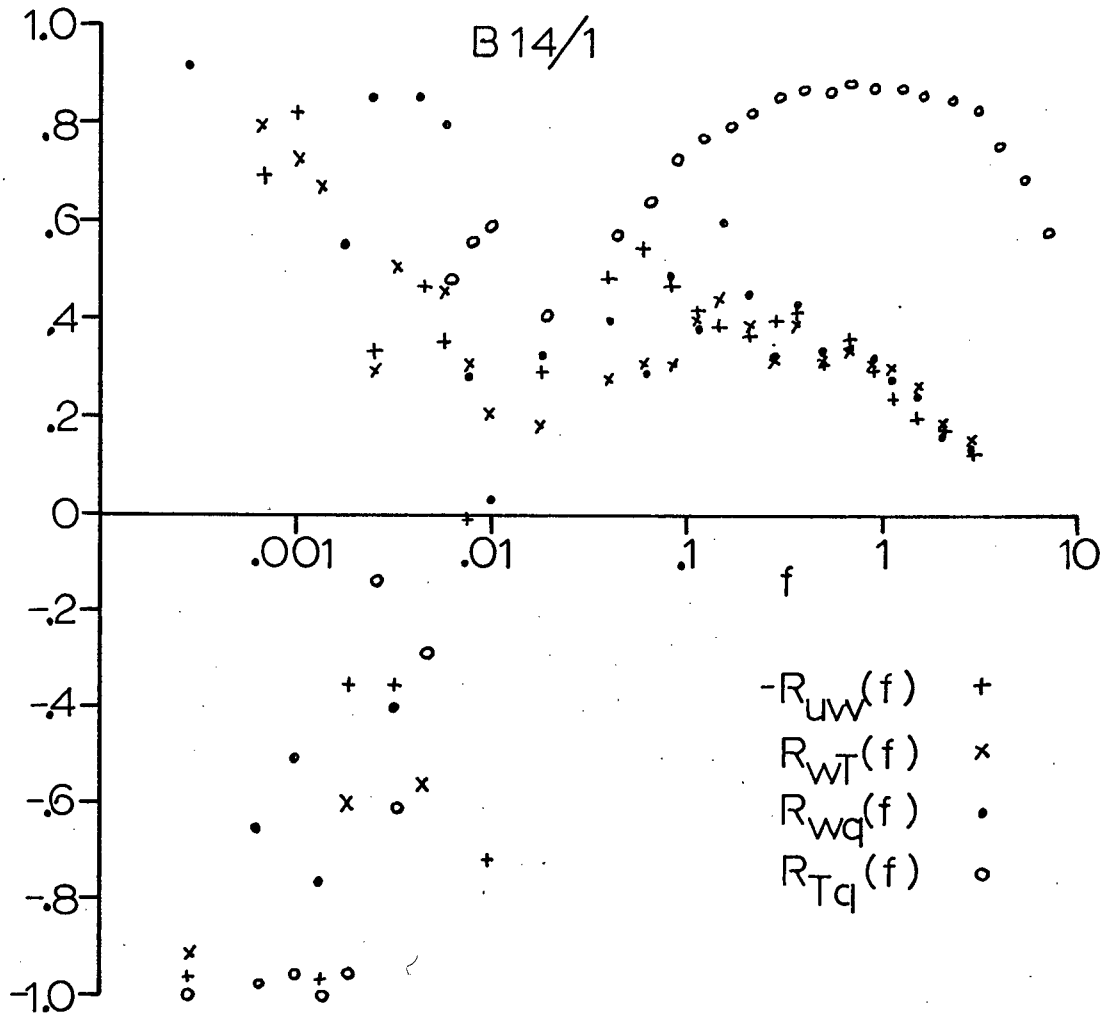

Figure 35. Spectral correlation coefficients for run B14/1

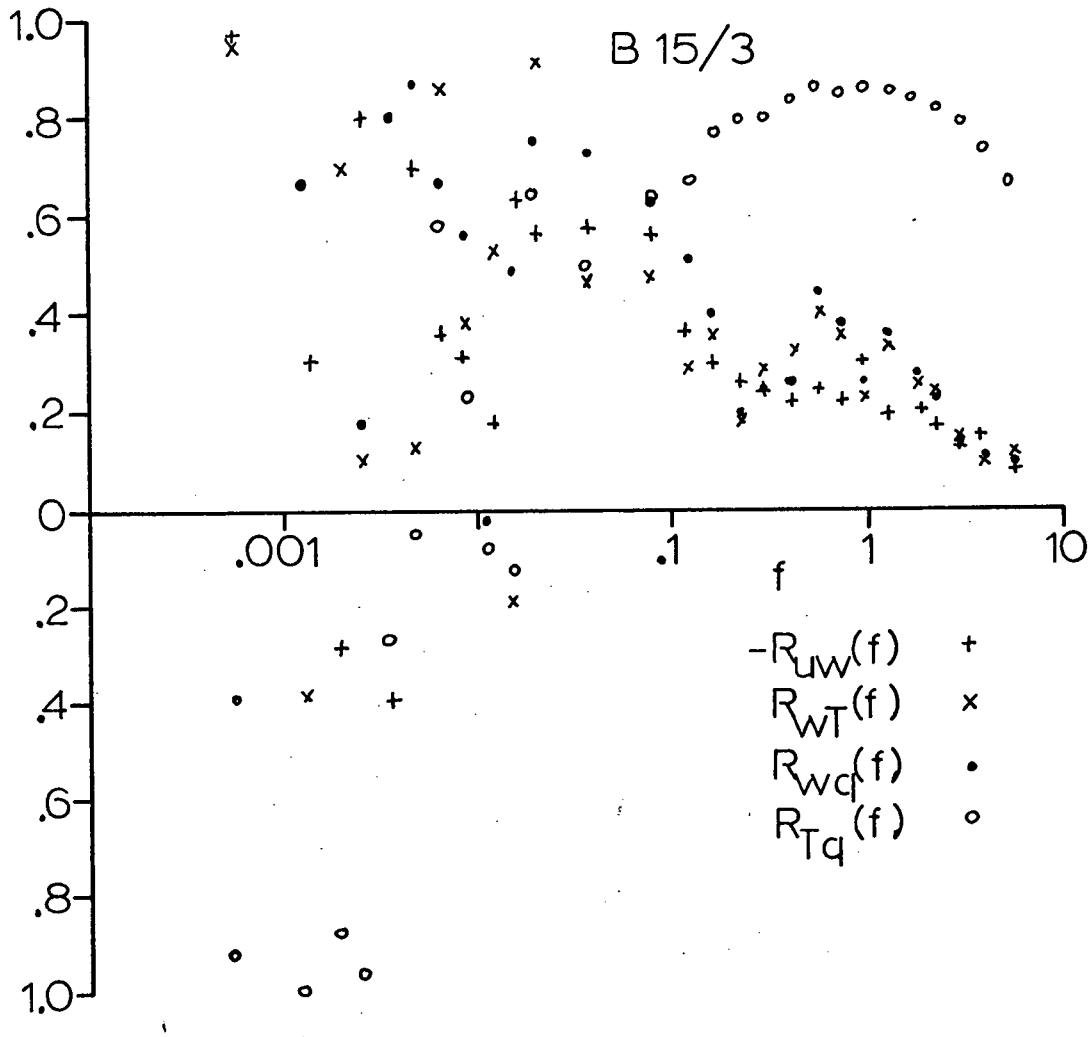

Figure 36. Spectral correlation coefficients for run B15/3.

more consistent. The spectral correlation coefficient for momentum transfer is largely determined by the analysis procedure (see Section 5.1). However, for f greater than 0.1, $R_{uw}(f)$ is approximately independent of tilt angle. For this reason the values of $R_{uw}(f)$ are only considered for $f > 0.1$. Note that in run B14/1 for $f > 0.2$, the three spectral correlation coefficients are similar, i.e., $R_{uw}(f) \triangleq R_{wT}(f) \triangleq R_{wq}(f)$. For the range f = 0.01 to about f = 0.2, $R_{wq}(f)$ is greater than $R_{wT}(f)$. For larger scales $R_{wq}(f)$ and $R_{wT}(f)$ are scattered and tend to have opposite signs. For B15/3 $R_{wq}(f)$ is greater than $R_{wT}(f)$ over the range of f from 0.01 to 0.1. The value of $R_{uw}(f)$ is the same as both $R_{wT}(f)$ and $R_{wq}(f)$ for f greater than 1.0 but is generally lower than both for f between 0.1 and 1.0. Over most of the range of f for which there is appreciable heat transfer, the w-T correlation is similar to the w-q correlation. Over the same range of f space there are significant temperature fluctuations (Fig 33) and the T-q correlation is high (Fig. 34). For scales between f = 0.01 and f = 0.1 the temperature spectrum is decreasing with decreasing f and the T-q correlation is also decreasing. It thus appears that the transfer mechanisms for heat and moisture transfers are similar over the range of f where temperature fluctuations are contributing to the buoyancy. For larger scales the buoyancy is mainly due to humidity fluctuations because the temperature fluctuations are small in magnitude. For these scales the T-q correlation is smaller and the transfer efficiency of moisture transfer, as gauged from $R_{wq}(f)$ is greater than that due to heat transfer. The results for $R_{uw}(f)$ indicate that momentum transfer for small scales (f less than 1.0) is as efficient as either heat or moisture transfer. Because the observation level at BOMEX was four times as high as at Ladner the sonic anemometer response to u fluctuations is not as important.

5.3 Turbulent Transfers: BOMEX and Ladner

The turbulent transfers at BOMEX differ from those at Ladner primarily for two reasons. During BOMEX the moisture fluctuations were large enough to be equally important with temperature fluctuations in causing buoyancy. Secondly the organized convective systems at BOMEX led to a quite different distribution with scale of the temperature variance from that observed at Ladner. The result was that the important scales contributing to the heat transfer were quite narrow during BOMEX as compared to Ladner; at BOMEX the range was $f = 0.03$ to $f = 3$ whereas at Ladner the range was $f = 0.001$ to $f = 3$ or 4. The scales contributing to the moisture and momentum transfer, from f about 0.001 to f about 1.0, were not significantly different between BOMEX and Ladner. The moisture transfer efficiency was, however, equal to that for heat transfer as a consequence of the fact that moisture was important in contributing to buoyancy. The BOMEX results agreed with the findings from Ladner that the parameter that causes buoyancy will have a high transport efficiency. These subtropical results from BOMEX will have to be verified by many further investigations but they do point out some of the features to look for.

CHAPTER 6

SUMMARY

The turbulent fluxes of momentum, heat and moisture, their similarities and the efficiencies of their transfers were examined. The cospectral analyses indicated that the dominant contributions to the fluxes of momentum, heat, and moisture at Ladner lie in the natural frequency range f = 0.001 to f = 5.0 for near neutral and unstable conditions. The cospectral shapes of all three transfers are similar for f less than 0.3 but the heat flux may fall off less rapidly at high f. The peaks of the cospectra shift from near f = 0.2 for near neutral stratifications to near f = 0.06 for $z/L \approx -0.5$. For stable stratifications the cospectra show marked shifts to higher natural frequency. It was also shown that atmospheric inertial wave motions can be important.

The spectral correlation coefficients were considered to be a measure of the transfer efficiency as a function of scale size. For momentum transfer the efficiency, $R_{uw}(f)$, decreased at all scales as instability decreased and the largest relative changes were at low frequencies. The heat transfer spectral correlation coefficients, $R_{wT}(f)$, increased at all scales as instability increased. The ratios $|R_{wT}(f)/R_{uw}(f)|$ were greater than 1 for most scales even for near neutral conditions. For more unstable conditions the ratio was between 2 and 3. These results indicated that even for near neutral conditions that the transfer mechanisms were not the same. It appears that only the slightest amount of buoyancy ($|z/L| < -0.02$ or perhaps smaller) is needed to make the transfer efficiency for heat transport more efficient than that for momentum transport.

As z/L decreases from zero the transfer efficiency of momentum transfer decreases. It was postulated that this was due to greater amounts of momentum being transferred in bursts of short duration thus making the spectral correlation coefficient for momentum transfer, averaged over sufficient time, smaller.

The ratio of the correlation coefficients calculated from the complete data signals could be approximated by $(|r_{wT}/r_{uw}|) = 3\,|z/L|^{\frac{1}{4}}$ for unstable conditions and a constant, about 1.2, for stable conditions.

The efficiency of moisture transfer, when moisture is a passive scalar, was found to depend on the correlation between moisture fluctuations and those of temperature, which is the active scalar. These results indicate that universal relationships pertaining to the transfer of passive scalars are unlikely and that the transfer mechanism will depend on both the surface boundary conditions and the larger scale circulations which effect the passive scalar-active scalar correlation.

The results from BOMEX pointed out the large differences in the distribution of temperature variance at large scales between the subtropics and mid-latitudes. Further the contributions to buoyancy due to humidity were significant at BOMEX and this is reflected in the transfer mechanisms. Whereas humidity and momentum transport were by scales between $f = 0.001$ and $f = 1$ (as at Ladner), the heat transfer was confined within the narrow band between $f = 0.03$ and $f = 5$.

BIBLIOGRAPHY

Blackman, R. B., and J. W. Tukey, 1958: The Measurement of Power Spectra. New York, Dover, 190 pp.

Businger, J. A., M. Miyake, A. J. Dyer, and E. F. Bradley, 1967: On the direct determination of the turbulent heat flux near the ground. J. Appl. Meteor., 6, 1025-1032.

Businger, J. A., J. C. Wyngaard, Y. Izumi, and E. F. Bradley, 1970: Flux-profile relationships in the atmospheric surface layer. (submitted to J. Atmos. Sci.).

Dyer, A. J., 1965: The flux-gradient relation for turbulent heat transfer in the lower atmosphere. Quart. J. R. Meteor. Soc., 91, 151-157.

_____, 1967: The turbulent transport of heat and water vapour in an unstable atmosphere. Quart. J. R. Meteor. Soc.,93, 501-508.

Elderkin, C. E., 1968: Experimental investigation of the turbulence structure in the lower atmosphere. AEC Research and Development Report, BNWL-329, Battelle Memorial Institute, Hanford, Wash.

Elliott, J. A., 1970: Microscale pressure fluctuations measured within the lower atmospheric boundary layer. Ph.D. Dissertation, Univ. of British Columbia.

Francisco, C. C., and D. J. Beaubian, 1965: An automatic dew point hygrometer with thermoelectric cooling. Humidity and Moisture, I, Reinhold Publ. Co., New York, 165-173.

Garratt, J. R., 1969: Spectral and bulk properties of turbulence in the surface layer of air over the sea. Ph.D. Dissertation, Univ. of London.

Garrett, J. F., 1970: Field observations of frequency domain statistics and nonlinear effects in wind-generated ocean waves. Ph.D. Dissertation, Univ. of British Columbia.

Haltiner, G. J., and F. L. Martin, 1957: Dynamical and Physical Meteorology. New York, McGraw-Hill, 470 pp.

Haugen, D. A., J. C. Kaimal, and E. F. Bradley, 1970: An experimental study of Reynolds stress and heat flux in the atmospheric surface layer. (submitted to Quart. J. R. Meteor. Soc.).

Kaimal, J. C., and J. A. Businger, 1963: A continuous-wave sonic anemometer-thermometer. J. Appl. Meteor., 2, 156-167.

_____, J. C. Wyngaard, and D. A. Haugen, 1968: Deriving power spectra from a three-component sonic anemometer. J. Appl. Meteor., 7, 827-837.

Kuettner, J.P., and J. Holland, 1969: The BOMEX project. Bull. Amer. Met. Soc., 50, 394-402.

Kukharets, V.P., and L.R. Tsvang, 1969: Spectra of the turbulent heat flux in the atmospheric boundary layer. Isv., Atmos. Oceanic Phys., 5, 1132-1142.

Lamb, H., 1945: Hydrodynamics, New York, Dover, 738 pp.

Laufer, J., 1954: Natl. Advisory Comm. Aeronaut. Tech. Repts. No 1174.

Lumley, J.L., and H.A. Panofsky, 1964: The Structure of Atmospheric Turbulence. New York, Interscience, 239 pp.

Mitsuta, Y., 1966: Sonic anemometer-thermometer for general use. J. Meteor. Soc. Japan, 44, 12-23.

Miyake, M., R.W. Stewart, and R.W. Burling, 1970: Spectra and cospectra of turbulence over water. Quart. J. Roy. Meteor. Soc., 96, 138-143.

Mollo-Christensen, E , 1969: Wind tunnel test of the superstructure of R/V Flip for assessment of wind field distortion. Rep. 68-2, Fluid Dyn. Lab., M.I.T., 31 pp.

Monin, A.S., and A.M. Obukhov, 1954: Basic laws of turbulent mixing in the ground layer of the atmosphere. Akad. Nauk SSSR Geotiz. Inst. Trudy, 151, 163-187.

Mordukhovich, M.I., and L.R. Tsvang, 1966: Direct measurements of turbulent flows at two heights in the atmospheric ground layer. Izv. Atmos. Oceanic Phys., 2, 786-803.

Panofsky, H.A., and E. Mares, 1968: Recent measurements of cospectra for heat-flux and stress. Quart. J.R. Meteor. Soc., 94, 581-585.

Paulson, C.A., 1967: Profiles of Wind Speed, Temperature and Humidity over the Sea. Ph.D. Dissertation, Department of Atm. Sci., Univer. of Wash., Seattle, 128 pp.

Phelps, G.T., S. Pond, and U. Gorner, 1970: Simultaneous measurements of humidity and temperature fluctuations. J. Atmos. Sci., 27, 343-345.

Phillips, O.M., 1966: The dynamics of the upper ocean. Cambridge, Cambridge University Press, 277 pp.

Pond, S., 1965: Turbulence Spectra in the Atmospheric Boundary Layer over the Sea. Instit. of Ocean., Univ. of British Columbia, Report No. 19.

Randal, D.L., T.E. Hanley, and O.K. Larison, 1965: The NRL Lyman-α humidiometer. Humidity and Moisture, I, Reinhold Publ. Co., New York, 444-454.

Rudnick, P., 1964: Flip: an oceanographic buoy. Science, 146, 1268-1273.

_____, 1967: Motion of a large spar buoy in sea waves. J. Ship Research, 11, 257-267.

Smith, S.D., 1967: Thrust-anemometer measurements of wind-velocity spectra and of Reynolds stress over a coastal inlet. J. Marine Res., 25, 519-532.

Stewart, R.W., 1969: Turbulence and waves in a stratified atmosphere. Radio Science, 4, 1269-1278.

Swinbank, W.C., 1968: A comparison between predictions of dimensional analysis for the constant-flux layer and observations in unstable conditions. Quart. J.R. Meteor. Soc., 94, 460-467.

_____, and A.J. Dyer, 1967: An experimental study in micro-meteorology. Quart. J.R. Meteor. Soc., 93, 494-500.

Taylor, G.I., 1954: The dispersion of matter in turbulent flow through a pipe. Proc. Roy. Soc., A, 223, 446-468.

Tsvang, L.R., 1960: Measurements of temperature pulse frequency spectra in the surface layer of the atmosphere. Izv. ANSSSR, Geophys. Ser. S. 1252.

Weiler, H.S., and R.W. Burling, 1967: Direct measurements of stress and spectra of turbulence in the boundary layer over the sea. J. Atmos. Sci., 24, 653-664.

Wexler A, (ed.), 1965: Humidity and Moisture, Reinhold Publ. Co., New York.

Zubkovsky, S.L., and B.M. Koprov, 1969: Experimental investigation of the spectra of turbulent heat and momentum fluxes in the atmospheric surface layer. Isv., Atmos. Oceanic Phys., 5, 323-331.

APPENDIX I

SPECTRAL ANALYSIS

All the data were collected in analog form and all analysis was done digitally. The analog to digital conversion was done using a converter designed and built at IOUBC. The converter gives 10 bits resolution for 10.24 volts full scale input, i.e. 10 mv resolution. The usual procedure was to simultaneously digitize ten channels of information. In the mode of operation used the ten channels were sampled sequentially with a 45 microsecond delay between channels. These "cross-channel sequences" were repeated at the rates given in Table IV. The analog signals were reproduced at tape speed 60 inches sec^{-1} (except Type I which was at 30 ips) to reduce the time required to digitize a data run. For Type I the ratio of the time between sampling channels to the time between cross channel sweeps is at most 1:17. The corresponding ratios for Types II and III were: 1:12; and 1:18. Before digitizing, all data were passed through a matched set of linear phase shift filters with a gain of -3db at 160 Hz in 'reproduce' time, with fall-off of 12 db per octave. This resulted in real time high frequency cutoffs at: 40 Hz for Type I; 20 Hz for Type II; and 5 Hz for Type III. In all analyses the spectral estimates were corrected for attenuation by the filters.

The output of the A-D converter was relayed to a Control Data Corp "8092 Teleprogrammer" (a small computer) which wrote the data onto a 7 track digital tape in a format that could be read on the IBM 360/67 of the UBC Computing Centre which was used to do the analysis.

The IOUBC spectral analysis system is outlined in Fig. 37. The programs TVERIF, FTOR, and SCOR were developed by two other graduate

Table IV. Digital Sampling Frequencies.

		Real Time	Playback Time
I	Ladner data (except in II)	80 Hz	320 Hz
II	Ladner 216,219,220,221,222.	60 Hz	480 Hz
III	Flip data	20 Hz	640 Hz

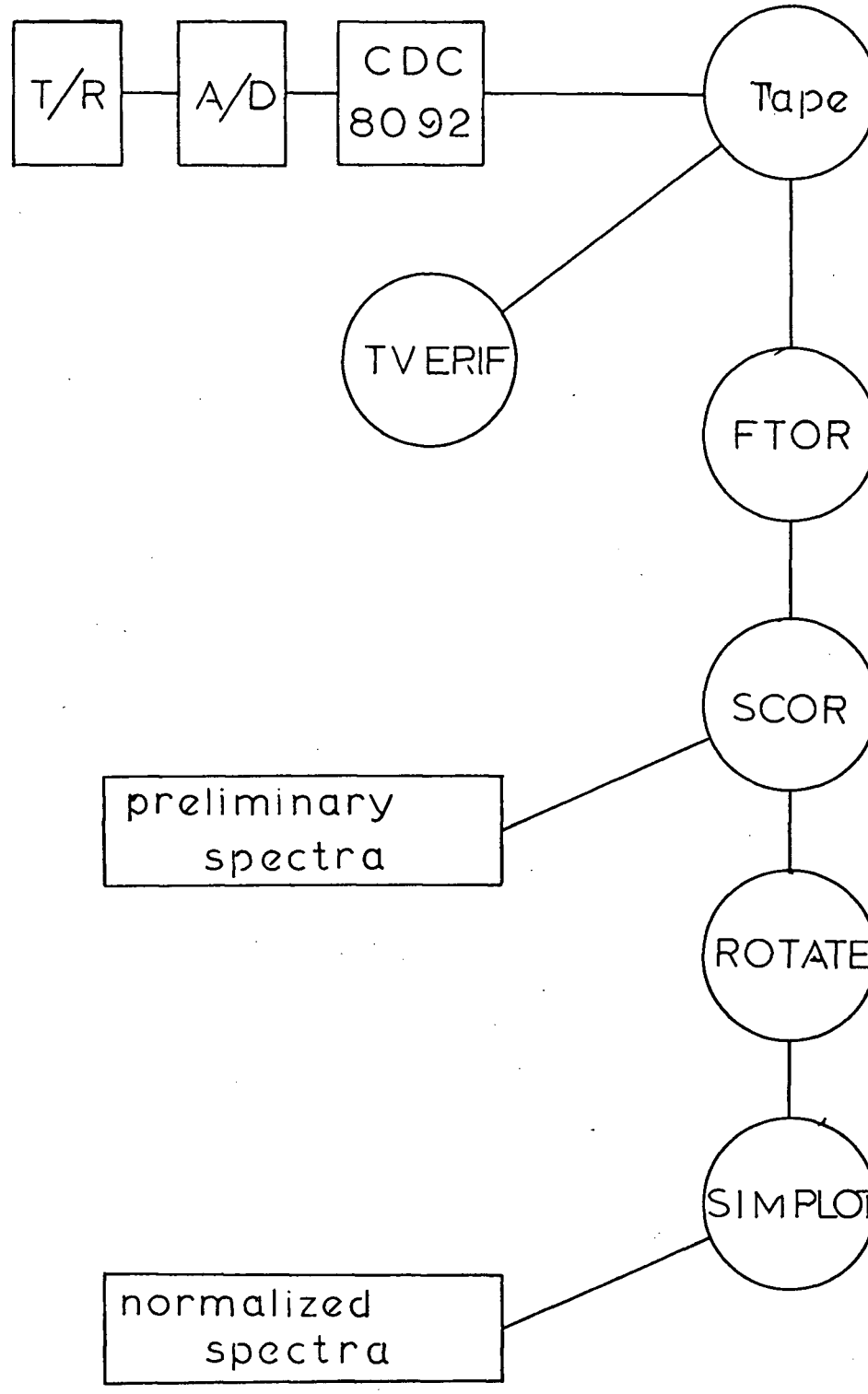

Figure 37. IOUBC spectral analysis system.

students, Dr. J.F. Garrett and J.R. Wilson. The author's contributions were the ROTATE and SIMPLOT programs and modifications to SCOR. The TVERIF or tape verify program was used to check the digital tape for errors. The technique used for this thesis was compute the Fourier coefficients of the time series by use of a "fast" Fourier transform (FFT) subroutine (see IEEE Transactions on Audio and Electro-acoustics, June, 1967) and then compute the spectra and cospectra from these coefficients. The details of this procedure have been given by Garrett (1970). The FTOR program computed the Fourier coefficients for data blocks containing 1024 samples from each of the ten channels. The SCOR program computed from the coefficients the required spectra and cross spectra. These spectral estimates were averaged over approximately one-eighth decade frequency bands.

For a typical Ladner data run, there was enough data for 64 data blocks. The range of frequency analysis was from $n_1 = 1/N\Delta t = 0.078$ Hz and Δt is the time between samples (=0.0125 sec.), to $n_{\frac{N}{2}} = 40$ Hz. This lower frequency limit, n_1 was too high to include all the low frequency energy for some variables. Hence a procedure was developed to extend the analysis to lower frequencies while at the same time not unduly extending the analyses procedure. In computing the Fourier coefficients for each block the average value of each signal over that block is automatically computed. These block averages (usually 64 in number) then constitute a new time series. The SCOR program was modified to include a small FTOR-like program to compute the Fourier coefficients of this new time series. The band-averaged spectra and cross spectra for this new time series were computed in SCOR in exactly the same manner as the others. The resultant new spectra are the same as if the time series had been "box car" averaged over 1024 data points and then sampled every 1024th point. The effect of

the box car average is to modify the spectrum with a sinc^2 function; i.e. the spectral estimates are multiplied by $\tau(n)$ where:

$$\tau(n) = \left[\sin 2\pi\tfrac{nT}{2} \Big/ 2\pi\tfrac{nT}{2}\right]^2 = \text{sinc}^2(\pi nT)$$

where T is the length of the average.

How this affects the data will now be investigated. For a typical Ladner case T was 12.8 seconds. The transfer function $\tau(n)$ is given in Fig. 38. Taking every 1024th point has the effect of aliasing the data or folding $\tau(n) * \phi(n)$ around the Nyquist frequency which in this case was $n_{Ny} = 1/2T$. The folded $\tau(n)$ is also shown in Fig. 38. If $n\phi_{33}(n) \propto n$ at low frequencies (see Miyake et al, 1970) then $\phi_{33}(n)$ = constant for low n and the effect of the transfer function is to distort the spectrum as shown. Also shown is the result for $\phi(n) \propto n^{-1}$. The spectral window for the low frequency analysis reduces the spectral energy density to 80% of its value at n_{Ny}. The typical value of n_{Ny} was 0.039 Hz which for z = 2m and $\bar{u}$ = 4 m/s gives $f = nz/\bar{u} = 0.02$. According to Miyake et al (1970) less than 20% of the momentum transfer occurs for $f < 0.02$. From the same data (Miyake et al, 1970; Weiler and Burling, 1968) the contributions to $\overline{w}$ for $f < 0.02$ are negligible. Hence although the transfer function $\tau(n)$ effects the spectral shape, the effect on the transfers is likely to be small.

The natural scatter of the spectral estimates tends to conceal the transfer function effects. In Fig. 39 values of $\log n\phi_{ww}(n)/\sigma_w^2$ for one run, computed by three separate techniques, are plotted. One method was the FFT technique used in this thesis. The second was by standard analog computer techniques on the IOUBC analog computer. The third was also an analog computation but done by the Soviet scientists of the Institute of Physics of the Atmosphere, Moscow (see Kukharets and Tsvang, 1969). The data run

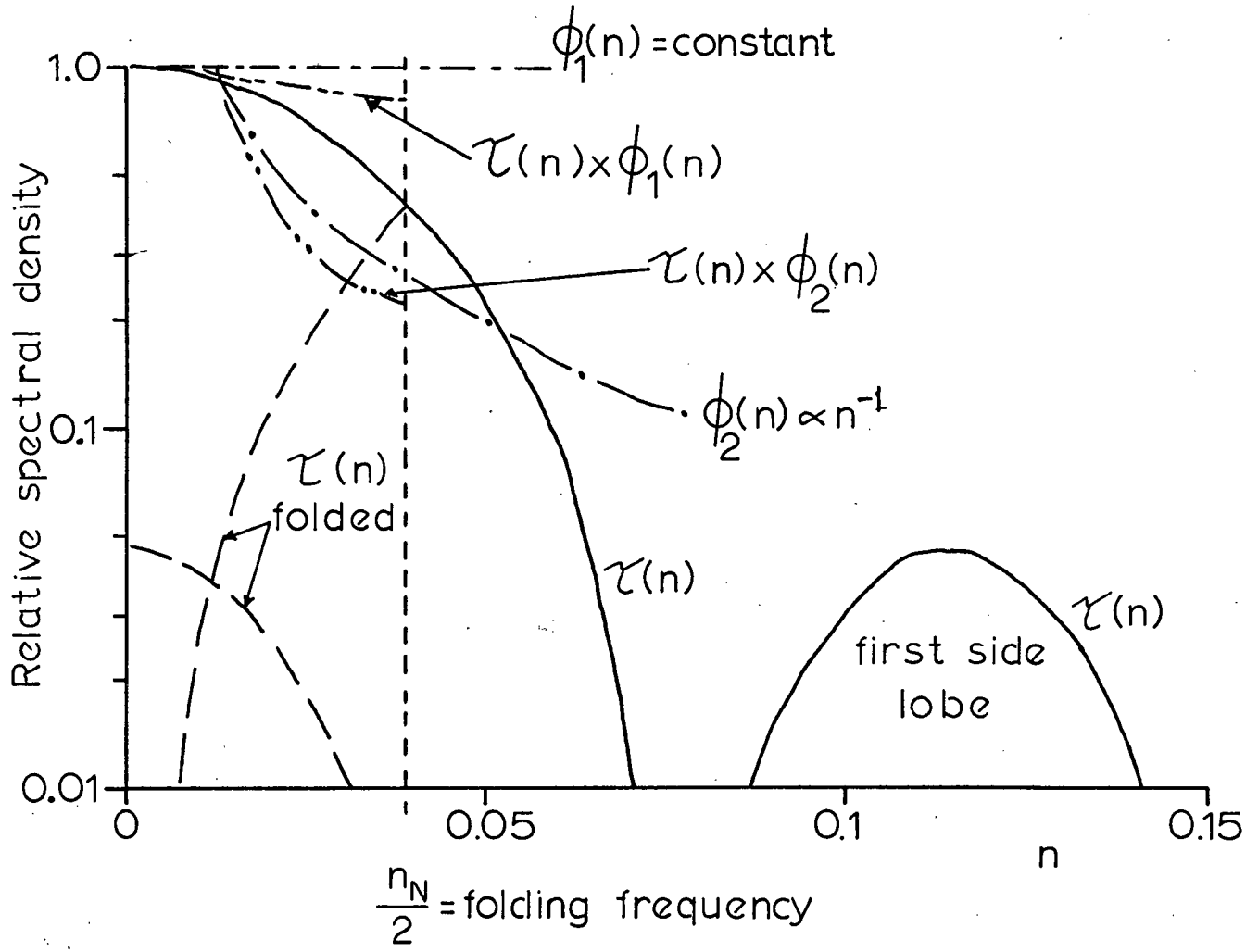

Figure 38. The low frequency analysis transfer function and its effect on spectra.

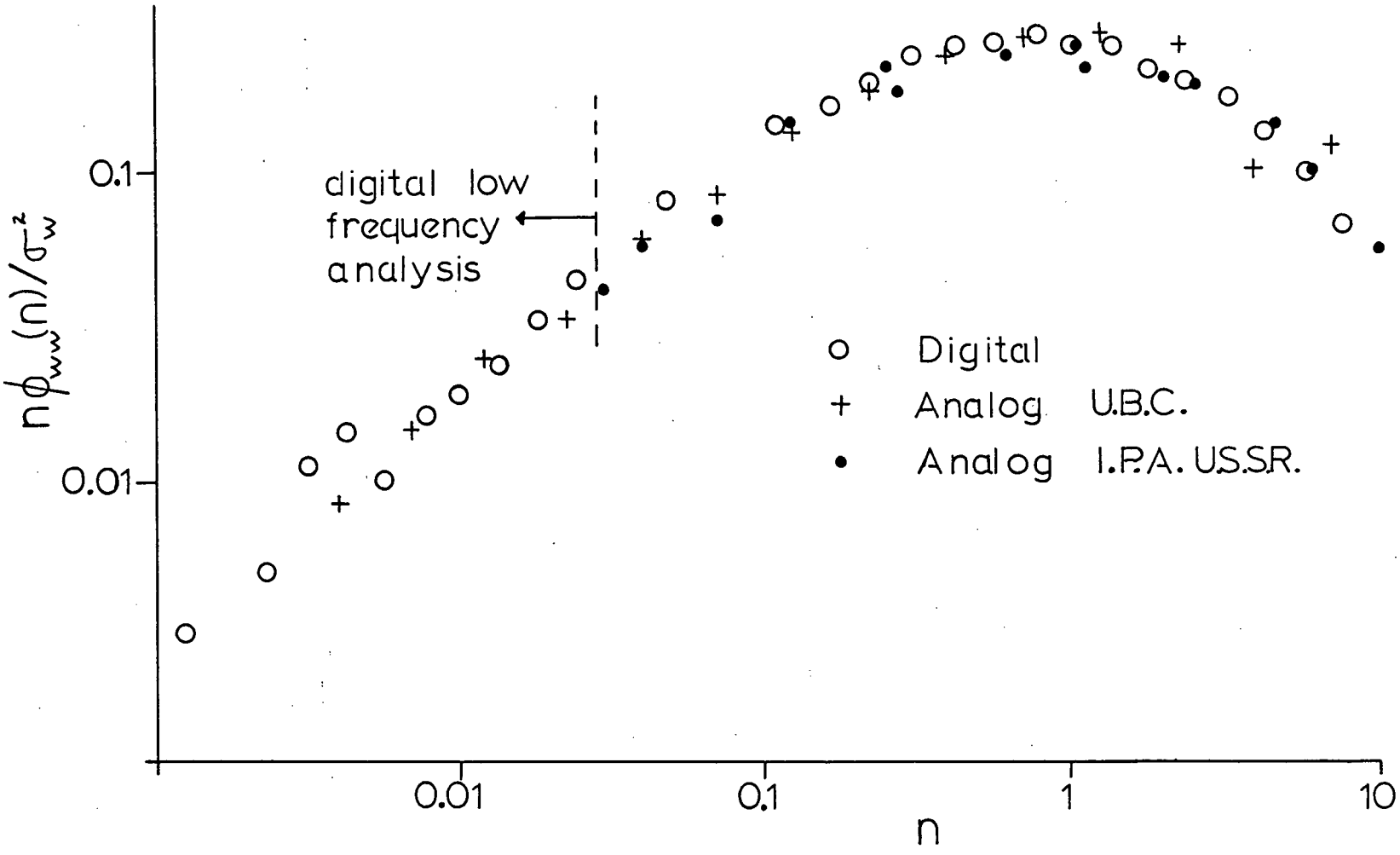

Figure 39. Comparison of three spectral analysis techniques.

analysed was collected during an IOUBC - I.P.A. "Instrument Inter-comparison" and is not included amongst those analysed for this thesis. The agreement in the spectral shapes is very good.

A forty minute section of data (also collected during the IOUBC - I.P.A. comparison) was digitized twice, once at 10 samples/sec and once at 60 samples/sec. The longitudinal velocity spectra are compared in Fig. 40. Because of the difference in digitizing rates the low frequency analysis begins at different places and its effect can be compared with the regular analysis. The horizontal bars represent the bandwidth over which each spectral estimate applies. The vertical bars represent the 80% confidence limits computed from the deviations of the estimates from block to block. For the low frequency analysis no such error estimates are available because these are only one block. However, an estimate of the variation can be obtained by computing the confidence limits based on the number of degrees of freedom of each spectral value (which, in this case, is the number of harmonics averaged over in the bandwidth). The eighty per cent confidence limits based on the number of degrees of freedom (Blackman & Tukey, 1958, p.22) are plotted for the low frequency estimates. The results of both analyses agree well within their expected error limits. These results indicate that the low frequency analysis technique is suitable for the type of analysis required.

The ROTATE program was used to convert the spectra and cospectra from the somic anemometer coordinate system (i.e. from two horizontal paths at 120° separation) to the normal x, y, z coordinate system with x in the mean wind direction and z vertical. The equations used have been given by Kaimal et al (1968). The SIMPLOT was developed to present spectra in convenient normalized forms. The outputs were both in the form of printed output and

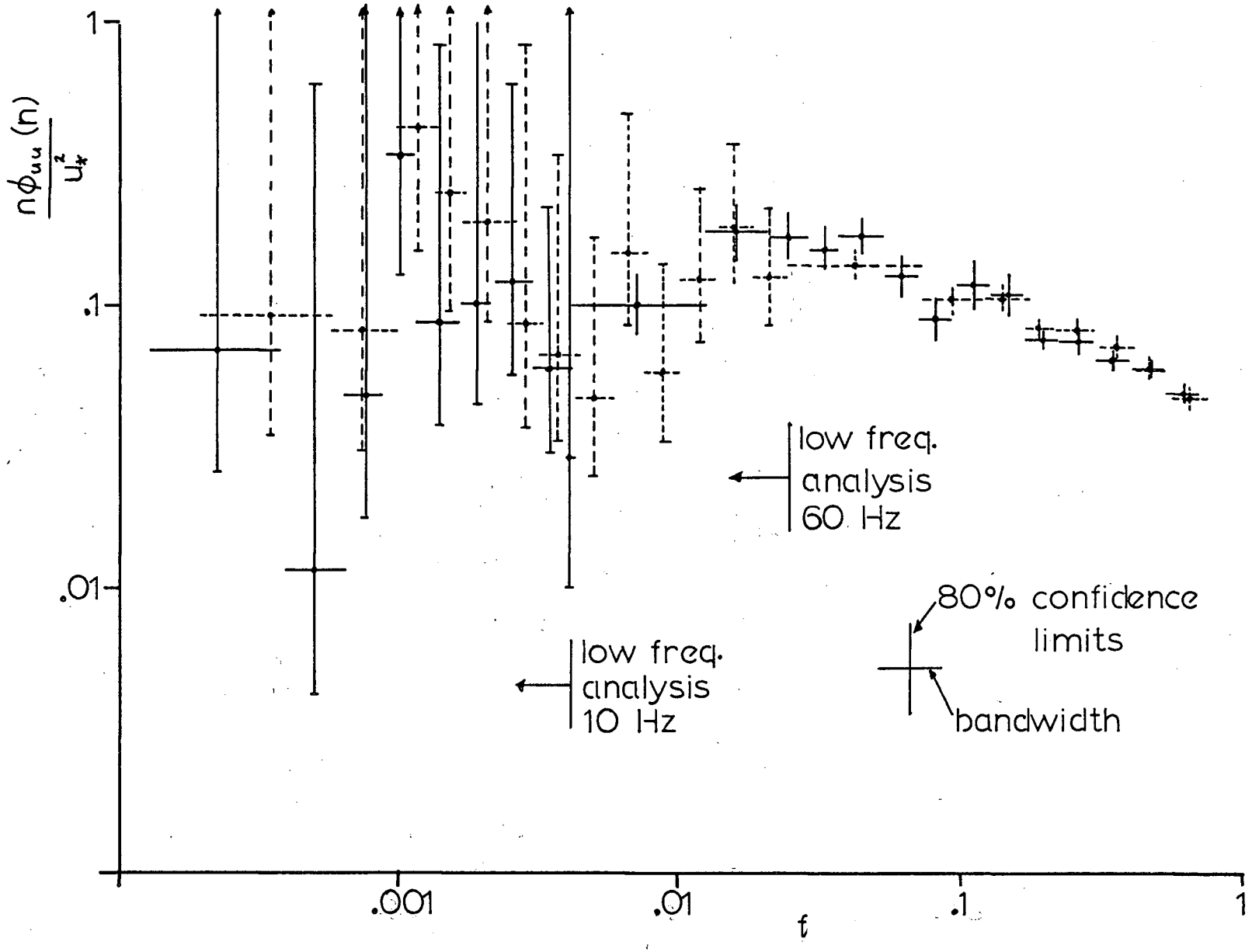

Figure 40. Check on low frequency analysis by comparing overlap of analysis regions.

graphical plots.

Since each spectral estimate was the average of estimates from each of the blocks of data it was possible to calculate the standard error of the average as:

$$S.E.(n) = \frac{\frac{1}{N}\sum_j [\phi^j(n)]^2 - \overline{\phi(n)}^2}{(N-1)^{1/2}}$$

where $\phi^j(n)$ is the spectral estimate for the j th data block

$\phi(n)$ is the average estimate for the total length of the run

N is the number of data blocks (normally 64).

The standard error of the mean is thus a measure of the variation of the spectral estimate for a given frequency n. When computing the average co-spectrum or spectral correlation coefficients for a stability group the standard error of the mean was computed as:

$$S.E.(f) = \frac{\frac{1}{M}\sum_k [\phi^k(f)]^2 - \overline{\phi(f)}^2}{(M-1)^{1/2}}$$

where $\phi^k(n)$ is estimate for frequency n for the k th run in the stability group

$\phi(n)$ is the average estimate for the group

M is the number of runs averaged (usually 7).

This standard error was plotted on the graphs of cospectrum or spectral correlation coefficients variation with stability.

APPENDIX II

HUMIDITY ANALYSIS

In measuring the humidity fluctuations it was necessary to use a 0.65 m long tube through which the air to be sampled passed. This had two major effects on the data. The first was to introduce a phase lag between the humidity fluctuations and the vertical velocity and temperature fluctuations. The second was that the tube turbulence damped out the small scale atmospheric humidity fluctuations. The simplest approach to the phase lag problem was to assume some advection velocity through the pipe, $\bar{u}_p$, and set the time lag $\tau_p = L/\bar{u}_p$ where L is the length of the pipe. This is surely an oversimplification but any more complicated correction would have required a detailed investigation of the pipe flow which was not felt to be justified. To determine $\bar{u}_p$, the tube and humidiometer were exposed to a wind in a similar experimental set-up as used during the measurements. A hot wire anemometer was used to measure the mean wind speed at the centre of the pipe near the emitter-detector tubes of the humidiometer. The measured speeds were assumed to be representative of $\bar{u}_p$. In mean wind speeds $\bar{u}$ ranging from 2 to 4 m/sec, the ratio $\bar{u}_p/\bar{u}$ scattered between 0.24 and 0.41 with no apparent wind speed dependence. Hence $\bar{u}_p = \bar{u}/3$ was assumed to be a reasonable value for all wind speeds. In computing the cospectrum of humidity and any other variable (usually vertical velocity) the cospectrum was corrected by the ratio $\cos(\Phi - 2\pi n\tau)/\cos\Phi$ where Φ is the phase angle and $2\pi n\tau = 2\pi nL/u_p$ is the correction due to the pipe. No corrections were attempted beyond $2\pi n\tau = 2\pi$ because the humidity fluctuations of higher frequencies were being damped out by the mixing in the pipe. The effect of the phase corrections was to raise the $w'q'$ correlation coefficient to nearly the value of

the coherence.

In the measurement of atmospheric humidity it is always difficult to determine the calibration of any sensor. The dew point hygrometer used in this experiment has the advantage that its calibration depends on the calibration of a platinum resistance thermometer which is comparatively easy to determine. This assumes, of course, that the dew point mirror is at the dew point temperature when dew forms on it; although contamination may have an effect it will be assumed that this is true. The Lyman-α humidiometer, on the other hand, has to be compared with another sensor that also measures humidity. The procedure adopted in this thesis was to field calibrate the humidiometer against the dew point hygrometer by running both instruments simultaneously during the experiment and comparing their low frequency spectral values.

The following approximation was developed to obtain humidity fluctuations in terms of dew point temperature fluctuations. The basic equation is the Clausius-Clapeyron equation, (for example, Haltiner and Martin, 1957, p. 23)

$$\frac{1}{e_s}\frac{de_s}{dT} = \frac{L_{lv}}{R_v T^2}$$

where e_s is the saturation vapour pressure

T is the absolute temperature

L_{lv} is the latent heat of vaporization

R_v is the perfect gas constant for water vapour.

Both L_{lv} and R_v can be assumed constant over the range of temperatures considered. This equation is equally valid for relating e, the actual vapour pressure, and T_d, the dew point temperature. Substituting e for e_s and T_d for T and integrating from T = 273° K to T gives:

$$\ln e - \ln e_o = \frac{L_{lv}}{R_v 273}\left(\frac{T_d}{T_d + 273}\right)$$

or

$$\ln e = 1.81 + 19.9\left(\frac{T_d}{T_d + 273}\right)$$

The relationship between specific humidity q and vapour pressure e is:

$$q = \frac{0.622\, e}{P - e} \simeq \frac{0.622\, e}{P}$$

Further making the substitution $q = \bar{q} - q'$ and $T_d = \bar{T}_d - T_d'$, leads to:

$$\ln\left(1 + \frac{q'}{\bar{q}}\right) + \ln\left(\frac{\bar{q}P}{0.622}\right) = 1.81 + 19.9\left(\frac{\bar{T}_d + T_d'}{273 + \bar{T}_d + T_d'}\right)$$

If the average of this equation is subtracted from it, then to first order in $q'/\bar{q}$ and T_d'/T_d:

$$q' = \left(\frac{19.9\,\bar{q}}{273 + \bar{T}_d}\right) T_d'$$

The mean $\bar{q}$ and $\bar{T}_d$ were determined for each run on the basis of sling psychrometer measurements. A linear approximation relating voltage fluctuation to humidity fluctuation was assumed for the Lyman-α humidiometer. Pond (personnel communication) has shown this to be valid for typical atmospheric humidity fluctuations. The spectra of the dew point hygrometer signal and the simultaneous humidiometer signal are shown in Fig. 41. The spectra compare very well up to f = 0.1.; at higher frequencies the response of the slower dew-point hygrometer falls off.

It is believed that the fall-off with frequency of the Lyman-α humidiometer output was due to increased mixing in the intake tubes. Taylor (1954) has determined the coefficient of mixing of matter in turbulent flow in a

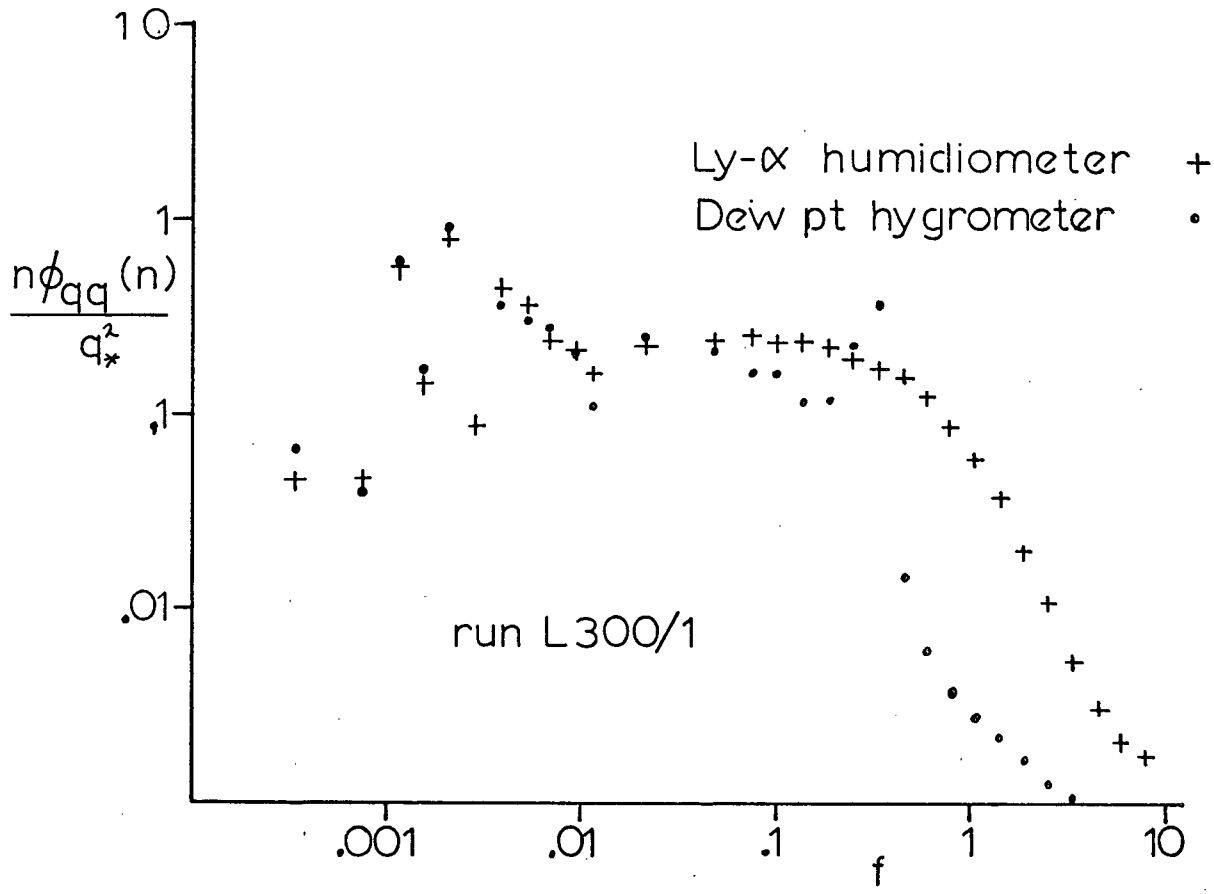

Figure 41. Comparison of spectral estimates of Lyman-α humidiometer and dew point hygrometer.

tube. Although the results are not exactly applicable because of length/diameter ratio of the humidiometer tube was only 20 (compared to several hundred for Taylor's measurements) some idea of the effects of mixing can be obtained. Taylor showed that $K = 10.1\ au(\frac{u_*}{\bar{u}})$ where K is the "virtual coefficient of mixing", a, the radius of the tube, and $\bar{u}$ the mean flow speed. For flow in smooth pipes (again when length/diameter is large enough) $u_*/\bar{u}$ depends only on the Reynolds number. For run 300/1, the pipe Reynolds number, $Re \sim 4 \times 10^3$ and hence $\bar{u}/u_* \simeq 14$ which gives $K \sim 200$. The Prandtl Number ν/K, is thus about 10^{-3}. For flows at low Prandtl Number the spectrum of a scalar should fall off from $k^{-5/3}$ near $k_c = (\nu/K^3)^{1/4}$. The dissipation in the pipe was estimated from $\epsilon = u_*^3/\kappa z$ to be about 5×10^3 cm sec^{-3} which agrees with Laufer's (1954) measurements of 4×10^3 $cm^2 sec^{-3}$ for a higher Re flow. Hence k_c for the pipe flow will be about $0.2 cm^{-1}$. For run 300/1 the change in slope occurred at n = 3 which corresponds to k_c $0.1 cm^{-1}$. This good agreement supports the hypothesis that the fall off from f 1.0 was due to mixing in the tube and hence not a result indicative of atmospheric humidity fluctuations.

APPENDIX III

TABULATION OF RESULTS

LADNER

All results in cm sec^{-1}, °C, or g/Kg.

TABLE AIII.I

#	RUN	DATE	DURATION	$\bar{u}$	z/L	z/L_q
1	216/1	15 AUG	2057-2109	277	-0.063	0.0
2	216/2	15 AUG	2109-2121	220	-0.000	0.0
3	216/3	15 AUG	2121-2132	163	-0.382	0.0
4	218/1	16 AUG	1358-1405	480	-0.173	0.0
5	218/2/1	16 AUG	1420-1434	435	-0.190	0.0
6	218/2/2	16 AUG	1434-1447	469	-0.157	0.0
7	219/1	16 AUG	1521-1536	394	-0.220	0.0
8	219/2	16 AUG	1536-1550	385	-0.240	0.0
9	219/3	16 AUG	1600-1605	361	-0.235	0.0
10	219/4	16 AUG	1605-1619	361	-0.212	0.0
11	220/1/1	21 AUG	1321-1338	334	-0.471	-0.034
12	220/1/2	21 AUG	1338-1355	294	-0.548	-0.039
13	220/2/1	21 AUG	1419-1434	352	-0.308	-0.017
14	220/2/2	21 AUG	1434-1443	403	-0.180	-0.009
15	221/1	21 AUG	1558-1613	339	-0.620	-0.039
16	221/2	21 AUG	1613-1629	307	-0.285	-0.022
17	221/3	21 AUG	1629-1636	245	-0.537	-0.049
18	222/1	21 AUG	1830-1847	319	-0.268	-0.006
19	222/2	21 AUG	1847-1905	297	-0.278	-0.007
20	222/4	21 AUG	1909-1927	263	-0.294	-0.004
21	223/1	21 AUG	2004-2015	155	-0.448	0.006
22	223/2	21 AUG	2015-2026	139	-0.303	0.010
23	217/1	22 AUG	933- 950	445	-0.136	-0.005
24	217/2	22 AUG	950-1007	501	-0.131	-0.004
25	217/3	22 AUG	1007-1024	492	-0.191	-0.004
26	224/1	22 AUG	1204-1218	526	-0.110	-0.004
27	224/2	22 AUG	1218-1231	508	-0.146	-0.005
28	224/3	22 AUG	1231-1249	487	-0.198	-0.008
29	224/4	22 AUG	1249-1254	487	-0.154	-0.006
30	300/1	22 AUG	1436-1449	637	-0.051	-0.002
31	300/2	22 AUG	1449-1502	596	-0.057	-0.002
32	300/3	22 AUG	1502-1515	586	-0.057	-0.002
33	300/4	22 AUG	1515-1528	585	-0.067	-0.002
34	300/5	22 AUG	1528-1542	557	-0.068	-0.003
35	300/LONG	22 AUG	1436-1530	592	-0.057	-0.002
36	301/1	22 AUG	1554-1607	552	-0.063	-0.005
37	301/2	22 AUG	1607-1620	567	-0.042	-0.003
38	301/3	22 AUG	1620-1633	562	-0.046	-0.003
39	301/4	22 AUG	1633-1646	578	-0.045	0.0
40	301/5	22 AUG	1653-1659	560	-0.053	0.0
41	302/1	22 AUG	1713-1727	472	-0.046	-0.003
42	302/2/1	22 AUG	1736-1750	509	-0.026	-0.001
43	302/2/2	22 AUG	1750-1802	486	-0.033	-0.002
44	302/3	22 AUG	1802-1816	463	-0.023	-0.002
45	303/1/1	22 AUG	1915-1929	327	0.039	-0.003
46	303/1/2	22 AUG	1929-1942	302	0.083	-0.002
47	303/2/1	22 AUG	1954-2005	155	0.658	0.001

TABLE AIII.1 (CONT.)

#	RUN	DATE	DURATION	$\bar{u}$	z/L	z/L_q
48	303/2/2	22 AUG	2005-2016	148	1.583	0.003
49	304/1	22 AUG	2057-2110	150	3.719	0.085
50	304/2	22 AUG	2124-2135	195	2.876	0.015
51	305/1/1	22 AUG	2208-2219	200	0.288	0.009
52	305/1/2	22 AUG	2219-2228	207	4.188	0.036
53	305/2	22 AUG	2228-2241	194	5.783	0.020
54	305/3/1	22 AUG	2242-2253	138	0.995	0.001
55	305/3/2	22 AUG	2253-2304	103	7.253	0.124
56	306/1	23 AUG	1016-1030	309	-0.384	-0.017
57	306/2	23 AUG	1034-1049	303	-0.321	-0.012
58	306/3	23 AUG	1054-1108	306	-0.499	-0.016
59	306/4	23 AUG	1110-1124	293	-0.366	-0.011
60	307/1	23 AUG	1210-1223	363	-0.357	-0.011
61	307/2	23 AUG	1223-1235	327	-0.380	-0.014
62	307/3	23 AUG	1235-1247	293	-0.567	-0.018
63	307/4	23 AUG	1247-1300	278	-0.364	0.0
64	307/5	23 AUG	1300-1312	251	-0.554	0.0
65	307/LONG	23 AUG	1210-1257	327	-0.383	-0.011
66	308/1	23 AUG	1334-1348	332	-0.428	-0.014
67	308/2	23 AUG	1354-1405	394	-0.248	-0.009
68	308/3/1	23 AUG	1407-1418	436	-0.221	-0.008
69	308/3/2	23 AUG	1418-1429	443	-0.195	-0.007
70	318/1/1	23 AUG	1524-1538	352	-0.083	0.0
71	318/1/2	23 AUG	1538-1551	328	-0.100	0.0
72	318/2/1	23 AUG	1623-1637	312	-0.083	0.0
73	318/2/2	23 AUG	1637-1650	324	-0.091	0.0
74	309/1/1	23 AUG	1746-1759	359	-0.137	-0.008
75	309/1/2	23 AUG	1759-1811	349	-0.117	-0.007
76	309/2/1	23 AUG	1813-1825	318	-0.142	-0.012
77	309/2/2	23 AUG	1825-1838	294	-0.008	-0.007
78	309/3	23 AUG	1843-1854	241	-0.071	-0.015
79	310/1	23 AUG	2034-2046	167	1.349	0.104
80	310/2	23 AUG	2049-2104	223	0.003	0.003
81	310/3	23 AUG	2115-2126	130	0.472	0.019
82	311/1/1	24 AUG	1011-1024	684	-0.049	-0.001
83	311/1/2	24 AUG	1024-1037	613	-0.063	-0.001
84	311/2/1	24 AUG	1043-1056	538	-0.143	-0.003
85	311/2/2	24 AUG	1056-1110	578	-0.109	-0.003
86	312/1/1	24 AUG	1137-1151	584	-0.131	-0.002
87	312/1/2	24 AUG	1151-1204	662	-0.082	-0.002
88	312/1/3	24 AUG	1204-1218	711	-0.075	-0.002
89	312/2/1	24 AUG	1219-1230	643	-0.061	-0.001
90	312/2/2	24 AUG	1230-1242	700	-0.080	-0.001
91	314/1	24 AUG	1336-1349	494	-0.172	-0.002
92	314/2	24 AUG	1349-1403	456	-0.121	-0.003
93	314/3	24 AUG	1403-1411	420	-0.105	-0.002

TABLE AIII.II

#	z/L	u_*	T_*	q_*	$\frac{\sigma_u}{u_*}$	$\frac{\sigma_v}{u_*}$	$\frac{\sigma_w}{u_*}$	$\frac{\sigma_T}{T_*}$	$\frac{\sigma_q}{q_*}$
1	-0.07	17.52	0.191	0.0	2.49	2.04	1.52	3.82	*******
2	-0.00	14.25	0.000	0.0	2.39	2.01	1.51	4103.37	*******
3	-0.38	11.09	0.428	0.0	2.58	2.59	1.32	1.59	*******
4	-0.18	26.46	1.162	0.0	2.69	2.72	1.86	0.42	*******
5	-0.19	25.30	1.136	0.0	2.68	2.57	1.74	0.42	*******
6	-0.16	27.20	1.084	0.0	2.34	2.25	1.66	0.44	*******
7	-0.22	21.28	0.933	0.0	2.49	2.72	1.84	0.39	*******
8	-0.24	20.00	0.896	0.0	2.61	2.72	1.84	0.36	*******
9	-0.24	20.00	0.879	0.0	2.79	2.88	1.80	0.40	*******
10	-0.21	20.17	0.808	0.0	2.78	2.68	1.79	0.41	*******
11	-0.47	21.21	1.838	0.800	2.59	2.51	1.57	0.46	0.51
12	-0.55	23.02	2.519	1.074	2.59	2.32	1.54	0.40	0.45
13	-0.31	27.93	2.121	0.704	2.16	2.11	1.37	0.51	0.58
14	-0.18	31.62	1.605	0.448	1.98	1.78	1.26	0.61	0.74
15	-0.62	18.71	1.911	0.720	2.93	2.93	1.82	0.42	0.51
16	-0.28	23.24	1.334	0.626	2.05	2.41	1.42	0.54	0.57
17	-0.54	17.89	1.467	0.820	2.75	2.86	1.62	0.44	0.51
18	-0.27	17.83	0.774	0.108	2.24	2.09	1.56	0.52	1.20
19	-0.28	16.58	0.693	0.106	2.18	1.88	1.51	0.53	1.04
20	-0.29	15.00	0.607	0.050	2.33	2.01	1.57	0.56	1.78
21	-0.45	9.85	0.409	-0.029	1.85	1.62	1.44	0.54	0.68
22	-0.30	9.22	0.247	-0.043	1.88	1.54	1.30	0.73	0.63
23	-0.14	24.90	0.756	0.155	2.59	2.28	1.64	0.67	1.10
24	-0.13	28.28	0.946	0.161	2.35	2.34	1.65	0.53	0.75
25	-0.19	24.49	1.041	0.119	2.85	2.60	1.82	0.55	1.09
26	-0.11	38.08	1.425	0.320	2.19	1.83	1.36	0.54	0.59
27	-0.15	32.56	1.298	0.260	2.43	1.84	1.40	0.59	0.73
28	-0.20	28.81	1.467	0.364	2.33	2.07	1.57	0.53	0.55
29	-0.15	31.46	1.359	0.317	2.35	1.90	1.43	0.60	0.57
30	-0.05	51.28	1.219	0.238	2.05	1.74	1.36	0.62	0.76
31	-0.06	47.54	1.183	0.214	2.15	1.92	1.35	0.60	0.89
32	-0.06	46.80	1.133	0.234	2.13	1.79	1.38	0.63	0.81
33	-0.07	44.50	1.208	0.256	2.17	2.12	1.46	0.60	0.78
34	-0.07	43.47	1.162	0.271	2.10	1.91	1.41	0.57	0.70
35	-0.06	47.75	1.178	0.237	2.24	1.97	1.38	0.65	0.85
36	-0.06	40.50	0.901	0.425	2.33	2.06	1.51	0.63	0.49
37	-0.04	47.22	0.826	0.361	2.14	1.80	1.29	0.68	0.55
38	-0.05	45.28	0.845	0.238	2.06	1.81	1.36	0.62	0.56
39	-0.04	43.01	0.779	0.0	2.12	1.94	1.42	0.56	*******
40	-0.05	40.37	0.811	0.0	2.08	1.97	1.53	0.53	*******
41	-0.05	40.25	0.652	0.222	2.05	1.73	1.35	0.67	0.58
42	-0.03	44.72	0.472	0.135	2.09	1.67	1.30	0.74	0.89
43	-0.03	35.50	0.366	0.105	2.26	1.97	1.41	0.79	1.24
44	-0.02	39.37	0.304	0.184	2.04	1.73	1.33	0.66	0.87
45	0.04	25.30	-0.251	0.087	2.26	1.94	1.48	0.80	0.95
46	0.08	20.74	-0.341	0.051	2.60	2.10	1.60	0.73	1.42
47	0.66	8.49	-0.442	-0.004	2.95	2.39	1.86	0.75	8.00

TABLE AIII.II (CONT.)

#	z/L	u_*	T_*	q_*	$\frac{\sigma_u}{u_*}$	$\frac{\sigma_v}{u_*}$	$\frac{\sigma_w}{u_*}$	$\frac{\sigma_T}{T_*}$	$\frac{\sigma_q}{q_*}$
48	1.58	5.74	-0.487	-0.004	3.46	3.31	2.09	0.80	4.37
49	3.72	2.83	-0.265	-0.035	2.93	3.96	2.37	1.36	1.41
50	2.88	3.16	-0.261	-0.008	4.24	3.42	2.31	0.92	1.77
51	0.29	7.21	-0.132	-0.024	2.40	2.12	1.59	1.90	1.28
52	4.19	2.37	-0.211	-0.011	3.68	2.87	2.28	0.99	2.46
53	5.78	2.12	-0.236	-0.005	4.43	3.03	2.26	1.06	7.09
54	1.00	3.87	-0.136	-0.001	3.00	2.45	1.69	0.96	196.89
55	7.25	0.73	-0.034	-0.003	4.53	2.88	2.61	2.33	0.61
56	-0.38	22.58	1.749	0.462	2.37	2.51	1.59	0.41	0.48
57	-0.32	25.69	1.907	0.405	2.09	2.30	1.50	0.43	0.59
58	-0.50	20.74	1.941	0.354	2.51	2.82	1.78	0.41	0.51
59	-0.37	22.14	1.626	0.281	2.89	2.47	1.52	0.49	0.64
60	-0.36	24.70	1.984	0.356	2.75	2.71	1.73	0.46	0.79
61	-0.38	26.46	2.410	0.520	2.74	2.50	1.67	0.43	0.58
62	-0.57	22.58	2.635	0.469	2.88	2.86	1.69	0.40	0.58
63	-0.36	27.02	2.498	0.0	2.48	2.36	1.49	0.48	*******
64	-0.55	22.36	2.605	0.0	3.09	3.14	1.83	0.40	*******
65	-0.38	24.49	2.102	0.337	3.09	2.84	1.60	0.47	0.80
66	-0.43	24.70	2.379	0.459	2.69	3.11	1.66	0.42	0.55
67	-0.25	28.28	1.803	0.382	2.38	2.15	1.51	0.49	0.55
68	-0.22	28.98	1.691	0.357	2.40	2.24	1.54	0.50	0.53
69	-0.19	30.50	1.648	0.353	2.35	1.91	1.41	0.54	0.68
70	-0.08	32.56	1.659	0.0	2.00	2.04	1.25	0.61	*******
71	-0.10	28.64	1.554	0.0	2.18	2.29	1.35	0.61	*******
72	-0.08	28.98	1.320	0.0	2.31	2.01	1.26	0.63	*******
73	-0.09	28.11	1.352	0.0	2.40	2.21	1.32	0.62	*******
74	-0.14	26.46	0.850	0.308	2.28	2.01	1.50	0.58	0.49
75	-0.12	26.83	0.745	0.258	2.33	1.98	1.46	0.56	0.50
76	-0.14	21.68	0.577	0.299	2.47	2.33	1.50	0.57	0.74
77	-0.01	19.49	0.001	0.147	2.66	2.28	1.45	54.58	61.97
78	-0.07	14.49	0.110	0.167	2.48	2.48	1.55	0.45	0.90
79	1.35	4.58	-0.240	-0.115	3.19	2.18	1.79	1.25	1.83
80	0.00	14.18	-0.002	-0.026	2.22	1.65	1.38	119.09	2.68
81	0.47	5.83	-0.141	-0.033	2.50	2.21	1.41	1.34	1.23
82	-0.05	39.24	0.675	0.098	2.47	2.23	1.60	0.64	1.00
83	-0.06	37.56	0.805	0.104	2.29	1.86	1.40	0.67	1.02
84	-0.14	29.48	1.128	0.148	2.66	2.22	1.64	0.57	1.56
85	-0.11	33.32	1.103	0.149	2.49	2.15	1.55	0.60	1.41
86	-0.13	33.62	1.361	0.147	2.34	2.39	1.63	0.59	1.49
87	-0.08	41.11	1.265	0.152	2.32	2.20	1.45	0.62	1.45
88	-0.08	41.83	1.213	0.137	2.38	2.09	1.50	0.66	1.60
89	-0.06	43.13	1.043	0.110	2.43	2.00	1.53	0.68	1.73
90	-0.08	36.06	0.957	0.069	2.65	2.31	1.60	0.66	2.74
91	-0.17	30.33	1.459	0.115	2.49	2.46	1.65	0.56	2.25
92	-0.12	28.98	0.932	0.121	2.30	2.22	1.54	0.54	1.57
93	-0.10	28.11	0.756	0.089	2.53	1.99	1.50	0.57	1.57

TABLE AIII.III

#	RUN	z/L	r_{uw}	r_{wT}	r_{wq}
1	216/1	-0.07	-0.26	0.07	*****
2	216/2	-0.00	-0.28	0.00	*****
3	216/3	-0.38	-0.21	0.14	*****
4	218/1	-0.18	-0.20	0.51	*****
5	218/2/1	-0.19	-0.21	0.54	*****
6	218/2/2	-0.16	-0.26	0.55	*****
7	219/1	-0.22	-0.22	0.56	*****
8	219/2	-0.24	-0.21	0.61	*****
9	219/3	-0.24	-0.20	0.56	*****
10	219/4	-0.21	-0.20	0.55	*****
11	220/1/1	-0.47	-0.25	0.55	0.50
12	220/1/2	-0.55	-0.25	0.65	0.58
13	220/2/1	-0.31	-0.34	0.57	0.50
14	220/2/2	-0.18	-0.40	0.52	0.43
15	221/1	-0.62	-0.19	0.52	0.43
16	221/2	-0.28	-0.34	0.52	0.49
17	221/3	-0.54	-0.22	0.56	0.48
18	222/1	-0.27	-0.29	0.50	0.21
19	222/2	-0.28	-0.30	0.50	0.25
20	222/4	-0.29	-0.27	0.46	0.14
21	223/1	-0.45	-0.38	0.52	-0.41
22	223/2	-0.30	-0.41	0.42	-0.49
23	217/1	-0.14	-0.23	0.36	0.22
24	217/2	-0.13	-0.26	0.46	0.33
25	217/3	-0.19	-0.19	0.40	0.20
26	224/1	-0.11	-0.34	0.55	0.50
27	224/2	-0.15	-0.29	0.48	0.39
28	224/3	-0.20	-0.27	0.48	0.46
29	224/4	-0.15	-0.30	0.47	0.49
30	300/1	-0.05	-0.36	0.48	0.39
31	300/2	-0.06	-0.35	0.49	0.33
32	300/3	-0.06	-0.34	0.46	0.36
33	300/4	-0.07	-0.32	0.45	0.35
34	300/5	-0.07	-0.34	0.50	0.41
35	300/LONG	-0.06	-0.32	0.44	0.34
36	301/1	-0.06	-0.28	0.42	0.54
37	301/2	-0.04	-0.36	0.46	0.56
38	301/3	-0.05	-0.36	0.48	0.53
39	301/4	-0.04	-0.33	0.50	*****
40	301/5	-0.05	-0.31	0.49	*****
41	302/1	-0.05	-0.36	0.44	0.51
42	302/2/1	-0.03	-0.37	0.41	0.34
43	302/2/2	-0.03	-0.31	0.36	0.23
44	302/3	-0.02	-0.37	0.46	0.35
45	303/1/1	0.04	-0.30	-0.34	0.28
46	303/1/2	0.08	-0.24	-0.34	0.18
47	303/2/1	0.66	-0.18	-0.29	-0.03

TABLE AIII.III (CONT.)

#	RUN	z/L	r_{uw}	r_{wT}	r_{wq}
48	303/2/2	1.58	-0.14	-0.24	-0.04
49	304/1	3.72	-0.14	-0.12	-0.12
50	304/2	2.88	-0.10	-0.19	-0.10
51	305/1/1	0.29	-0.26	-0.13	-0.20
52	305/1/2	4.19	-0.12	-0.18	-0.07
53	305/2	5.78	-0.10	-0.17	-0.03
54	305/3/1	1.00	-0.21	-0.26	-0.00
55	305/3/2	7.25	-0.08	-0.07	-0.02
56	306/1	-0.38	-0.26	0.61	0.53
57	306/2	-0.32	-0.32	0.62	0.45
58	306/3	-0.50	-0.22	0.54	0.44
59	306/4	-0.37	-0.23	0.54	0.41
60	307/1	-0.36	-0.21	0.50	0.29
61	307/2	-0.38	-0.22	0.55	0.41
62	307/3	-0.57	-0.21	0.59	0.41
63	307/4	-0.36	-0.27	0.56	*****
64	307/5	-0.55	-0.18	0.54	*****
65	307/LONG	-0.38	-0.20	0.54	0.31
66	308/1	-0.43	-0.22	0.57	0.44
67	308/2	-0.25	-0.28	0.54	0.48
68	308/3/1	-0.22	-0.27	0.52	0.49
69	308/3/2	-0.19	-0.30	0.52	0.42
70	318/1/1	-0.08	-0.40	0.52	*****
71	318/1/2	-0.10	-0.34	0.48	*****
72	318/2/1	-0.08	-0.34	0.51	*****
73	318/2/2	-0.09	-0.32	0.49	*****
74	309/1/1	-0.14	-0.29	0.46	0.55
75	309/1/2	-0.12	-0.29	0.48	0.54
76	309/2/1	-0.14	-0.27	0.46	0.36
77	309/2/2	-0.01	-0.26	0.01	0.00
78	309/3	-0.07	-0.26	0.57	0.29
79	310/1	1.35	-0.18	-0.18	-0.12
80	310/2	0.00	-0.33	-0.00	-0.11
81	310/3	0.47	-0.28	-0.21	-0.23
82	311/1/1	-0.05	-0.25	0.39	0.25
83	311/1/2	-0.06	-0.31	0.43	0.28
84	311/2/1	-0.14	-0.23	0.43	0.16
85	311/2/2	-0.11	-0.26	0.43	0.18
86	312/1/1	-0.13	-0.26	0.42	0.16
87	312/1/2	-0.08	-0.30	0.45	0.19
88	312/1/3	-0.08	-0.28	0.40	0.17
89	312/2/1	-0.06	-0.27	0.38	0.15
90	312/2/2	-0.08	-0.22	0.36	0.09
91	314/1	-0.17	-0.24	0.44	0.11
92	314/2	-0.12	-0.28	0.48	0.16
93	314/3	-0.10	-0.26	0.47	0.17

APPENDIX IV

TABULATION OF RESULTS

BOMEX

All results in cm sec^{-1}, °C, or g/Kg.

TABLE AIV.I

#	RUN	DATE	DURATION	$\bar{u}$	z/L	z/q
1	B14/1	6 MAY	1145-1226	670	-0.080	-0.046
2	B14/2	6 MAY	1431-1523	620	-0.067	-0.036
3	B15/1	6 MAY	1811-1854	580	-0.140	-0.080
4	B15/2	6 MAY	1902-1937	530	-0.129	-0.068
5	B15/3	6 MAY	1959-2043	370	-0.360	-0.140

TABLE AIV.II

#	z/L	u_*	T_* [1]	q_* [1]	$\frac{\sigma_u}{u_*}$	$\frac{\sigma_v}{u_*}$	$\frac{\sigma_w}{u_*}$	$\frac{\sigma_T}{T_*}$	$\frac{\sigma_q}{q_*}$
1	-0.08	27.8	0.70	0.89	2.0	2.0	1.20	1.0	0.8
2	-0.07	25.9	0.62	0.91	2.0	1.9	1.15	1.1	0.8
3	-0.14	21.7	0.88	0.50	1.9	2.0	1.15	0.8	0.5
4	-0.13	20.8	0.86	0.50	2.0	1.6	1.10	0.7	0.4
5	-0.36	15.6	0.69	0.42	2.1	1.8	1.44	0.8	0.5

1 - uncalibrated

TABLE AIV.II

#	RUN	z/L	r_{uw}	r_{wT}	r_{wq}
1	B14/1	-0.08	-0.40	0.26	0.34
2	B14/2	-0.07	-0.43	0.31	0.45
3	B15/1	-0.14	-0.46	0.32	0.55
4	B15/2	-0.13	-0.41	0.41	0.65
5	B15/3	-0.36	-0.34	0.33	0.53

APPENDIX V

SPECTRUM ANALYSIS RESULTS

In this appendix the composite cospectra and spectral correlation coefficients of momentum, heat, and moisture transfer for stability Groups II, V, VI, VIIIA, and VIIIB are presented. On each figure up to seven data runs are presented and the symbols can be identified with runs by use of Table AV.I. All cospectra are normalized and plotted on double logarithmic coordinates

TABLE AV.I Identification of Runs on Composite Plots

See Table AIII.I to identify run numbers.

Stability Group	•	×	+	○	△	□	▽
I	11	12	15	17	58	62	64
III	13	16	19	25	57	68	69
V	30	32	34	37	39	41	88
VI	42	43	44	45	46	77	80
VIIIA	48	49	50	79			
VIIIB	52	53	55				

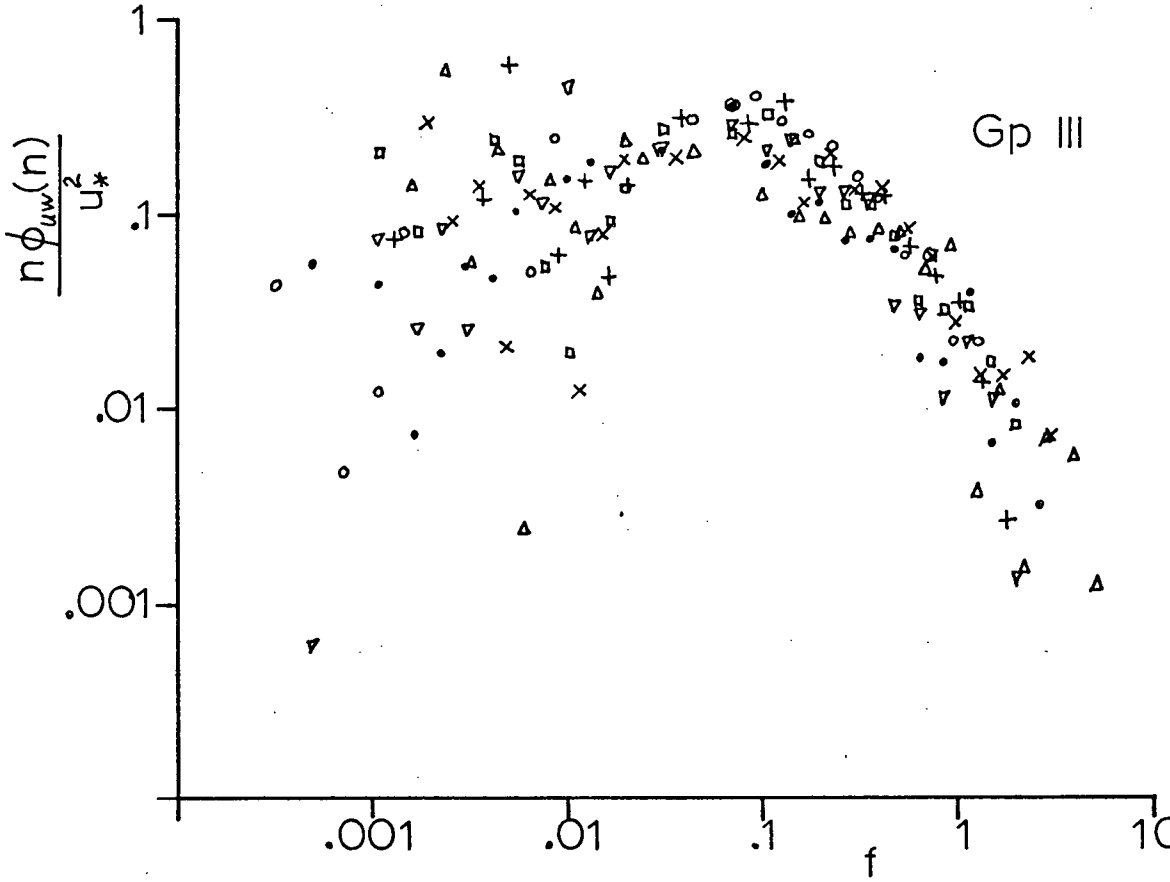
Gp III
$\frac{n\phi_{uw}(n)}{u_*^2}$
1
.1
.01
.001
.001
.01
.1
1
10
f

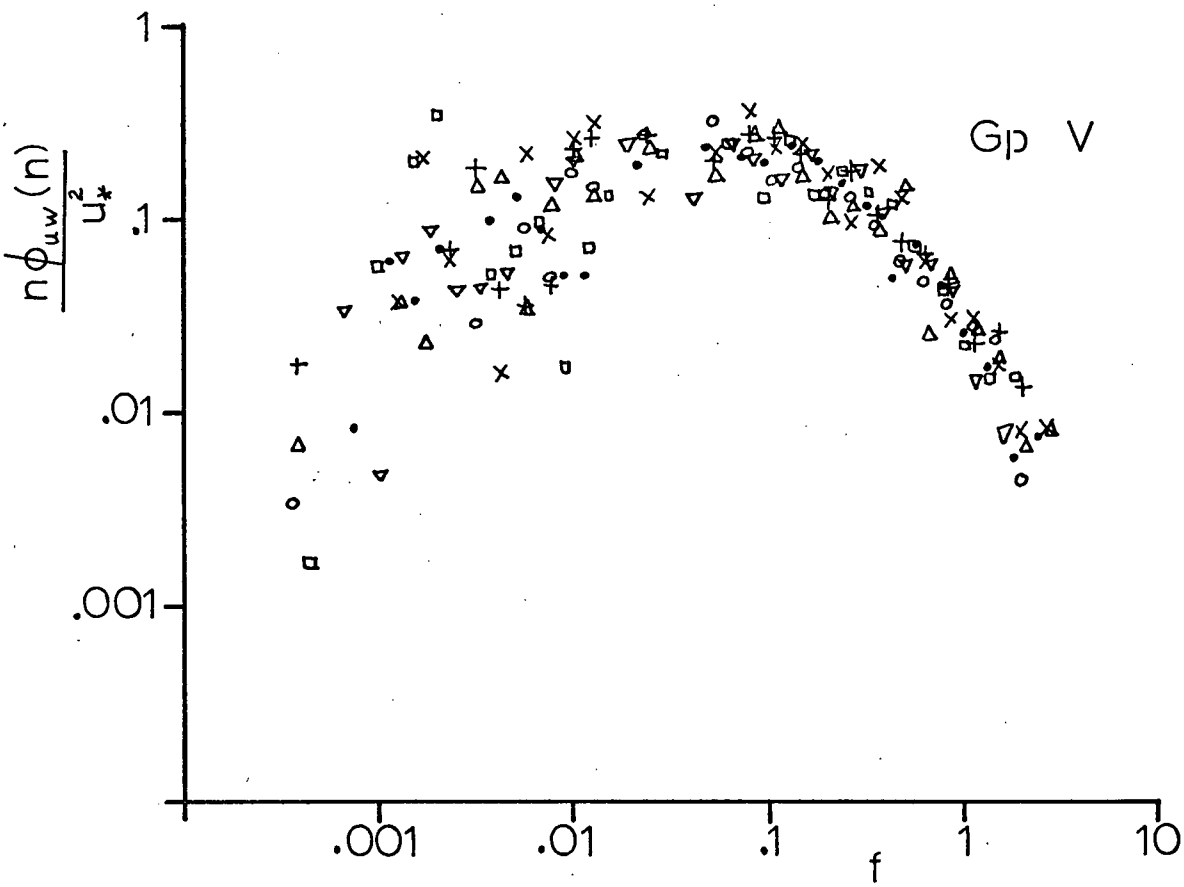
Gp V
$\frac{n\phi_{uw}(n)}{u_*^2}$
1
.1
.01
.001
.001
.01
.1
1
10
f

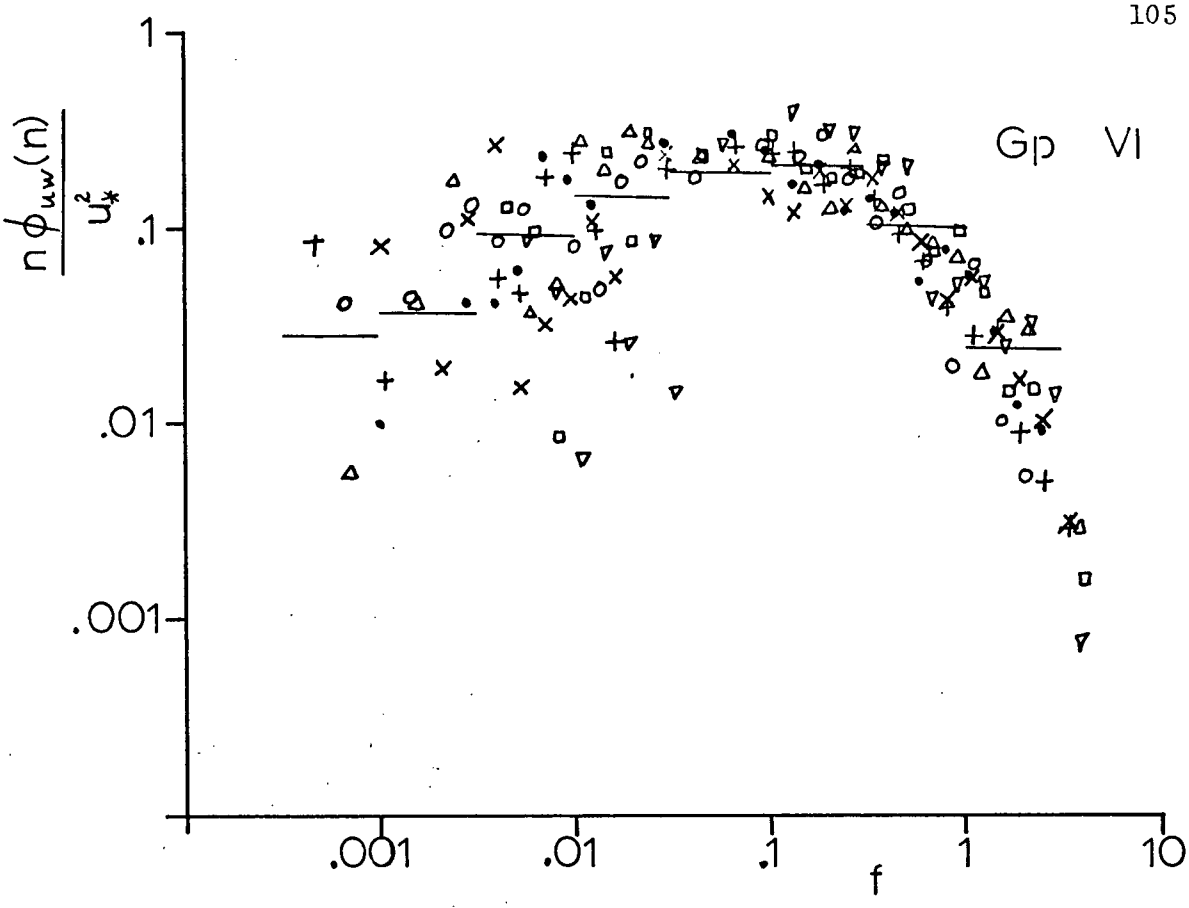
Gp VI
$\frac{n\phi_{uw}(n)}{u_*^2}$
1
.1
.01
.001
.001
.01
.1
1
10
f

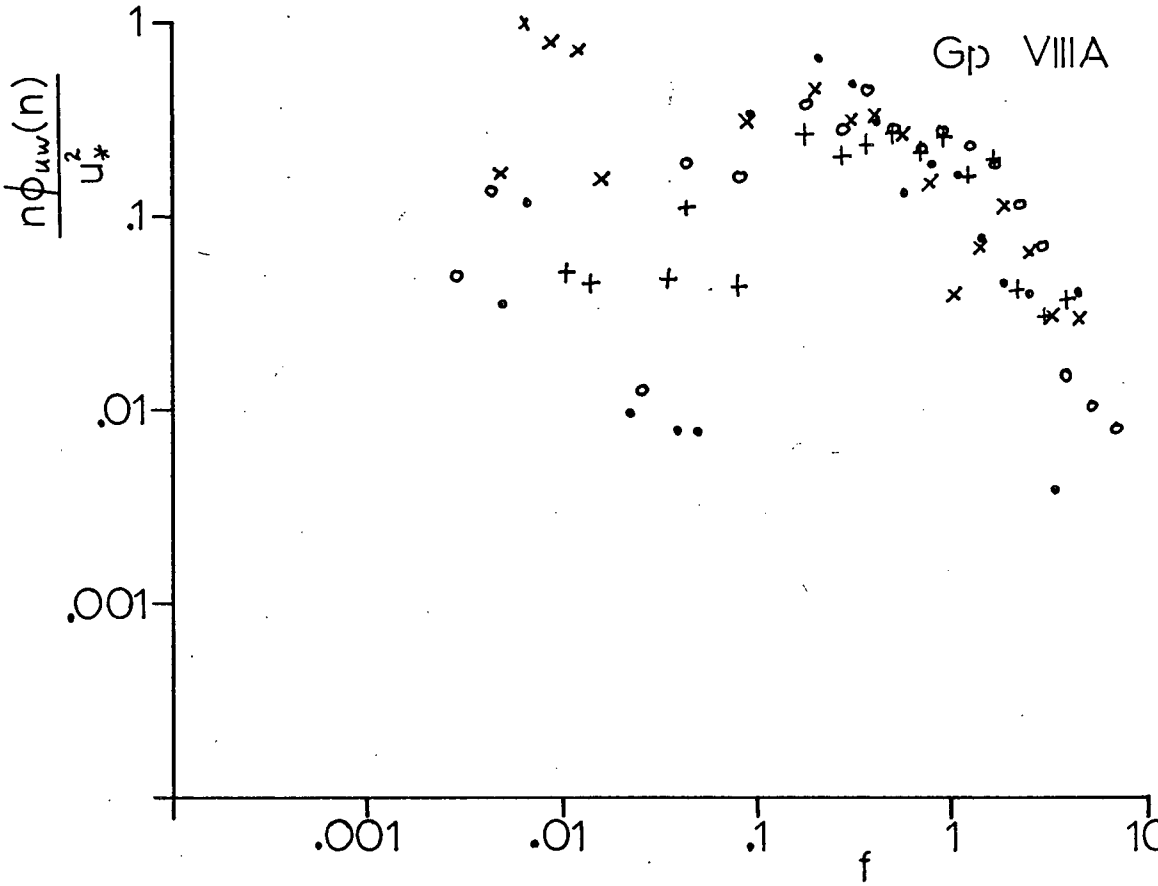
Gp VIIIA
$\frac{n\phi_{uw}(n)}{u_*^2}$
1
.1
.01
.001
.001
.01
.1
1
10
f

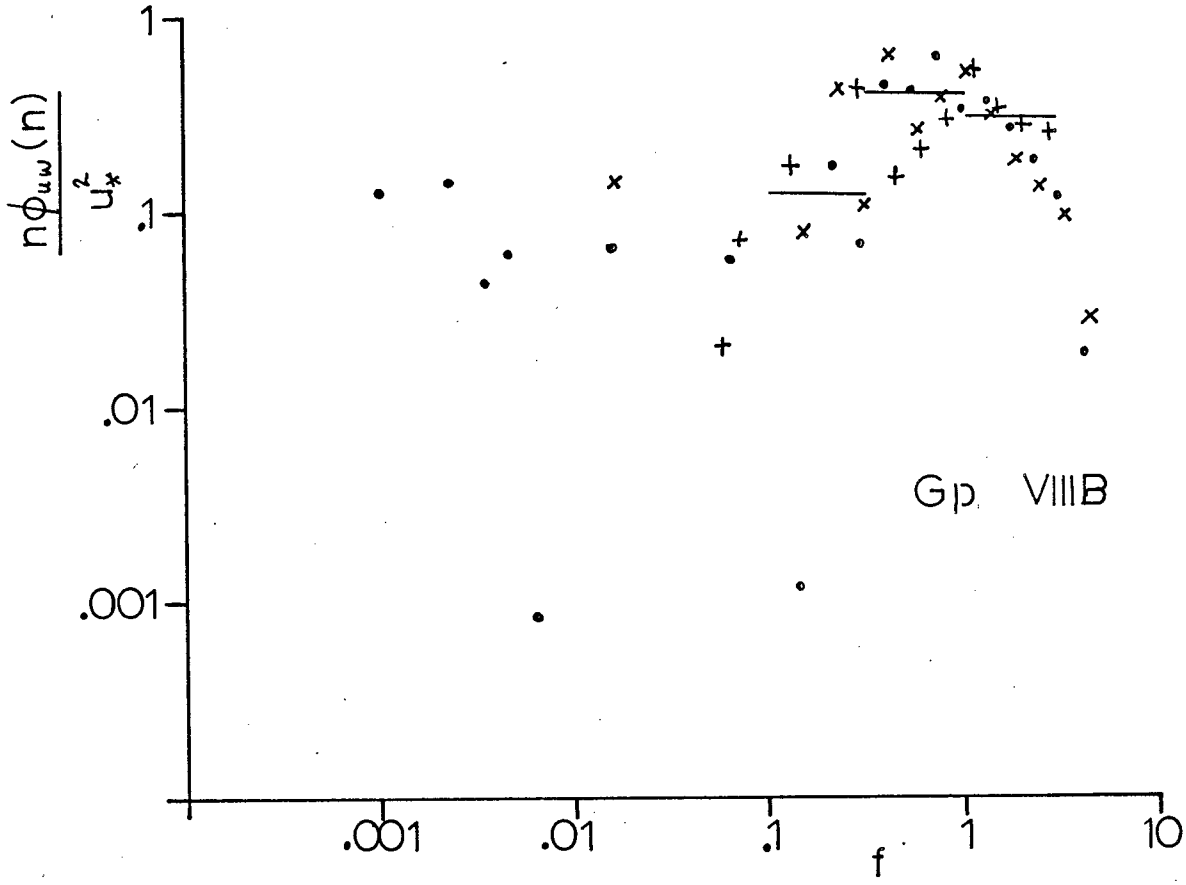
$\frac{n\phi_{uw}(n)}{u_*^2}$
1
.1
.01
.001
Gp VIIIB
.001
.01
.1
1
10
f

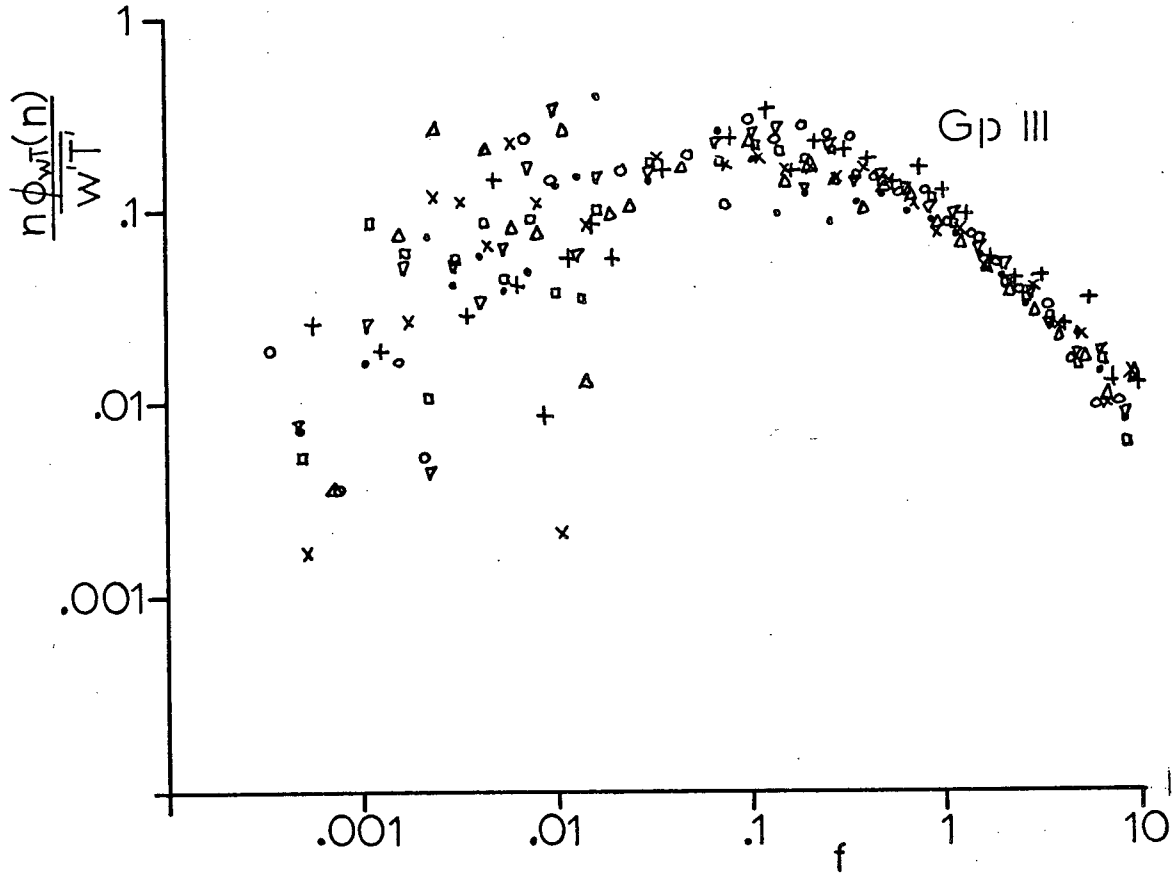
$\frac{n\phi_{wT}(n)}{\overline{w'T'}}$
1
.1
.01
.001
Gp III
.001
.01
.1
1
10
f

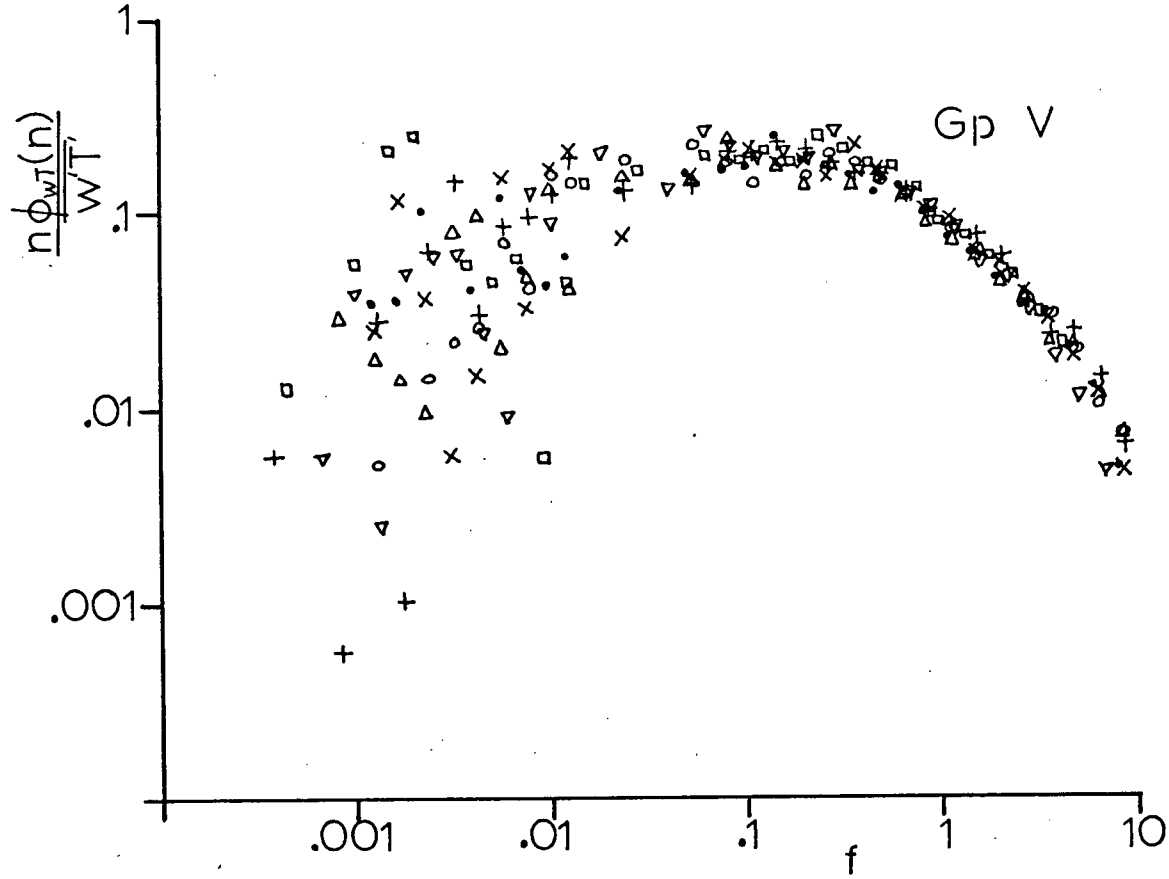
Gp V
1
.1
.01
.001
$\frac{n\phi_{WT}(n)}{W'T'}$
.001
.01
.1
1
10
f

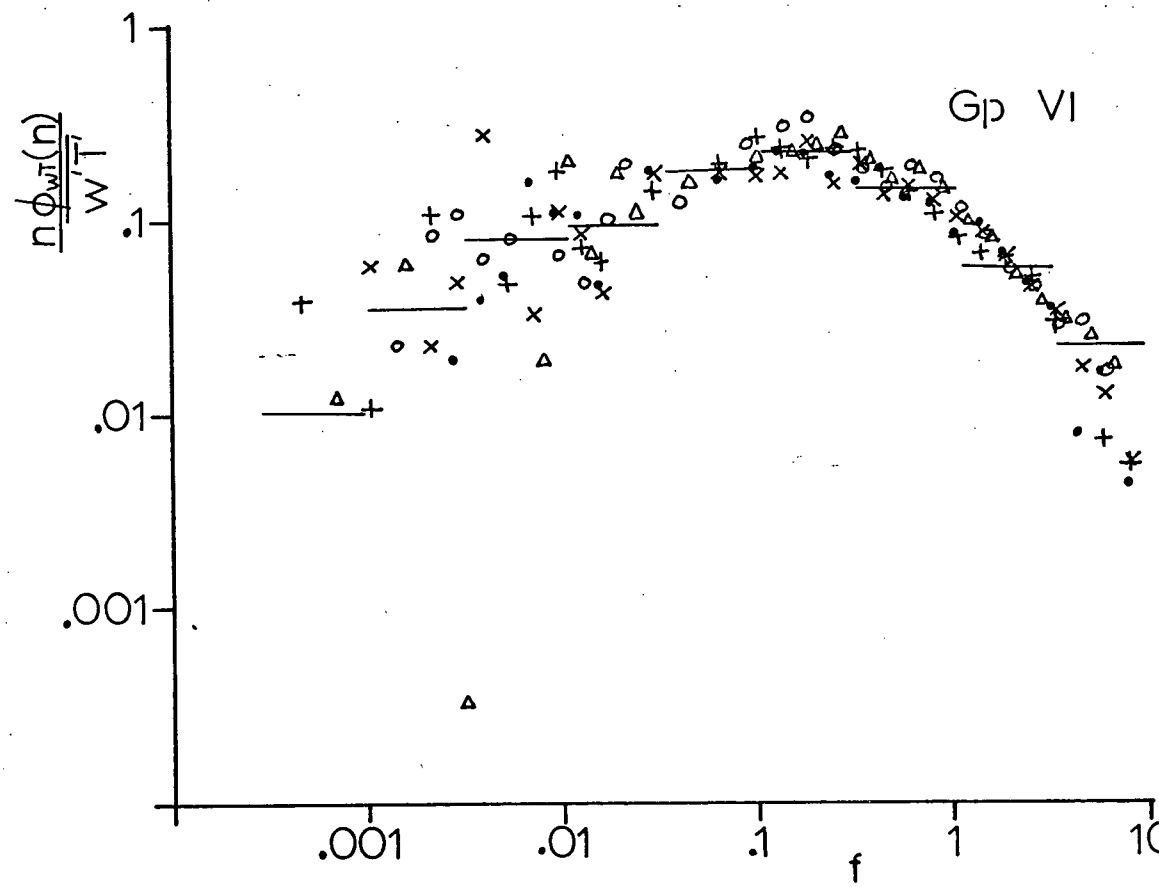
Gp VI
1
.1
.01
.001
$\frac{n\phi_{WT}(n)}{W'T'}$
.001
.01
.1
1
10
f

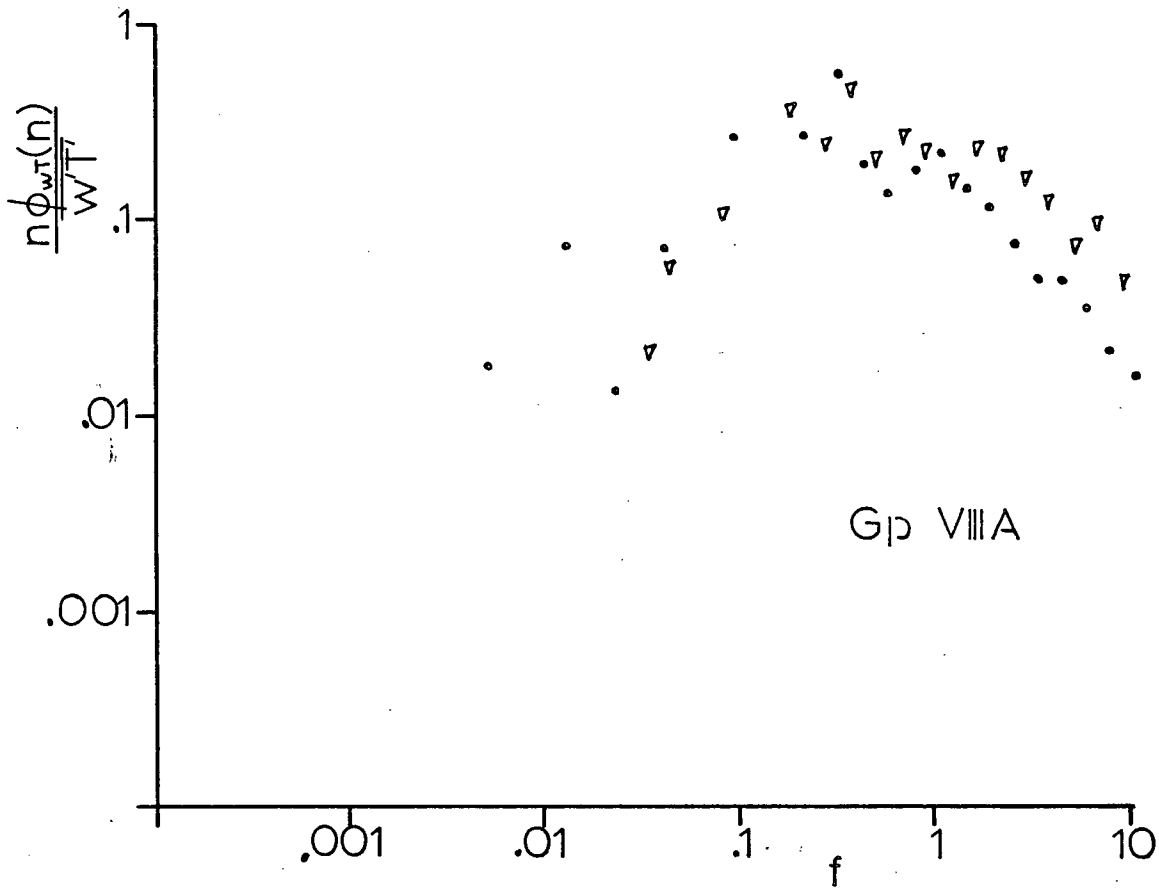
1
.1
.01
.001
$\frac{n\phi_{wT}(n)}{W'T'}$
.001
.01
.1
1
10
f
Gp VIIIA

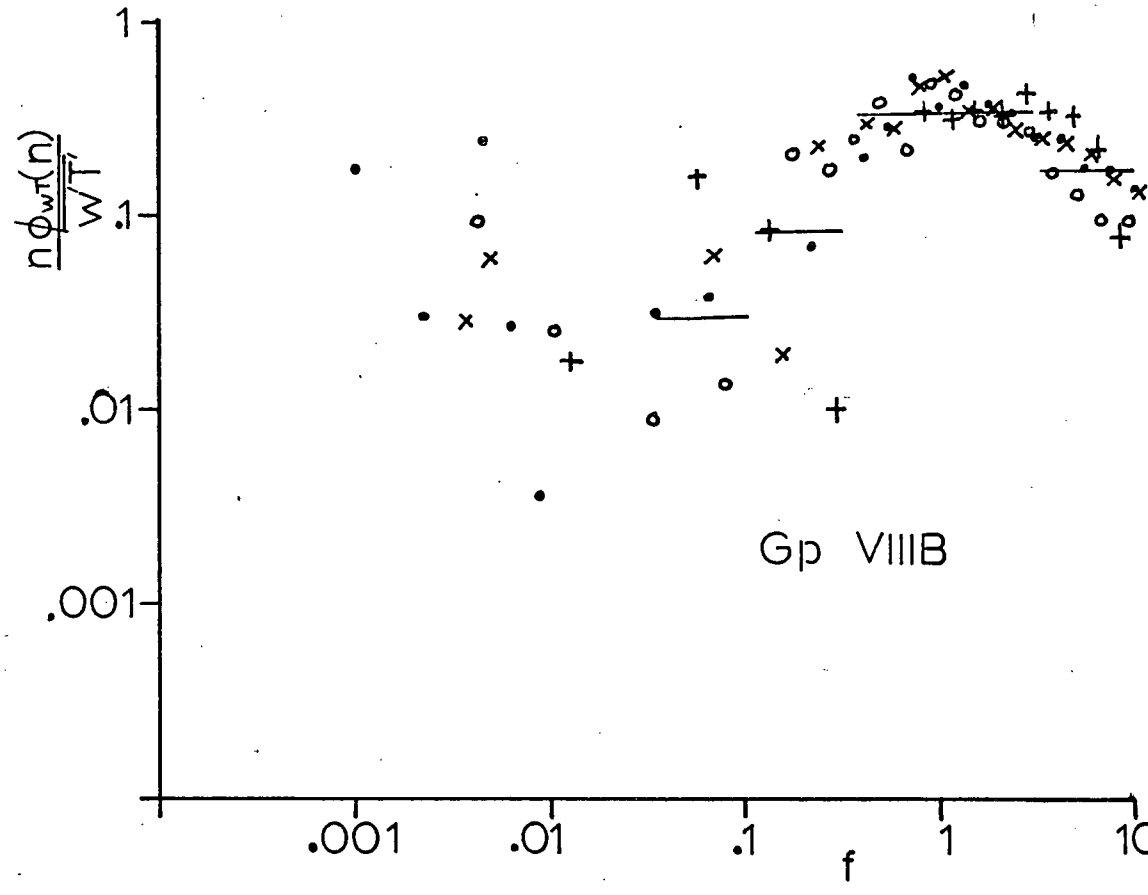
1
.1
.01
.001
$\frac{n\phi_{wT}(n)}{W'T'}$
.001
.01
.1
1
10
f
Gp VIIIB

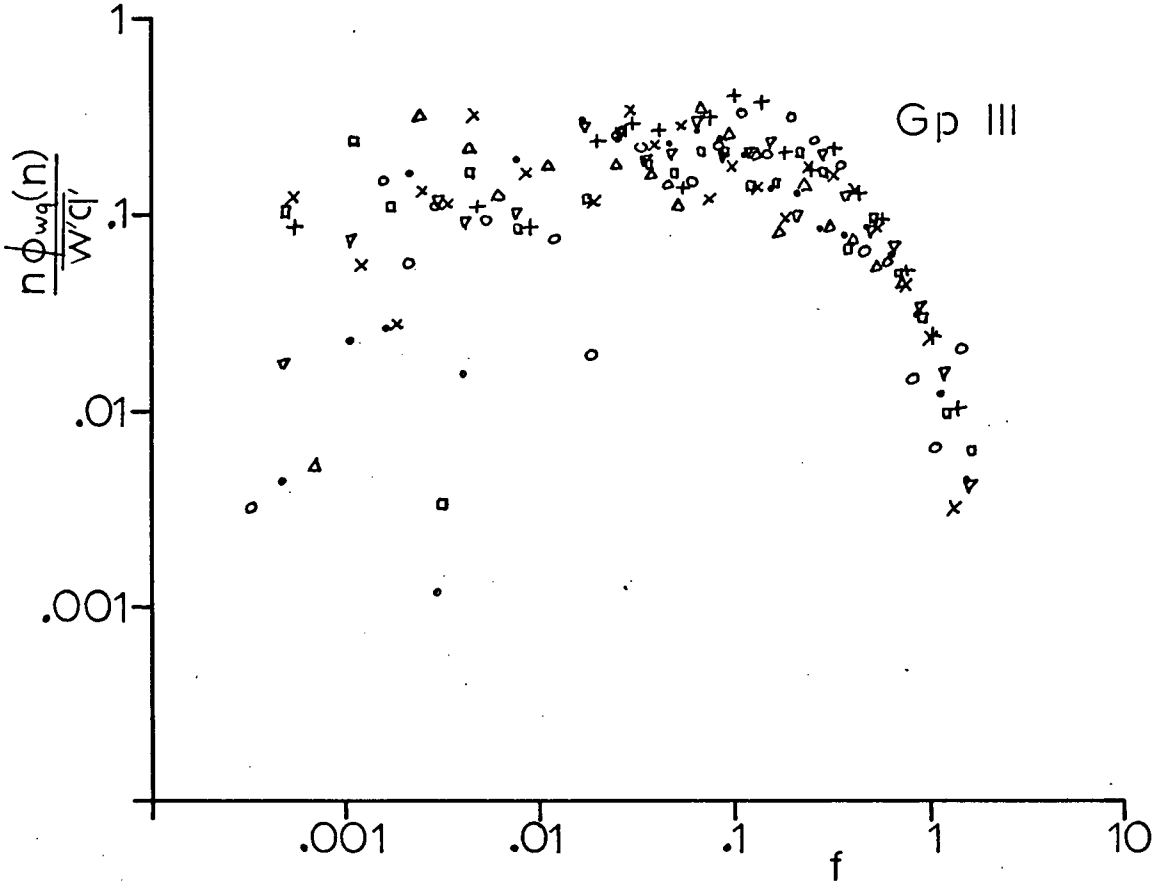
Gp III
$\frac{n\phi_{wq}(n)}{W'c'}$
1
.1
.01
.001
.001
.01
.1
1
10
f

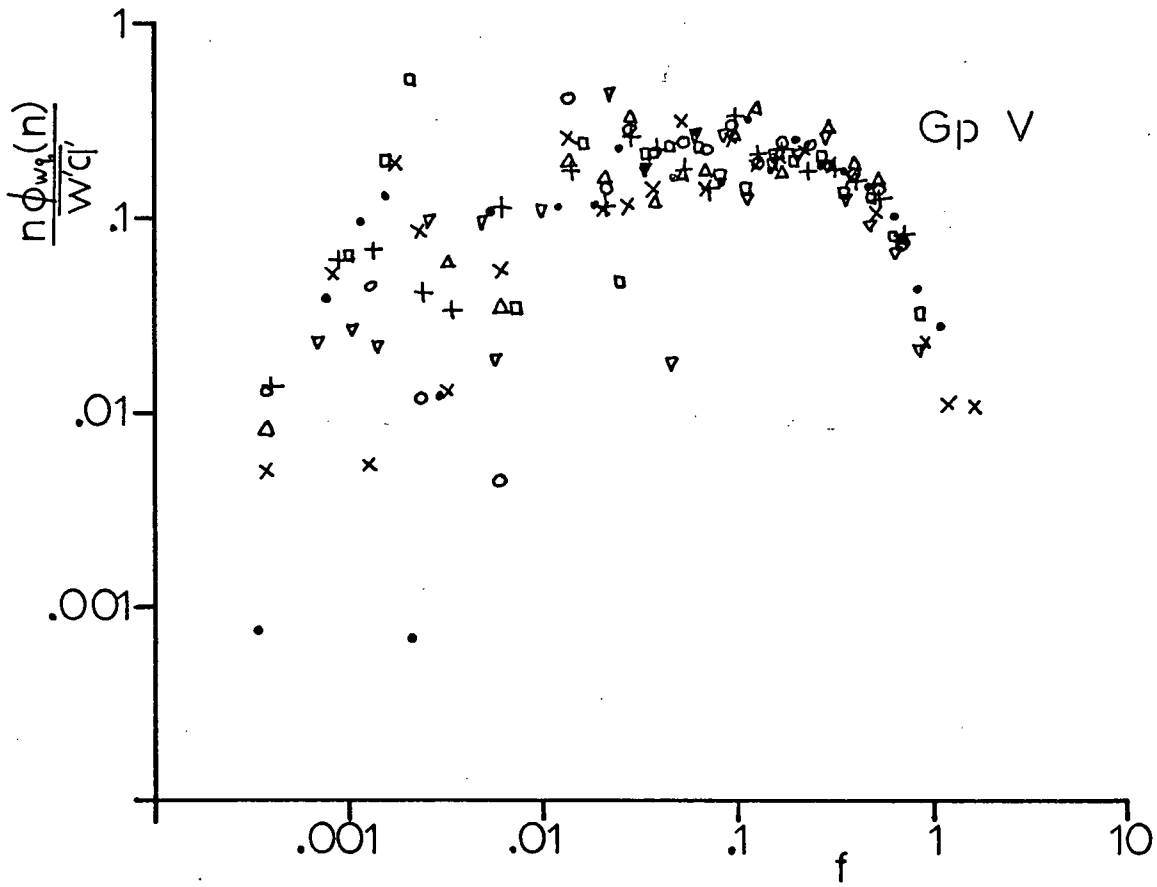
Gp V
$\frac{n\phi_{wq}(n)}{W'c'}$
1
.1
.01
.001
.001
.01
.1
1
10
f

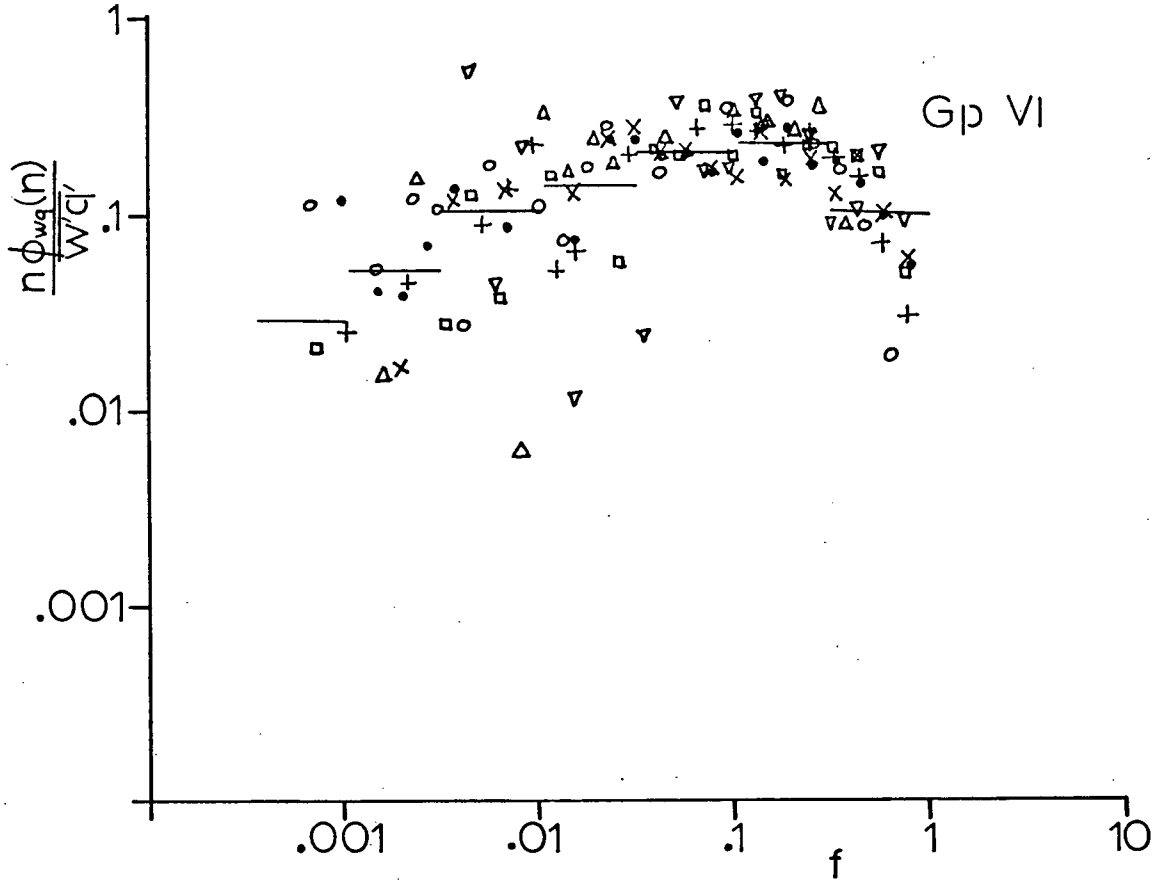
Gp VI
1
.1
.01
.001
$\frac{n\phi_{wq}(n)}{\overline{w'c'}}$
.001
.01
.1
1
10
f

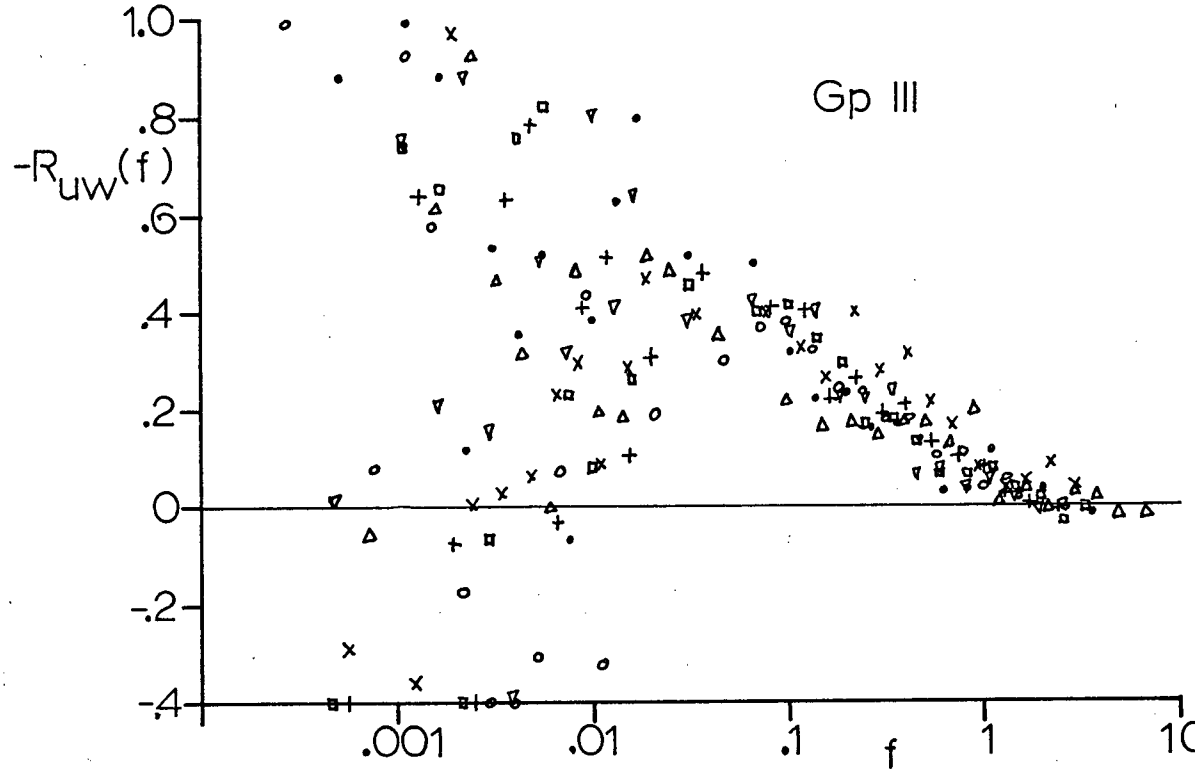
Gp III
$-R_{uw}(f)$
1.0
.8
.6
.4
.2
0
-.2
-.4
.001
.01
.1
f
1
10

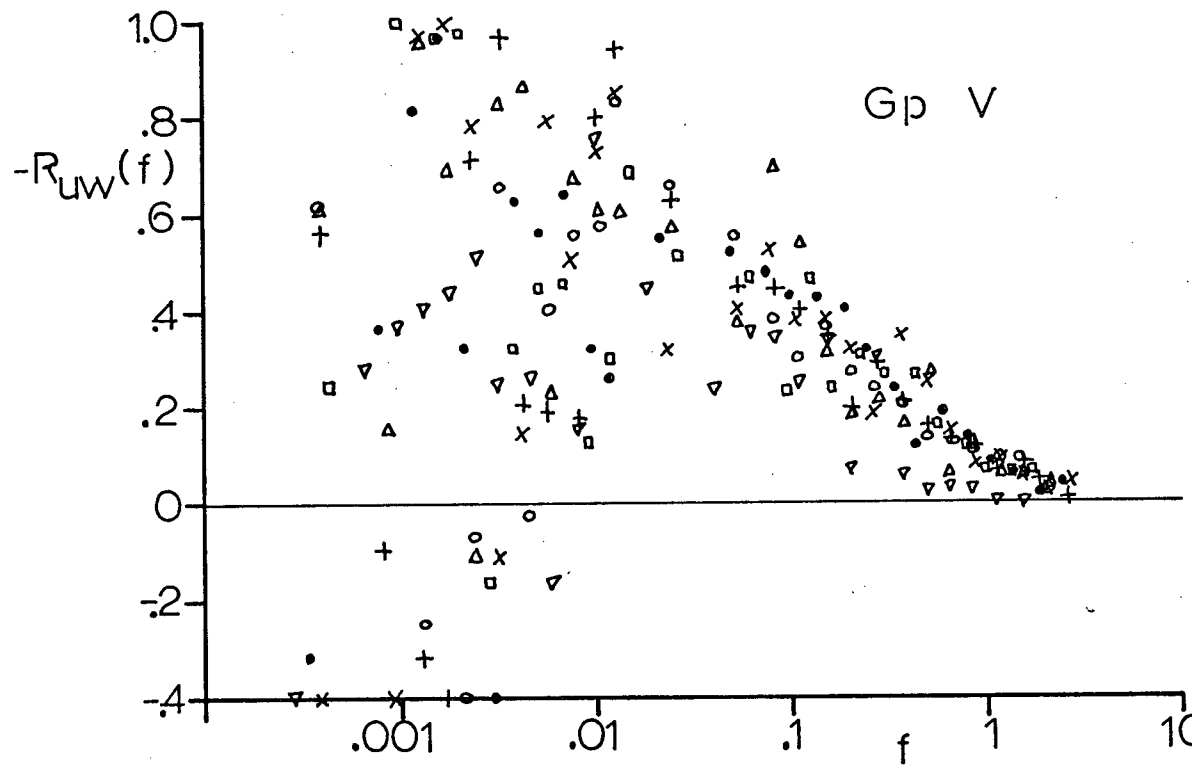
Gp V
$-R_{uw}(f)$
1.0
.8
.6
.4
.2
0
-.2
-.4
.001
.01
.1
f
1
10

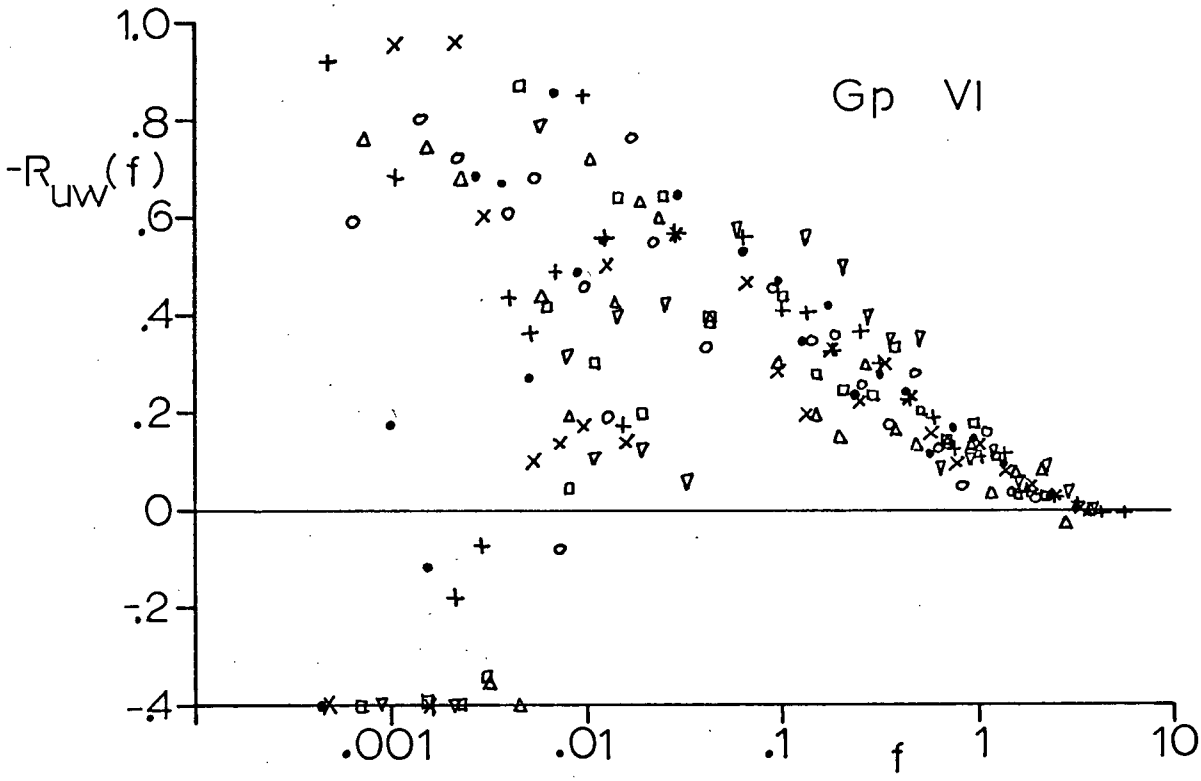
Gp VI
$-R_{uw}(f)$
1.0
.8
.6
.4
.2
0
-.2
-.4
.001
.01
.1
1
10
f

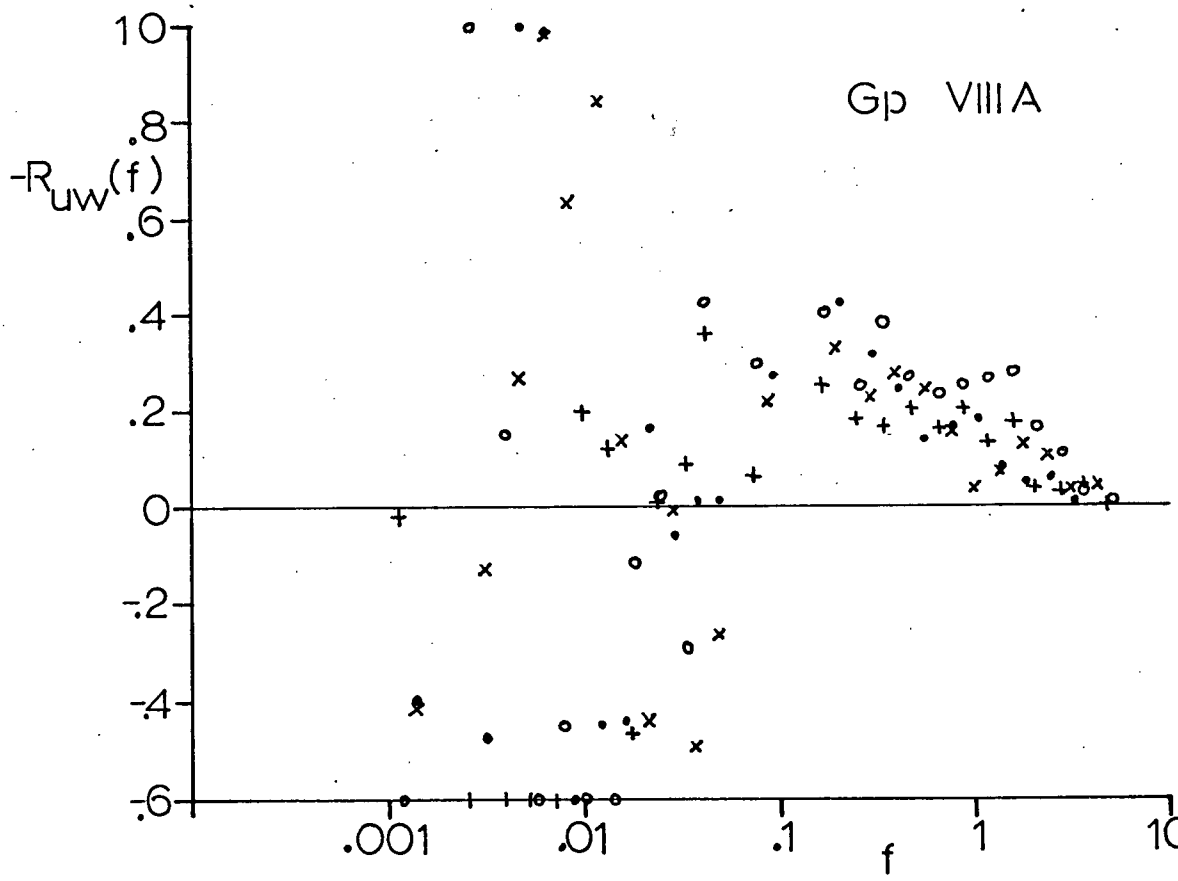
Gp VIII A
$-R_{uw}(f)$
10
.8
.6
.4
.2
0
-.2
-.4
-.6
.001
.01
.1
1
10
f

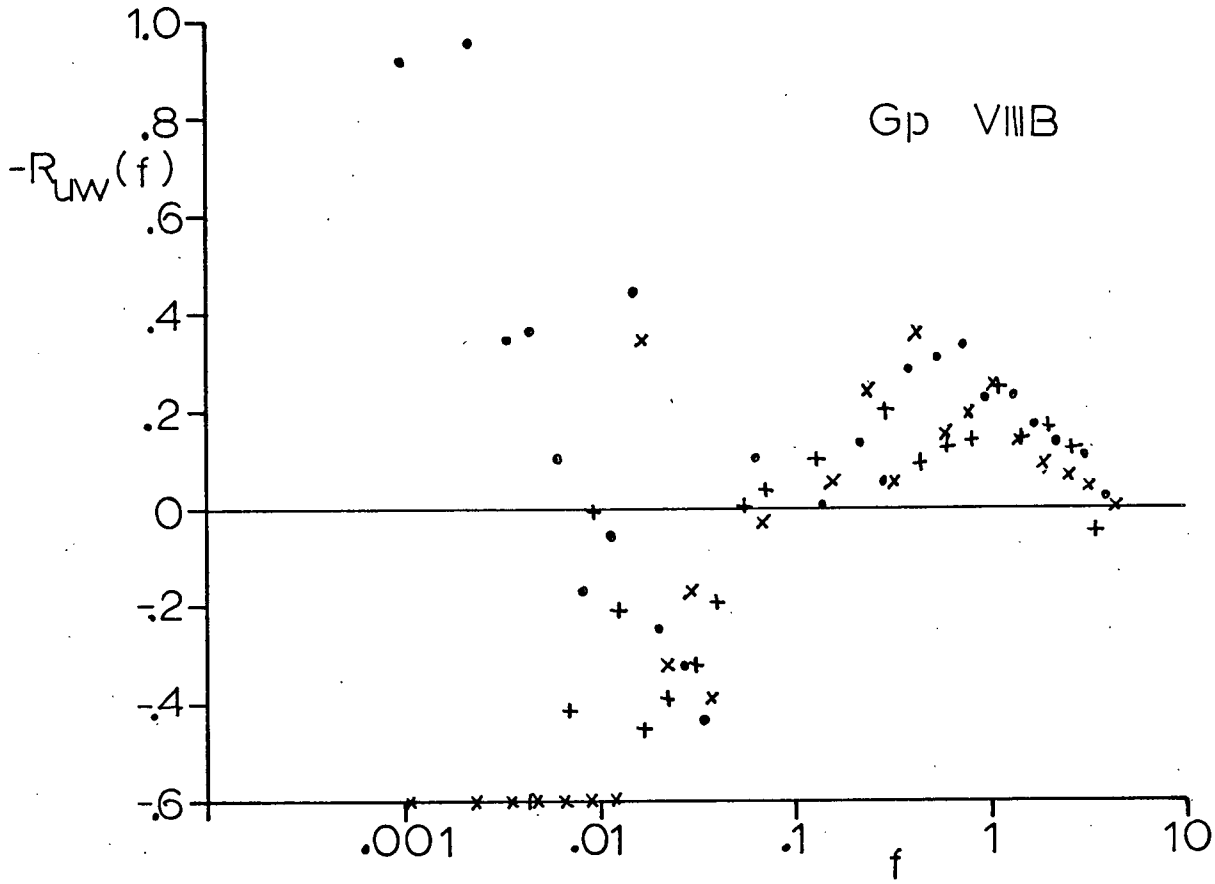
Gp VIIIB
$-R_{uw}(f)$
1.0
.8
.6
.4
.2
0
-.2
-.4
-.6
.001
.01
.1
1
10
f

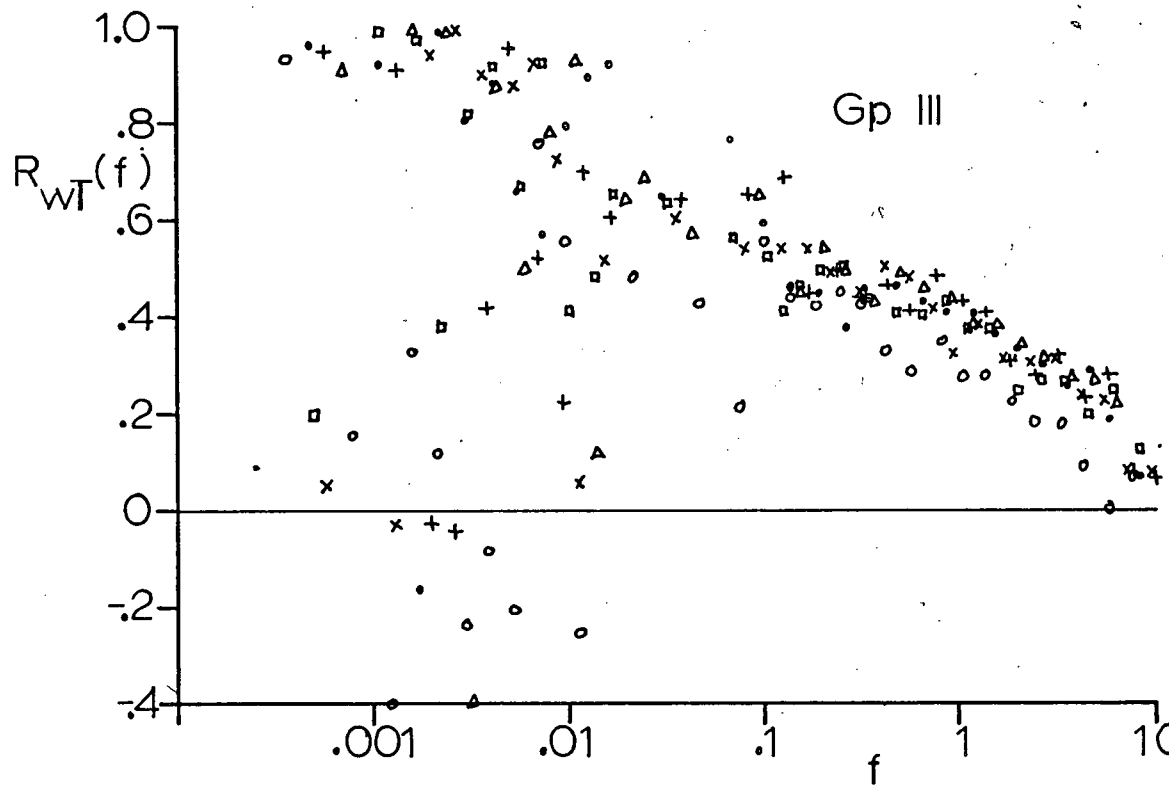
Gp III
$R_{wT}(f)$
1.0
.8
.6
.4
.2
0
-.2
-.4
.001
.01
.1
1
10
f

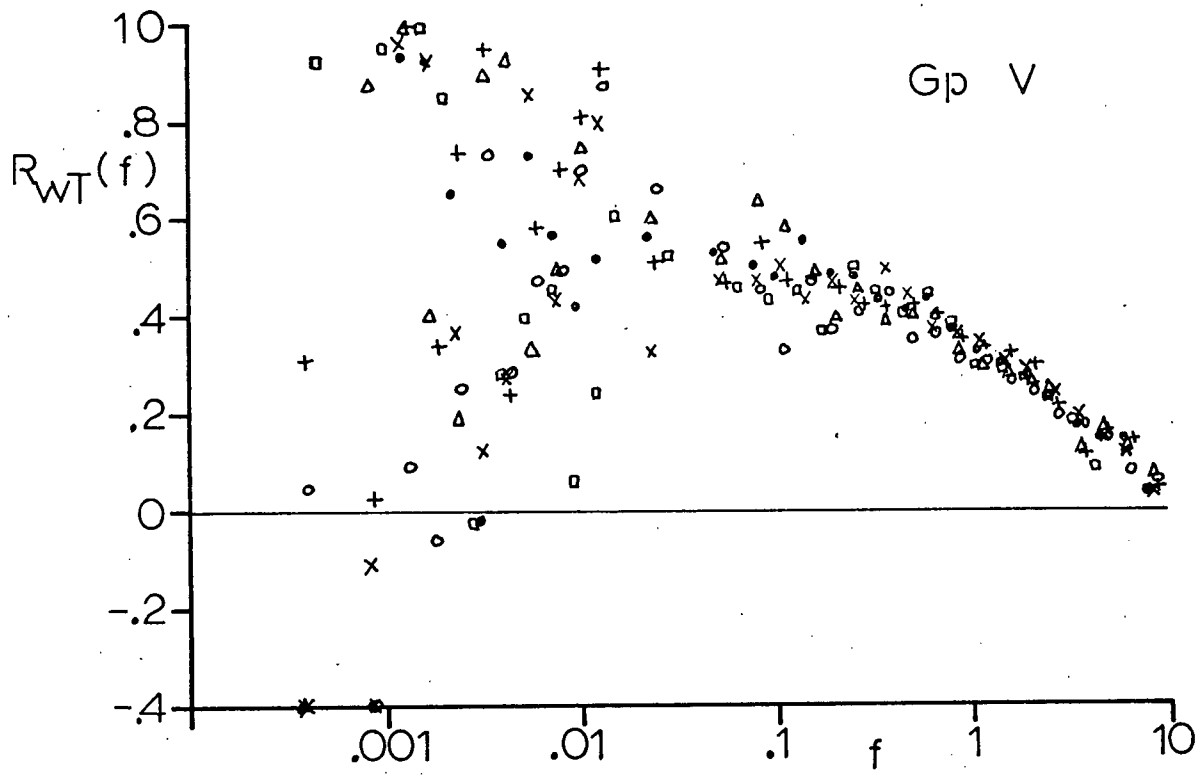
Gp V
$R_{WT}(f)$
10
.8
.6
.4
.2
0
-.2
-.4
.001
.01
.1
f
1
10

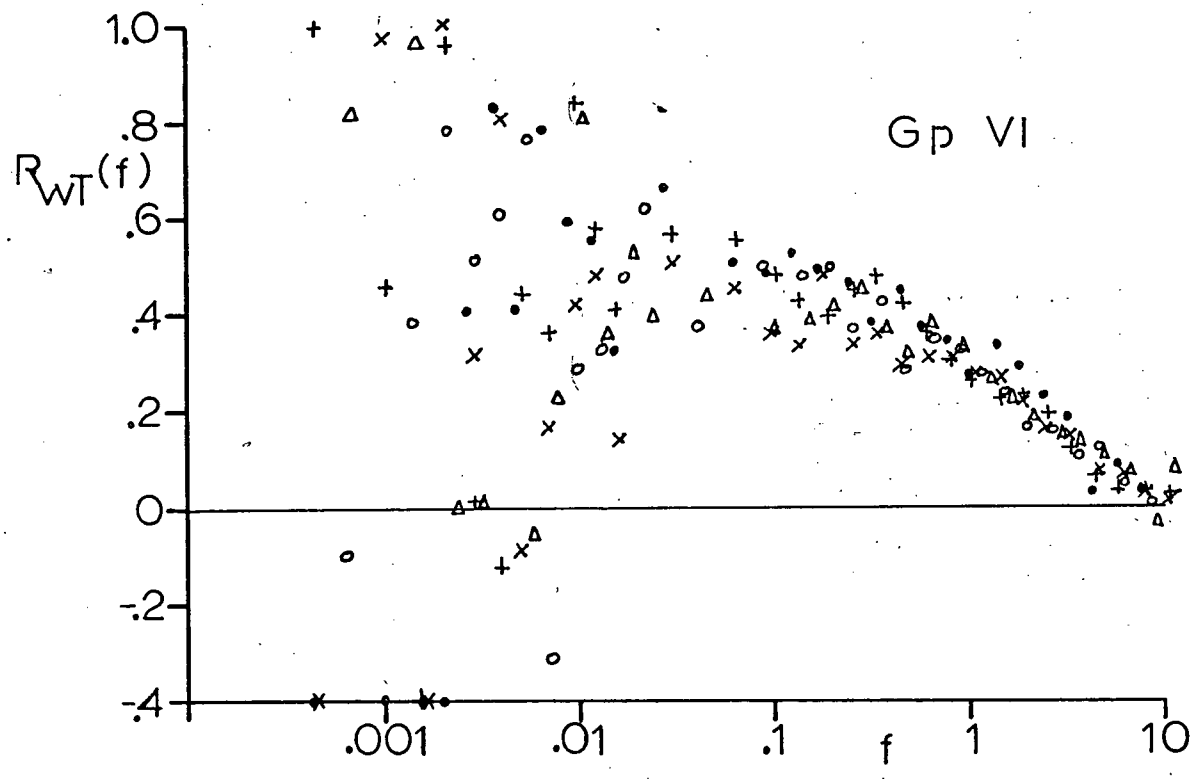
Gp VI
$R_{WT}(f)$
1.0
.8
.6
.4
.2
0
-.2
-.4
.001
.01
.1
f
1
10

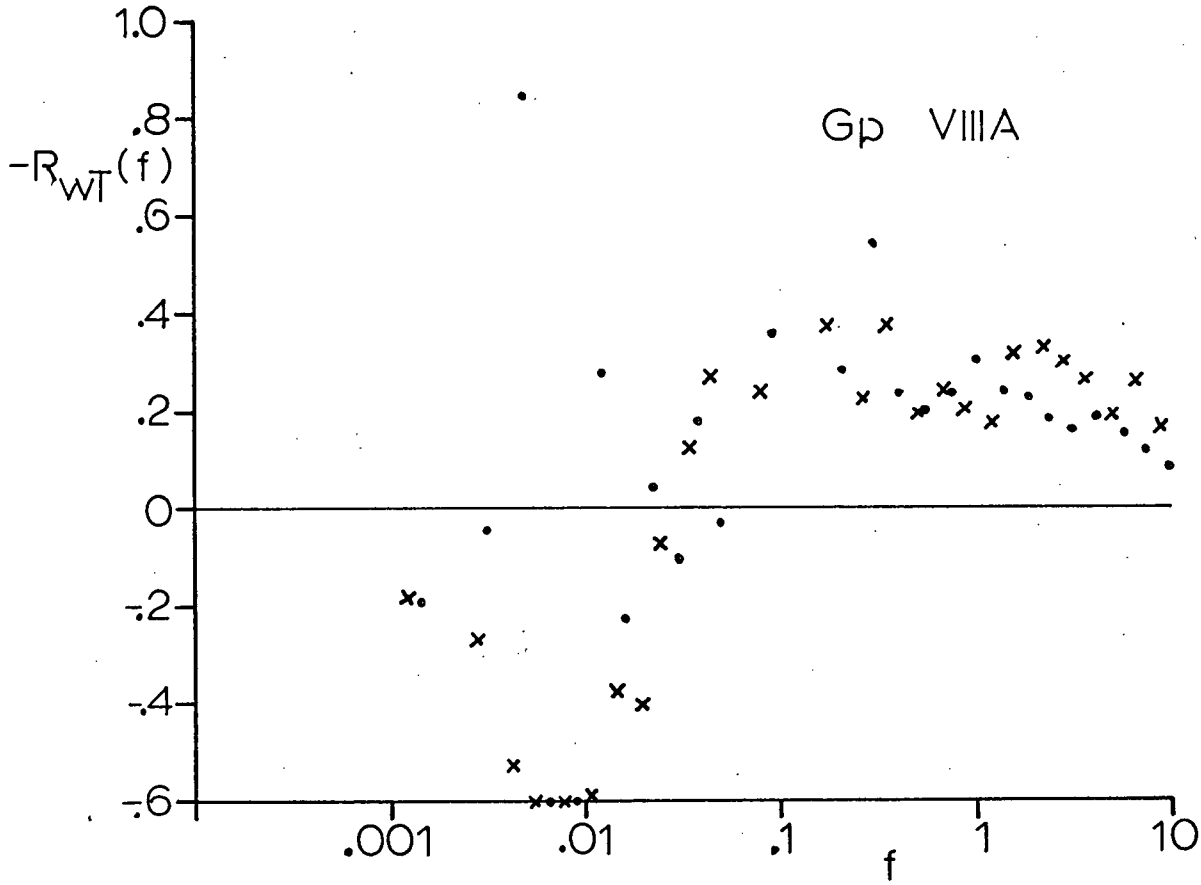
Gp VIIIA
$-R_{WT}(f)$
1.0
.8
.6
.4
.2
0
-.2
-.4
-.6
.001
.01
.1
1
10
f

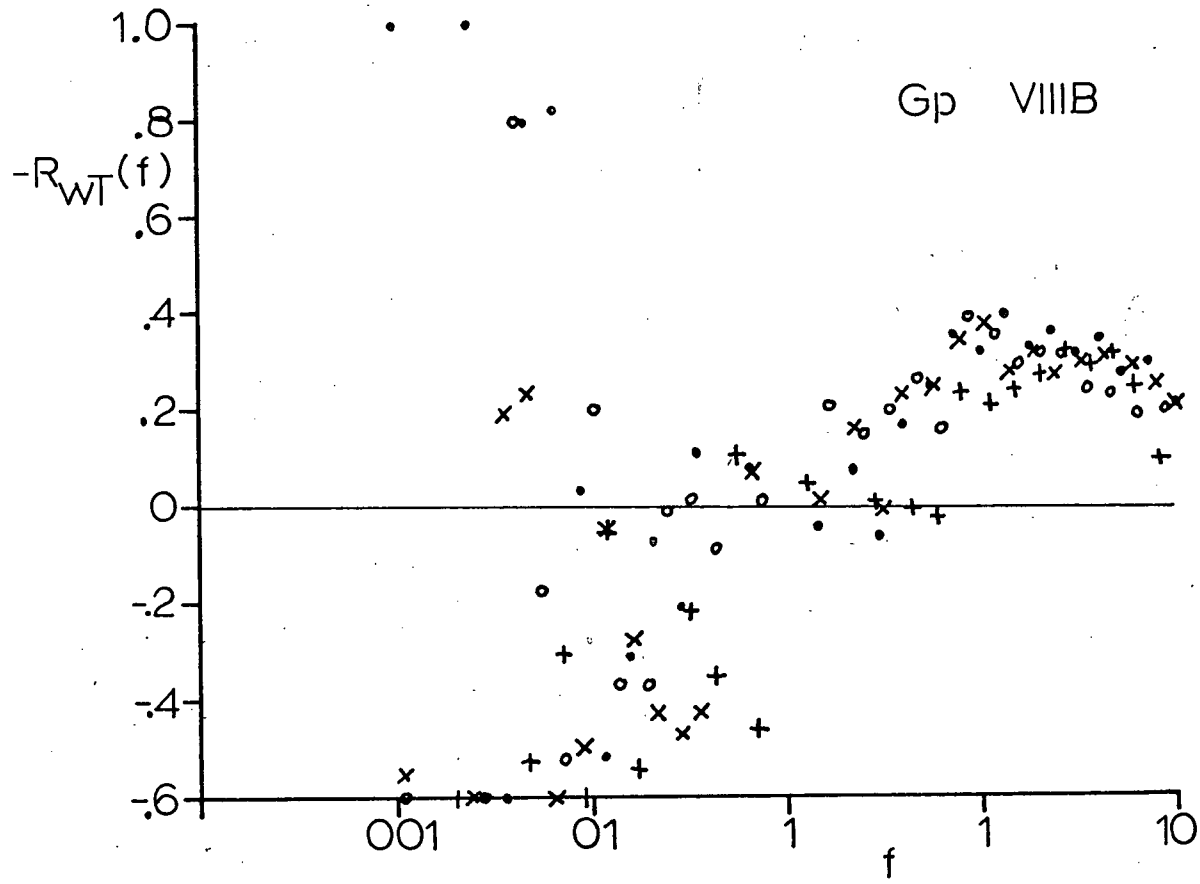
Gp VIIIB
$-R_{WT}(f)$
1.0
.8
.6
.4
.2
0
-.2
-.4
-.6
001
01
1
1
10
f

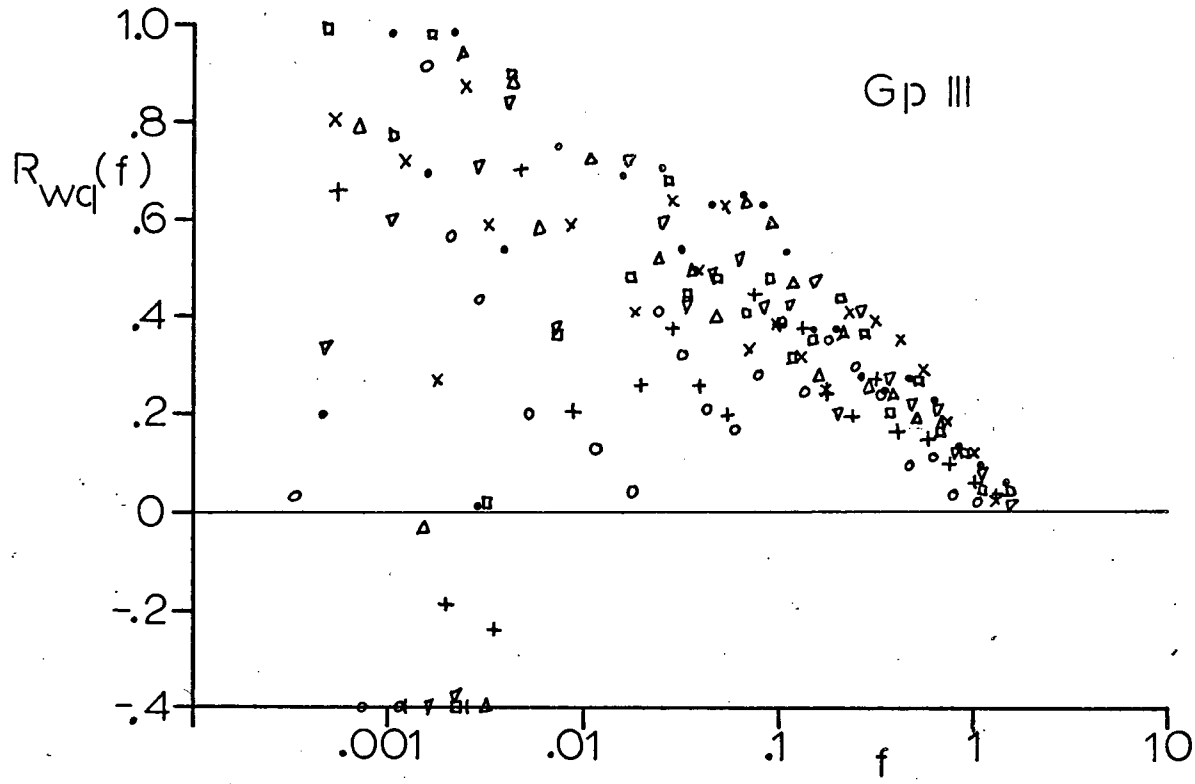
1.0
.8
.6
.4
.2
0
-.2
-.4
$R_{wq}(f)$
Gp III
.001
.01
.1
1
10
f

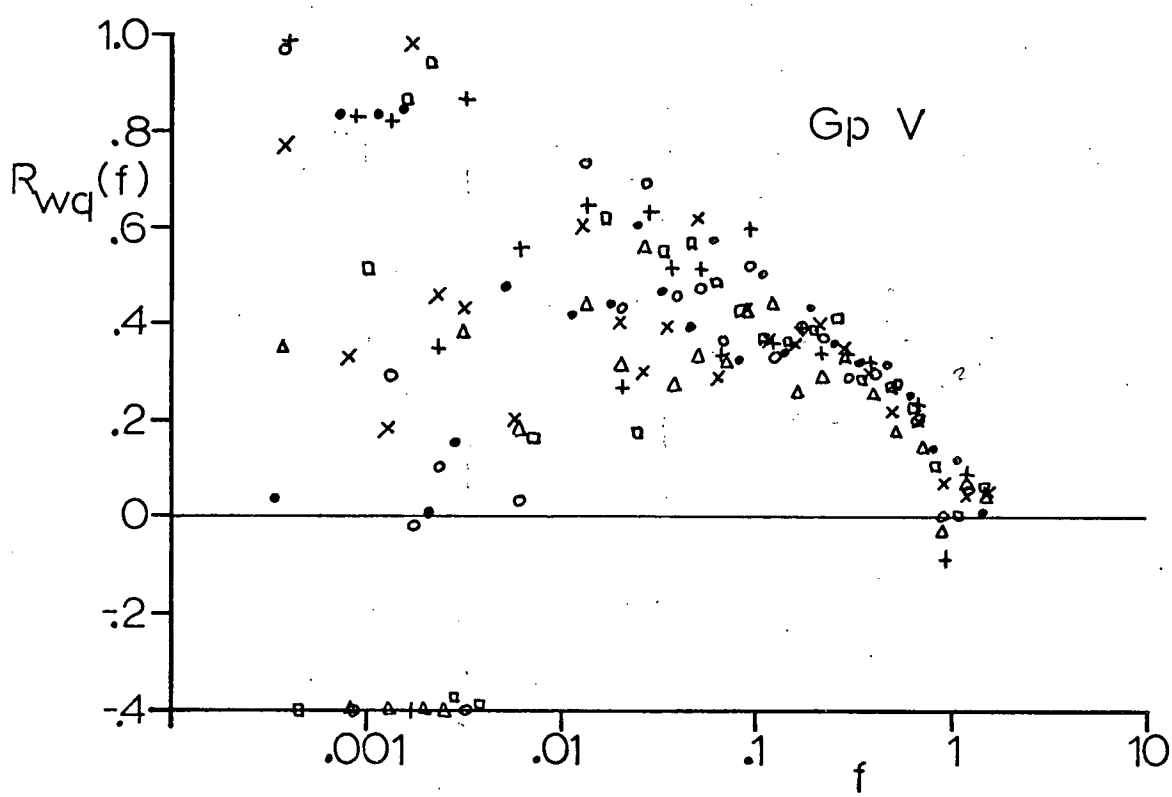
1.0
.8
.6
.4
.2
0
-.2
-.4
$R_{wq}(f)$
Gp V
.001
.01
.1
1
10
f

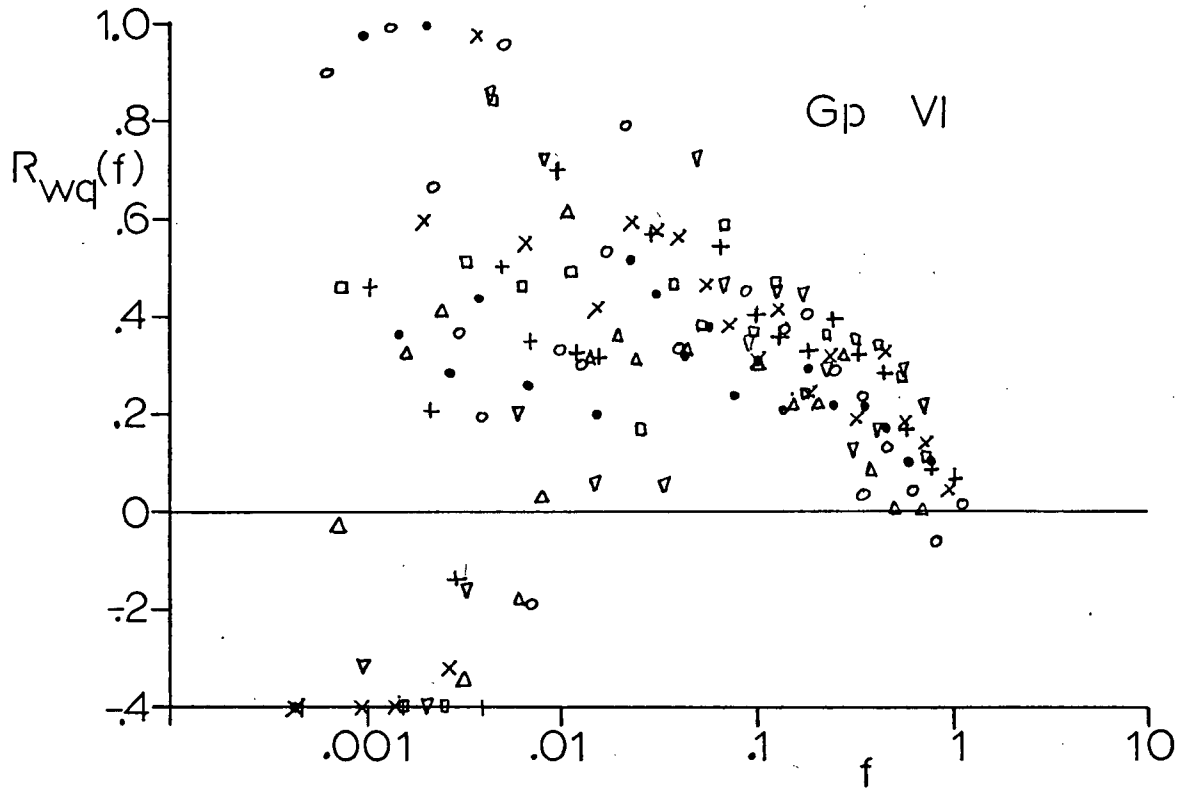
1.0
.8
.6
.4
.2
0
-.2
-.4
$R_{wq}(f)$
Gp VI
.001
.01
.1
1
10
f

List of Symbols

c_p	specific heat of air at constant pressure.
D_q	molecular diffusivity of water vapour.
D_T	molecular conductivity for heat.
ϵ_{ijk}	= 1 for i,j.k, cyclic; = -1 for i,j,k not cyclic; = 0 for any of i,j,k equal.
f	natural frequency, = $nz/\overline{u}$.
g_i	i th component of earth's gravity.
$\phi_{ij}(n)$	cospectral energy density between i and j at frequency n (eqn. 2.3).
K	turbulent diffusivity (eqn. 2.8).
κ	von Karman's constant,= 0.4.
L	Monin-Obukhov length (eqn. 2.6).
n	frequency, in Hz.
P	atmospheric pressure.
q	specific humidity.
q_*	scaling parameter for humidity (eqn. 2.7c).
$R_{ij}(f)$	spectral correlation coefficient function (eqn. 2.5).
r_{ij}	correlation coefficient (eqn. 2.7).
ρ	density of air.
σ_x	standard deviation of x.
T	temperature.
T_v	virtual temperature.
T_*	scaling parameter for temperature (eqn. 2.7b).
u_i	velocity component in the x_i direction.
$\overline{u}$	mean wind speed.

u_* friction velocity (eqn. 2.7a).

Ω_j j th component of the earth's rotation vector.

μ molecular viscosity.